LONG TERM FATIGUE

OF GLASS FIBER REINFORCED COMPOSITE MATERIALS

FOR WIND TURBINE BLADES

by

Robert Michael Reed

A thesis submitted in partial fulfillment
of the requirements for the degree

of

Master of Science

in

Chemical Engineering

MONTANA STATE UNIVERSITY
Bozeman, Montana

May 1991

APPROVAL

of a thesis submitted by

Robert Michael Reed

This thesis has been read by each member of the thesis committee and has been found to be satisfactory regarding content, English usage, format, citations, bibliographic style, and consistency, and is ready for submission to the College of Graduate Studies.

_5/20/91_
Date

_____
Chairperson, Graduate Committee

Approved for the Major Department

_5/20/11_
Date

_____
Head, Major Department

Approved for the College of Graduate Studies

_5/30/91_
Date

_____
Graduate Dean

STATEMENT OF PERMISSION TO USE

In presenting this thesis in partial fulfillment of the requirements for a master's degree at Montana State University, I agree that the Library shall make it available to borrowers under rules of the Library. Brief quotations from this thesis are allowable without special permission, provided that accurate acknowledgment of source is made.

Permission for extensive quotation from or reproduction of this thesis may be granted by my major professor, or in his absence, by the Dean of Libraries when, in the opinion of either, the proposed use of the material is for scholarly purposes. Any copying or use of the material in this thesis for financial gain shall not be allowed without my written permission.

Signature _Robert Michael Reed_

Date _May 5 1991_

ACKNOWLEDGEMENTS

TABLE OF CONTENTS

TABLE OF CONTENTS-<u>Continued</u>

LIST OF TABLES

LIST OF FIGURES

LIST OF FIGURES-<u>Continued</u>

LIST OF FIGURES-Continued

LIST OF FIGURES-<u>Continued</u>

ABSTRACT

This thesis presents the results of the initial phase of a study of the long term fatigue resistance of composite materials for use in wind turbine blades. There is a severe shortage of information on the high cycle fatigue resistance of composite materials in general, and particularly for the E-glass fiber reinforced plastic composites used in wind turbine rotor blades. As wind turbine blades experience roughly 40 million major loading-unloading cycles per year, the fatigue resistance of blade materials is critical.

Different arrangements of unidirectional and triaxial E-glass reinforced polyester and vinyl ester matrices were supplied by blade manufacturers, using fabrication techniques representative of blade manufacturing. Tests were run on a servo-hydraulic machine equipped with hydraulic grips, under sinusoidal tensile fatigue loading. Test results included cycles to failure, damage development, stiffness changes, and surface temperature changes.

The results show a fatigue sensitivity in these composites which is generally greater than that of similar materials of more uniform microstructure. The unidirectional material lifetime data are well fit by a power law trend line, which suggests that the lifetime is dominated by splitting parallel to the poorly aligned fibers. The exponent of the power law fit is similar to that obtained directly in delamination fatigue crack growth tests. The matrix material had little effect on the unidirectional fatigue sensitivity.

The [0/±45] triax materials were significantly more fatigue sensitive that expected. Although they contained some unidirectional strands in the load direction (0°), they failed in high cycle fatigue at the lower strain levels where the off-axis plies failed. This may be related to the details of the triax cloth structure and preparation as well as to the presence of a significant content of ±45° layers.

The stiffness decrease in fatigue was up to 10-20 % for the unidirectional material, but significantly higher for the triax. Extrapolation of the lifetime trends beyond the 40 million cycle data approximated the allowable strain level at 10^9 cycles. The results are very dependent on the assumed model, but show substantially higher allowable strains for the unidirectional than for the triax materials.

CHAPTER ONE

INTRODUCTION

The current cost of producing wind-generated electricity is more expensive than that of coal and hydro-electric, but generally similar to nuclear [1]. To make wind energy more competitive, wind turbine blade manufacturers have begun to design more efficient airfoil shaped blades utilizing the high strength to weight ratio of composite materials. In order to keep costs down, the wind industry can only afford the lower strength, less expensive, glass fiber reinforced polyester and vinyl ester thermosetting matrix materials.

As low performance materials are generally of little concern to the aerospace-military industry which generates the majority of composite materials research on fatigue properties, there exists a shortage of information on the mechanical properties of glass fiber reinforced composite materials. This general lack of mechanical property data, as well as poor blade designs, has resulted in premature blade failures. A critical area of concern to blade designers is the ability of their blades to resist long term cyclic loading-unloading conditions called fatigue. Only through an understanding of the basic long term fatigue behavior of materials can blades be designed efficiently and safely and

can the best materials be selected and developed.

Generation of the required basic material property data is typically performed through static and dynamic fatigue testing. Appropriate theoretical models are adapted or developed to correlate and clarify the experimental results and to allow extrapolations to longer time periods in the absence of appropriate data. Ultimately the results may be used as design parameters and as a basis for materials selection. Understanding of the material behavior may lead to the development of improved materials for fatigue applications. A long term study has been undertaken at Montana State University to address these problems; the initial phase of this project is the subject of this thesis.

CHAPTER TWO

WIND POWER HISTORY

The wind has been enslaved for centuries: the earliest records (before Christ) describe Egyptian boat sails and Chinese water pumps [2]. By the 11th century, mills driven by the wind were scattered across Persia and the Middle East. The Dutch refined this technology and adapted it to other uses such as draining lakes and marshes [2]. Europeans immigrating to America transported this technology to pump water on their new farms and ranches.

By the 1890's the Dutch had wind power generated electric plants, but such systems in America were still in their infancy [2]. As a result, the advent of less expensive steam and gasoline powered generators led to a decline in the development of wind driven systems across the U.S. The usage of wind driven power plants on ranches and farms dwindled even further when the U.S. Government financed Rural Electrification programs [2]. Despite early failure to compete with other technologies, wind power conversion did survive, gradually improving in efficiency and expanding in usage.

One tale of the perseverance of wind technologists is the story of two Montana brothers, Joseph and Marcellus Jacobs. In the early 1900's, they decided to experiment with wind to

electric power conversion. Through their ingenuity, research, and experimentation, they created the Jacob Wind Electric plant. By 1956, their company had sold over 50 million dollars worth of wind turbine equipment and they now have over 25 patents [3]. Even today, their equipment can be reconditioned by such companies as North Wind Power Company. Through similar devotion world wide, most countries had wind turbines by the 1930's [2].

Cost has always been the major detraction for wind generation plants: the cost of electricity from wind plants has typically been higher than that from other types of plants. It was not until the inflation of oil prices during the 1970's that the price of wind energy generated electricity showed some hope of becoming competitive. With this economic boost, and a drive for independence from foreign oil, substantial government research funding became available: government subsidies for alternative energy were offered to encourage both public and private usage and development. With this new effort and interest, many concepts and designs developed.

Today, the U.S. Government funds research for only two designs (see Figure 1). The horizontal axis wind turbine (HAWT) is currently researched by the Solar Energy Research Institute (SERI). The vertical axis wind turbine (VAWT) is currently researched by Sandia National Laboratories. Both organizations perform their research through funding by the

Department of Energy (DOE).

Research on wind energy conversion has provided a number of insights into basic system design parameters. Most importantly, the wind at each site was found to be a complex parameter for system design [2,3]. Airflow was documented not only to gust randomly with time, but with height above the ground, and position along the ground at various wind sites. This established the need for careful wind flow pattern studies of direction, wind speed velocity, consistency, and gusts. A typical study will record wind behavior at specific locations throughout a site for an entire year. This insight gained into the annual wind spectrum allows a thorough evaluation of the potential of a proposed wind site to produce economical power.

The research has also provided a multitude of design choices within the two basic formats of Figure 1 [3]. Depending on the system requirements and available wind power, any number of various design parameters can be selected. Tower height and type, generator size and type, and blade number and size are just a few options open to designers. Depending on the requirements, either a truss or a tube tower may be selected. One of three basic generator types may be chosen: constant speed induction, constant pole induction, or magnetic dipole. Additionally, a two, three, or four blade system design may be chosen.

A significant aspect of the technology which originated

around 1975 was the wind farm concept [2]. The logic behind this concept is that if a site containing one 2-megawatt HAWT is shut down for maintenance or repair, no power will be generated. However, if the same site operates 80 smaller HAWTs of the 25-kilowatt generation class, the same total power can be generated, and, when any individual turbine is shut down, the remaining 79 can still generate power (see Figure 2). Turbines typically either store energy in batteries or directly wire into a central utility power grid [3].

One of the continuing research efforts is in the basic design of the turbine blades. The old HAWT designs were made with wood. Composite materials are now being exploited, but the need for low cost materials has created a two-fold problem. First, low cost composite materials typically exhibit lower mechanical properties, particularly fatigue resistance, as compared to more expensive composite materials such as graphite/epoxy. Second, only limited research has been performed on the lower grade materials. As wind power companies have limited resources, they cannot perform the tests necessary to ensure the most efficient designs. Even aircraft manufacturers which typically perform substantial research in this area do not perform the high-cost long-term fatigue tests which run past the million cycle range [4]. However, wind turbine blades must withstand roughly forty million cycles each year, for twenty to thirty years.

Problems with early wind turbines have resulted in many design errors and service failures, so that today only the best machines and blade manufacturers have survived. Still, there remains a lack of data necessary to improve systems, especially in the area of long term fatigue. This study is intended to correct this deficiency.
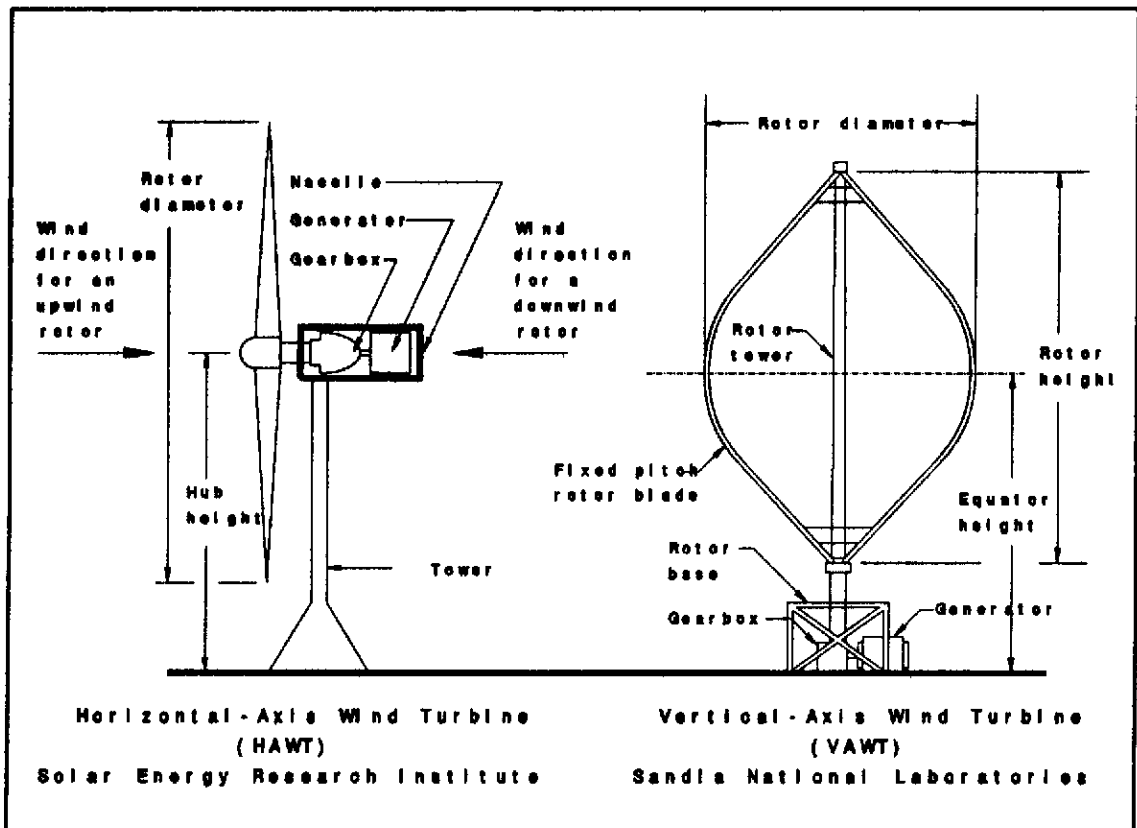
Figure 1. Two basic types of Wind Turbine Systems, From Ref. 2.
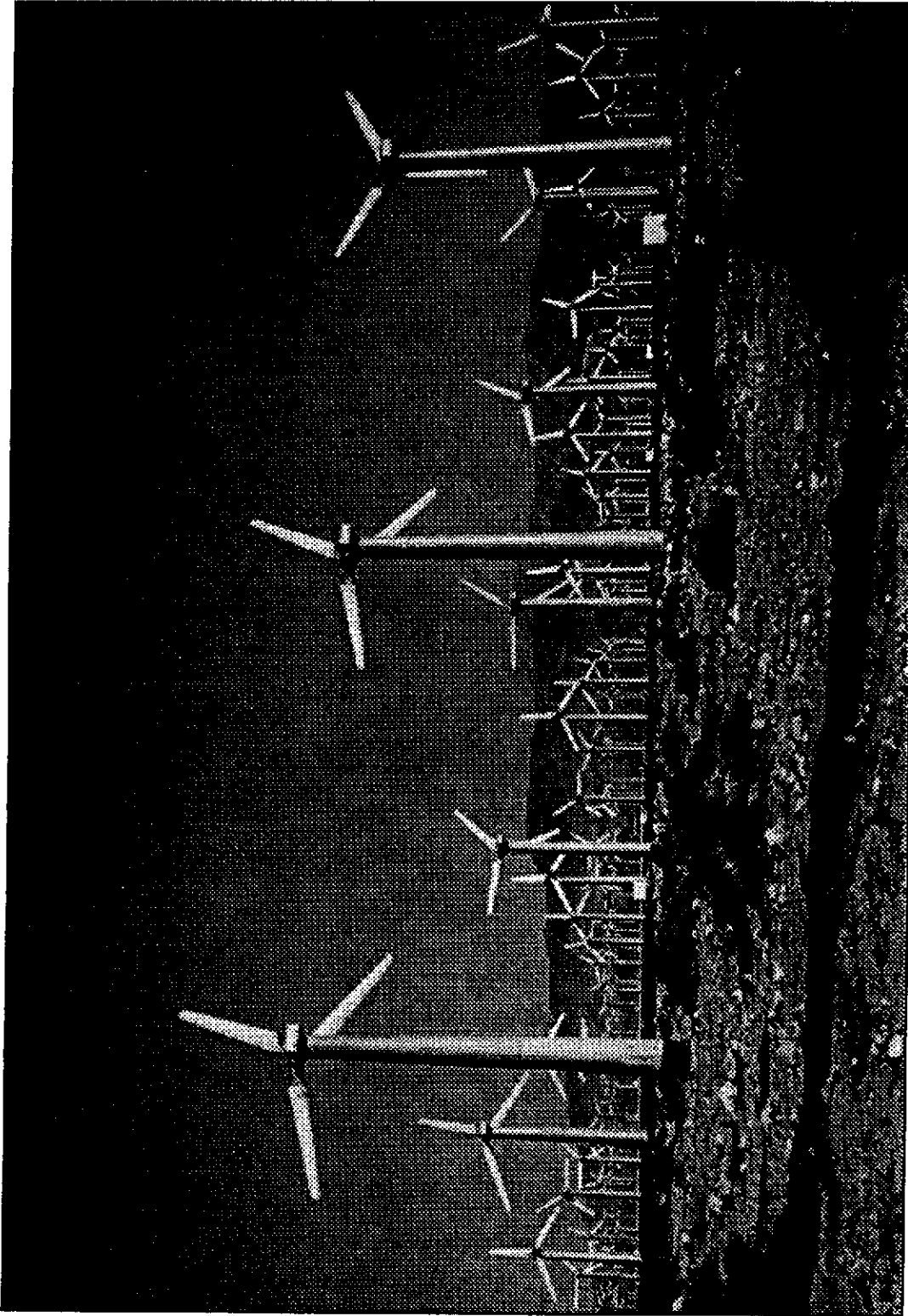
Figure 2. San Gorgonio Wind Farm Owned and Operated By Sea West Energy Group of San Diego, California.

CHAPTER THREE

BACKGROUND

Review of Composite Composition and Terminology

A composite is defined as a material which is comprised of several distinct components. The composites reviewed here are comprised of glass fibers reinforcing plastic matrices. As such, the basic properties can be explored in four categories: matrix, fiber, interface, and composite properties.

Polymeric Matrices

The matrix material has the tasks of holding the load bearing fibers in designed orientations, and in transferring stresses among individual fiber bundles. Therefore, a liquid material which can first permeate and surround fibers, and then cure to become a solid mass capable of transferring load, makes an ideal matrix material. Thermoset polymers can be transformed from viscous liquids into rigid solids through a chemical reaction called crosslinking, where individual molecules are joined together into a three dimensional network of strong covalent bonds. This ability allows flexible materials containing fibers and matrix to be laid-up and then cured into final rigid parts of the desired shape.

There are two temperature ranges which are typically important in defining the level of mobility of the molecular chains in polymers. The temperature where crystallization may begin to occur (or break down) in a noncrosslinked thermoplastic is called the melt temperature (T_m). Below this temperature, there exists a second transition where the chains not arranged in crystals first note a dramatic decrease in their freedom of relative movement. This second temperature range is called the glass transition temperature (T_g).

The chemical composition and molecular architecture play key roles in molecular movement. The chemical composition describes the basic chain units as to their size, shape, pendant (side) groups, and bond strengths. The chemical composition also tends to determine properties such as the glass transition temperature [5]. The molecular architecture is a term which includes the degree of polymerization, the molecular weight distribution, the average molecular weight, and the chain patterns (linear, branched, 3-d network). The chain patterns in conjunction with the stereo regularity determine how tightly the chains will pack together. The chain structures with more regular and uniform patterns are able to form more dense substructures which result in stronger matrices. The highest degree of packing may result in crystallization. The more irregular and complex chain structures tend to result in a less dense amorphous structure. Within this realm of morphology, there exist two basic

subcategories: thermosets and thermoplastics [6]. The thermoset material is defined by a more permanent covalently bonded network or set macro-molecular structure which cannot be made to flow like a liquid by the addition of heat or pressure. However, molecules of thermoplastic materials are held together by weak secondary bonds, such as Van der Waals forces. With sufficient energy the secondary bonds can be broken and reformed, allowing the material to flow [6]. In thermosets such movement can only occur between the crosslink points of the network.

There are a wide variety of basic resin materials from which to choose. The selection is determined by factors such as the method of fabrication, the ability of the matrix to wet and bond to the reinforcement, the desired resultant properties, the environment to which the composite will be exposed, and the total overall cost. Due primarily to cost and ease of fabrication, wind turbine blade manufacturers are currently relying on two relatively inexpensive, widely used polymeric materials: unsaturated polyester thermosets which cost from 0.5 to 1.0 \$/lb, and unsaturated vinyl ester thermosets which are slightly more expensive [7]. The term unsaturated is used to describe the double bonded carbon atoms (C=C) which, during curing, become the reactive sites which enable network formation [6].

Unsaturated Polyester Thermosets

Unsaturated polyester resin (UPR) materials can be cured
at room temperature, which make them ideal for hand laid-up
composites where no additional heat or pressure is applied.
Their curing reactions are exothermic, and enough heat is self
generated to help in rapidly converting an estimated 90% of
the reactive double bonds to single bonds [8]. With a strong
covalent attraction bonding individual monomers together, a
strong carbon backbone is created with typical molecular
weights ranging from 2000 to 20000 [7]. In addition, there
are shorter chains of a monomer such as styrene which can
bridge together the longer polyester chains into a permanent
three dimensional network.

UPR fabrication is performed in three basic steps (see
Figure 3) [6]. First, the starting material is prepared by
reacting maleic anhydride with a glycol (ethylene or
propylene) to form the polyester. Second, the polyester is
dissolved in a reactive monomer diluent. The third stage is
to add a catalyst which will quickly decompose into free
radicals. When these free radicals break the C=C bonds of the
diluent and the polyester, the monomer reacts with the
reactive sites of the polyester molecules forming bridges.
The end result is a complex three dimensional network of
bonded chains (see Figure 3) [6].

A wide range of morphologies can exist depending on the
type of reactants used: the basic polyester molecules,

crosslinking molecules, catalysts, promoters, accelerators, and additives. Monomers such as styrene or vinyl acetate, which greatly reduce the viscosity of the curing matrix, allow easier spreading and better wetting of the fibers. Additives can also adjust the brittleness or thermal expansion or conduction, give ultraviolet degradation protection, or increase fiber bonding. Another type of additive, inhibitors, may be added to increase the length of time in achieving a certain degree of cure. For heat applied cures, the most common catalyst is benzoyl peroxide which is stable at room temperature. For room temperature cures, methyl ethyl ketone peroxide (MEKP) is generally used but requires an accelerator such as cobalt naphthenate to provide a full cure [8]. Within the UPR family, there are currently five commonly used formulas: orthophthalic, isophthalic (or terephthalic), Bisphenol A (BPA), chlorendics, and dicylopentadiene [8]. Orthophthalic polyesters are typically used for general applications [9].

The wide range of chemical compositions result in a wide range of material properties. UPR yield strengths may range from 6.0 to 13.0 ksi, and tensile strengths from 5 to 15 ksi with up to 5% elongation to failure [6,9]. Elastic moduli are listed between 300 and 600 ksi with relative specific volumes ranging from 19 to 25 in^3/lb [6,9]. The mechanical strength is often dependent on effects such as physical aging, time under load, environment, and the temperature.

Unsaturated Vinyl Ester Thermosets

Vinyl ester resins are formed by combining an epoxy resin with an unsaturated carboxylic acid, like acrylic or methacrylic acid, which is then dissolved in a reactive diluent such as styrene monomer (see Figure 4) [6]. During the curing reaction, the diluent forms crosslinks only at the reactive ends of the vinyl ester chains. This leads to fewer crosslinks as compared to UPR. Vinyl esters matrices also contain hydroxyl (OH) pendant groups (see Figure 4). These hydroxyl groups can form hydrogen bonds to the surface molecules of glass fiber coupling agents, providing a strong interface [6].

Although the physical properties vary with the type and quantity of additives, vinyl esters are considered to exhibit slightly higher mechanical properties than the polyesters. Their tensile strengths range from 10 to 12 ksi with elongation to failure from 3.5 to 5.5 % [6]. Vinyl esters exhibit moduli around 440 to 510 ksi with specific volumes from 21 to 25 in^3/lb [6].

Glass Fibers

Glass fibers, or filaments, are composed of three-dimensional random-arrays of silicon and oxygen tetrahedra randomly interspersed with other additives [10]. The type and amount of additives can change the properties significantly. This has led to three basic glass fiber compositions, electrical (E-glass), structural (S-glass), and chemical

resistant (C-glass). The less expensive E-glass, herein termed glass, is the most widely used type of glass reinforcement and the only fiber used in this study.

Most glass fibers are approximately 10 microns in diameter and are typically individually coated with a protective size to prevent excessive handling damage. The individual filaments are then typically wound together in groups of 200 or so, and held together with a chemical binder. These thin strands of glass fibers are called ends. Multiple ends may then be grouped together to form thicker strands typically called bundles, strands, or tows. By adjusting the number of ends grouped together, thicker or thinner strands may be produced. Again, these ends may be held together with a chemical binder. A typical binder for glass fiber reinforced UPR would be a solution of the condensate of maleic anhydride and ethylene glycol in styrene [7]. The relative degree of tightness with which these filaments are bound is termed the bundle integrity. The integrity can play a crucial role in fiber-fiber friction, which is an important concern as will be seen later. Mandell (Reference 11) gives properties of glass bundles comprised of 204 fibers, each 9 microns in diameter, as 400 ksi tensile strength and 10600 ksi elastic modulus, which are notably greater than the corresponding values for the matrix materials. Glass fibers may be purchased in many arrangements, one of which is in the form of a sheet comprised of individual bundles aligned in the same

direction. This type of sheet or ply is termed unidirectional.

Interfacial Properties

The degree of interaction between the matrix and the reinforcement can significantly impact the properties of the composite. This interfacial strength depends upon the physical and chemical bonding characteristics at the fiber surface.

The degree of chemical bonding between the matrix and the fibers depends on the type of resin and size used. In cases where poor bonding or environmental stability is expected, as is typical of glass fiber reinforced composites, the addition of a coupling agent can be used to improve the interfacial bond strength. Glass fiber composites typically use silane coupling agents [6]. The specific type of silane coupling agent depends on the type of resin material. For polyester and vinyl ester thermosetting polymer matrix materials, γ-Methacryloxypropyltrimethoxysilane, vinyl triethoxysilane, or vinyl tris(ß-methoxyethoxy)silane are recommended [6]. After the size is burned from the fiber surfaces, the fibers are dipped into a silane solution. In theory, the fiber surface oxygen atoms chemically bond to the silicon atoms of the silane molecule (see Figure 5). The other end of the silane molecule contains a reactive functional group designed to react and chemically bond with the matrix material. Hydroxyl groups on the fiber surface develop additional but

weaker bonds to those in the silane solution [6]. Much of the role of the coupling agent is to provide environmental stability at the interface, particularly to resist water.

Differences in the thermal expansion properties of the constituents may also enhance their interfacial strength. With the thermal expansion coefficient for glass fibers in the range of 2.8 (10^{-6} in/in/°F), and the matrix coefficient around 50 to 100 (UPR) and 40 to 100 (vinyl ester), cooling from the cure temperature may result in the matrix shrinking around the fibers, depending on local fiber packing geometries [9]. Radial compression generated by the matrix against the fiber enables better mechanical load transfer [6].

Glass Fiber Reinforced Composites

The properties of glass fiber reinforced composites typically depend on the relative amounts of the constituents, their arrangement, and their properties. An example of this is the Young's modulus of elasticity (E_L) for a unidirectional composite in the direction parallel to the fiber axis, herein termed the longitudinal direction. With the volume fraction of fibers in the composite represented by V_f, and the volume fraction of matrix as V_m, the tensile longitudinal modulus of the composite is approximated well by the rule of mixtures, Equation 3.1 [10]. In the direction perpendicular to the fiber axis, herein termed the transverse direction ($_T$), the modulus depends more strongly on the matrix, but still depends directly on the relative amounts and properties of both

constituents. The approximation for E_T in Equation 3.1 is less accurate than for E_L

$$E_L = (V_f * E_F) + (V_m * E_M)$$
$$E_T = (E_F * E_M) / [(V_m * E_F) + (V_f * E_M)]$$

(3.1)

where E_f is the fiber modulus and E_m is the matrix modulus.

Another critical property is the composite strength. The efficiency with which the composite can carry load depends primarily on the relative amount and alignment of the fibers relative to the loading direction. A higher fiber content not only increases the longitudinal stiffness, but also the longitudinal tensile strength (to a point). A rough approximation for the tensile strength is to use a rule of mixtures, or an approximate version, where the fiber ultimate tensile strength is multiplied by V_f, as the contribution of the matrix tends to be minimal [10]. However, if the composite is loaded in directions other than nearly parallel to the fibers, then the strength of the matrix and interface are critical. In either case, mathematical modeling of strength can yield only an approximation: due to the strong effect of the interfacial strength between the fibers and the resin, a variety of potential flaws, a wide degree of scatter within individual component strengths, and imperfect alignment of fibers, only testing can provide an accurate composite strength.

As fiber alignment plays a critical role in strength and stiffness, differently oriented sheets of unidirectional fibers, called laminae or plies, will exhibit different properties. As both the modulus and Poisson's ratio (ν) of the fiber ($\nu=.22$) and matrix ($\nu=.35$) are different, the reaction of a laminae to loading depends entirely on the load distribution. Hashin and Rotem (Reference 12) give a review of the load sharing between fibers and matrix. The relationship between shear (τ) and normal (σ) stresses, and the angle (θ) between load and fiber axes for the basic laminae is summarized in Equation 3.2. These laminae can be carefully stacked together to tailor the overall composite properties. This stacking results in what is termed a laminate. The stacking sequences are typically symmetric about the center of the laminate, which allows symmetry to exist in the distribution of load, and the composite reaction, thus avoiding warping under membrane loads or temperature changes.

$$\sigma_L = \sigma \ \cos^2\theta$$
$$\sigma_T = \sigma \ \sin^2\theta$$
$$\tau_{LT} = \sigma \ \sin\theta \ \cos\theta \tag{3.2}$$

σ: uniaxial stress in the 0° direction.

The mnemonic for the stacking sequence describes the relative direction of the fiber axis to the load for each ply (see Figure 6): a typical description of a laminate might be $[0/\pm45/90]_s$, where the s relates symmetry of the given

sequence about the central plane (mid-thickness) of the laminate. Figure 7 relates a carpet plot for the tensile modulus and strength of a laminate with various percents of laminae orientations [6]. For example, a $[0/\pm45/90]_s$ laminate would have 25% 0° plies, 50% ±45° plies, and 25% 90° plies. The modulus or strength could then be approximated by taking the intercept of the 0° and 45° percentages. As the laminate overall reaction also depends upon the interlaminar properties between plies in the thickness direction, any chart or graph can only predict approximate properties.

Static Strength of Composite Materials

The ultimate tensile strength (UTS) of a material is defined as the maximum short time stress above which the specimen can no longer carry load. The UTS of a composite not only depends on its constitutive elements, but also on their relative ability to provide strong interfacial bonds [13]. The actual stress to cause failure may be reached by: 1. an applied stress over a long period of time (static fatigue or creep), 2. an extreme loading in a short time, 3. a cyclic loading (cyclic fatigue), or 4. stress applied in conjunction with an attacking environment (environmental stress cracking). This section will discuss the first two modes of failure. The third will be covered in the next section. Environmental effects cannot be ruled out for wind turbine applications, but are not within the scope of this thesis.

Matrix Materials

Due to molecular vibration and wriggling, polymeric material deformation occurs mostly through relative movement between molecular chains. The ability of the material to deform depends entirely on the morphology and the degree of molecular motion (temperature relative to T_g). Time dependent phenomena in the absence of load cycling may be classified as either stress relaxation or creep. Two basic methods for inducing these phenomena are presented in Figure 8. Analytical models have been developed to represent such behavior: the Kelvin-Voigt and the Maxwell (fluid) elements (see Figure 9). Although most sources reiterate that these individual models do not represent actual polymeric system behavior, Malvern (Reference 14) reports that through the addition of multiple elements, actual creep (strain versus time at constant stress) data can be fit to a mathematical equation with a high degree of accuracy (see Figure 9).

It has been established that these behavioral patterns follow two principles [5]. As applied to polymeric creep, the Boltzmann superposition principle states that the effects of various stress levels applied at various times can be equated by the summation of the individual stresses and their corresponding time of application if the material is linear viscoelastic. The second is a time/temperature equivalence principle wherein the material responses at high and low temperatures can be equated on a single master curve through

time shifting, with shorter times corresponding to lower temperatures.

The effects of morphology on creep and relaxation have been detailed by Alfrey and Gurnee (Reference 5), who report two major morphological trends. First, for a constant chemical composition, if the molecular architecture is altered, only the long time creep response (and not the short time response) will be affected; classification of molecular weights and crosslink densities can establish relative responses of a given material. Second, for constant molecular architecture at a given temperature, chemical compositions with lower T_g's exhibit quicker short time response than those with higher T_g's [5].

The ultimate static strength of a polymer may be defined as the upper limit of a creep rupture (applied stress vs time) curve. Although the UTS may be reached by extremely rapid loading, the UTS values are dependent on the loading rate. Since load application on a time scale faster than molecular movement (thermal fluctuation) is impossible, the actual UTS can only be an interpretation of approximate values. Tests performed at faster loading rates give higher UTS values, while the slower loading rates result in lower, more creep affected values. The testing temperature should also reflect the usage temperature. Far below the T_g, the polymeric material exhibits a relatively high modulus and tensile strength with a correspondingly low elongation to failure [5].

The deformation tends to remain linear elastic up to brittle failure. As the temperature increases towards T_g, the modulus and strength are reduced while elongation to failure increases, and the material may even exhibit yielding prior to ductile failure. Molecular architecture plays a crucial role in the UTS limit: as the molecular weight, crosslink density, and/or percent of chain orientation in loading direction increases, so does the tensile strength [5].

Glass Fibers

Glass fibers exhibit a much higher resistance to creep than do organic matrix materials, but they do suffer a loss of strength with time under load. The mechanism of static fatigue, termed stress corrosion, is the propagation of minute surface flaws to a critical length [15]. This propagation may be further enhanced by chemical reactions with small amounts of water. Many sources reiterate that the reduction in tensile strength of E-glass under constant stress is three to five percent of the short time strength for each decade of time under load. (The term decade of time refers to a change of a factor of 10, best represented on a logarithmic scale.) Glasses of higher sodium content exhibit roughly a ten percent reduction from the ultimate tensile strength per decade of time under load [16]. Strong statistical distributions exist for strengths of fibers due to surface flaw size distributions. As fiber surfaces cool during the formation process, they develop micro-cracks. Further processing, such

as winding filaments into bundles, can aggravate micro-cracks or induce new ones. The resulting fiber strength then depends on the size of the worst flaw.

Glass Fiber Reinforced Composites

As previously discussed, the strength of glass fiber reinforced (GFR) composite materials depends primarily on the amount, type, and orientation of the glass reinforcement. The UTS of a 0° ply (fibers in the load direction) tends to primarily depend on the fiber strength and the V_f, whereas that of a 45° or 90° ply tends to depend more on the strength of the matrix and interface (see Figure 10).

The laminate UTS may be roughly calculated by multiplying the 0° ply UTS by the percent of 0° plies (see Figure 7) [13]. For a laminate which is comprised of uniaxial and off-axis plies, the static stress-strain curve may exhibit a knee or bend from which point the modulus is reduced. This knee represents the strain or stress level where matrix and/or interfacial damage within the off-axis ply redistributes the load to the uniaxial plies [17]. Due to distributions in the constituent material and interfacial strengths, and variations in fiber alignment, there will be a range of composite UTS, creep, and relaxation rates. Appendix B gives typical laminate theory calculations for the properties of composites of interest in this study.

Fatigue Strength of Composite Constituents

Material damage from cyclic loading is typically more severe than from static loading: a material which initially survives an applied static stress may catastrophically fail when the same stress is repeatedly applied. Furthermore, a material will usually fail from cyclic loading in much less time than from steady loading [18]. Glass fiber reinforced composites are no exception to this rule.

Material fatigue strength tests may typically be performed by the sinusoidal application of load. The number of loading cycles which is required to cause failure, N, is then typically reported on a load vs. cycles (S-N) curve (Whöler diagram) for the given ratio of minimum to maximum stress (R value). The ability of a composite material to withstand cyclic fatigue depends primarily on the fatigue resistance of the constituents, with some geometric complications.

Matrix Materials

A comparison of fatigue curves for various matrix materials is presented in Figure 11 [7]. Note that changes in composition not only affect the UTS, but also the trends (curve shapes) of the fatigue strength. When a fatigue curve flattens out horizontally a fatigue limit is reached: loading below this level will not induce fatigue degradation in the absence of other complicating factors. Fatigue damage and

eventual failure of a polymeric material may occur from the initiation and propagation of a single crack [19], or may develop from a complex array of multiple cracks [20,21]. The type of damage which develops depends on the type of material and the test method. In either case, typical crack growth has been classified in three stages: crack initiation, stable crack growth, and unstable crack growth.

Crack initiation usually develops at flaws by means of molecular chain reorientation, disentanglement, and scission (primary bond breakage) [21]. Browstow and Coneliussen (Reference 21) indicate that as much as 80% of the fatigue life may be spent initiating cracks. In other instances, particularly at high stresses, damage may develop on the first loading cycle.

Initially, crack propagation tends to be stable. As the crack tip passes through thermally softened or crazed material, gradual growth can typically occur on each cycle, or it may strike through an entire craze zone after a period of cycling. Generally, cyclic fatigue crack growth rates are a function of the crack tip stress intensity range or maximum value. Unstable crack growth occurs at the end of the fatigue life, when the size of the crack reaches the critical length for brittle fracture.

The most widely accepted relationship which correlates the stress level to the fatigue life of polymeric materials is the power law relation [17]

$$S/S_o = C*N^{-1/m} \qquad (3.3)$$

where S is the applied maximum stress, S_o is the UTS, C is a constant, N is the number of cycles to failure, and m is a power law exponent. If C is equal to 1.0, the S-N curve will pass through the static UTS at one cycle. Typical m values for thermoset materials lie in the range of 11 to 14 [17]. This observed behavior trend correlates with fatigue crack growth predictions generated using fracture mechanics. The Paris power law relates the crack propagation for each loading cycle (da/dN) to the stress intensity change at the crack tip (ΔK_I):

$$da/dN = A * (\Delta K_I)^m \qquad (3.4)$$

By relating this stress intensity factor to the applied stress (σ) through fracture mechanics, and performing the complex integration from crack initiation to failure, a power law relationship between cycles and stress develops.

$$N \propto S^{-m} \qquad (3.5)$$

Thus, both observations and the theoretical calculations support the use of a power law S-N trend for fatigue lifetimes dominated by matrix crack growth. If specimen lifetime is determined by fatigue crack growth, then the exponent, m, should be the same value in Equations 3.3 and 3.5.

As mentioned earlier, an increase in material temperature is typically indicative of cyclic fatigue damage [18,21]. As the specimen forms deformation zones and releases energy in the form of heat, the specimen temperature increases. When

the energy released per cycle matches the heat loss rate to the environment, an equilibrium temperature is reached. However, if the loading frequency is too high and/or the heat transfer conditions are poor, this equilibrium temperature may exceed T_g and cause a thermal softening failure. This condition is distinct from the mechanical failure which usually occurs under service conditions at lower stresses, and does not represent the actual fatigue resistance. Therefore, to provide accurate and comparable data, test reports should contain not only the maximum stress, strain, and R values, but the loading frequency and waveform, the ambient and internal temperatures, environmental effects, specimen geometry, and crack initiation and propagation times [18].

Even in well controlled tests, there typically exists a wide degree of scatter in fatigue data. This scatter band exists both in static and cyclic fatigue, and is the result of a complex fracture process [21]. Care should also be taken to avoid generalized assumptions. For example, one might expect a matrix with a higher UTS to exhibit a similarly higher resistance to cyclic fatigue, as compared to that of a weaker polymer. But as Figure 11 indicates, characteristics which endow a material with higher UTS do not necessarily endow that material with higher fatigue resistance.

Currently, no data is known to exist on the cyclic fatigue trends of unsaturated vinyl ester materials. Information of this type would be beneficial in determining

whether the matrix cyclic fatigue resistance shows trends towards an endurance limit.

Glass Fibers

There have been limited direct studies of the cyclic fatigue of glass fibers, with considerably more research into their static fatigue behavior. Mandell and coworkers (Reference 16) report results on single fiber, fiber bundle, and surface compressed macro fiber tests with and without an epoxy matrix. Their results indicate that surface compressed macrofibers experienced no fatigue, supporting the contention that fatigue is induced by the propagation of minute surface flaws. The single filaments with no surface compression experienced linear strength reduction loss of roughly three percent of the UTS per decade of cycles under load. (The term decade of cycles refers to a change of a factor of 10, best represented on a logarithmic scale.) Fiber bundles, however, experienced a decreased fatigue resistance: a linear reduction of about ten percent strength loss per decade, similar to their parent composite. The conclusion of the study was that glass fiber failure is most probably associated with the severity of surface damage to the fiber, which is well established for static fatigue. In bundles, this mechanism of failure is aggravated by contact between the filaments, causing greater surface damage and thus shorter lives.

Mandell and coworkers (Reference 13) report on tests of impregnated and unimpregnated strands of E-glass under cyclic

fatigue, with the results of 11.6% and 11.0%/decade S-N curve slope, respectively, similar to many full scale composites. Thus, the overall behavior of axially-loaded glass fiber bundles under tensile cyclic fatigue is expected to approximately follow the 10%/decade reduction rule for the medium to high stress range under loading conditions of R = 0 - 0.1 for which the tests were reported (R = minimum stress/ maximum stress per cycle). As few, if any, data are available for more than one million cycles, it is not known whether fatigue limits exist for single or multiple glass fibers.

Interfacial Properties

Fatigue damage within fiber reinforced composites typically initiates at the fiber-matrix interface [17]. The basic load distribution between fiber and matrix results in high interfacial stress, particularly under transverse loading. No direct fatigue tests of interfaces have been reported, but data have been reported [17] for the stress conditions when debonding initiates at the edges of composite specimens. These data trends are generally similar to the fatigue S-N trends of the matrix material [17].

Once initiated, however, interface damage will steadily propagate via further cycling [17]. The crack typically advances in a direction parallel to the fibers. Poor fiber-matrix bonding may result in increased crack growth rates, whereas increased interfacial bond strength generally increases fatigue crack propagation resistance [17].

Glass Fiber Reinforced Composites

The ability of a GFR composite to withstand cyclic fatigue depends on the amount and orientation of the constituents, the interlaminar fatigue resistance, and the overall mode of fatigue loading, as well as the fatigue resistance of the individual constituents.

The relative amount and orientation of the reinforcement to the loading direction are the primary factors which determine the mechanisms or modes of failure. The tensile fatigue failure of unidirectional GFR composites tends to exhibit (1) fiber dominated failure modes (modes requiring fiber failure) for axially loaded composites, and (2) matrix/ interface dominated failure modes for off-axis loaded composites or plies.

Glass fiber dominated composites fatigued under medium to high stress tend to follow the 10%/decade strength reduction trend regardless of fiber arrangement or content, matrix material or interface, and void or filler content (R=0-0.1) [13,20]. Thus, the tensile fatigue resistance for glass fiber dominated composites is similar in the longitudinal, transverse, and shear directions which enable a broad range of GFR composites to exhibit the same rate and mode of failure, but also makes it difficult to associate particular fracture modes with the trend of the data [13,20]. By way of comparison, carbon fiber composites are much more fatigue resistant in the longitudinal direction [17].

Typical composite failures are not due to propagation of a single crack [19]. The damage state of the composite is progressive, and careful monitoring of a composite structure could yield signs of deterioration prior to catastrophic failure. The same three stages of matrix cracking which were described earlier may also occur within an off-axis loaded composite, but the cracks now develop parallel to the fibers. The first stage $n/N = 0.0 - 0.02$ (n:cycles; N:cycles to fail) tends not to show any significant decrease in static strength, even with the initiation at high stresses of many cracks in the resin near the fibers which are off-axis from the load direction. The second stage $n/N = 0.02 - 0.5$ typically involves crack accumulation which now begins to cause a decrease in the composite residual strength. At this stage, the number of cracks tends to remain constant while the cracks propagate through the ply, up to any adjacent longitudinal fibers which will then carry the load directly. The third stage, $n/N = 0.5 - 1.0$ displays a relatively rapid reduction in residual ultimate strength until the fatigue life is reached (the specimen fails).

Although matrix toughening additives may increase the overall composite initial static strength, their contribution to long term fatigue resistance tends to be negligible: the fatigue trend curves converge around one million cycles [17].

Multidirectional ply laminates, such as $[0/\pm45/90]_s$, typically experience multiple types of damage. In addition to

those described above, interlaminar separation may occur. Reference 19 reports one instance where the R = 0.1 fatigue of a $[0/\pm45/90]_s$ GFR composite experiences such progressive damage. The 90° plies first develop matrix cracks parallel to the fibers, perpendicular to the load. Then, as the loading shifts about these discontinuities, cracks develop parallel to the fibers in the 45° plies. The matrix cracks in a 45° ply experience both opening displacement (Mode I) and sliding displacement (Mode II) [22]. As cracks coalesce in these plies, the interface of the 45° and 90° plies may delaminate. Increasing levels of damage force the 0° plies to carry more load, until they eventually fail.

The exceptions to fiber dominated modes of failure in GFR composites occur when a more severe fatigue mechanism operates [20]. Woven fabrics may exhibit an increase in fiber friction and wear at weave crossover points which delaminate at relatively low strains and cycles. Therefore, although typical properties may be expected, mechanisms which might accelerate the degradation process such as the influences of test procedures or material construction should not be overlooked.

As the mechanical properties of constituents of GFR composites tend to be sensitive to loading time, rates, and temperature, such testing parameters may also affect the fatigue behavior of the composite structure and thereby influence the interpretation of the data. Mandell and Meier

(Reference 23) provide data on the effects of load rate, time under load, and stress ratio (R) on relative fatigue strength. The results of their analysis were that: (1) the upper limit of a GFR composite S-N curve is established by the static fatigue strength of the material, (2) any test parameter which resulted in more time at maximum load on a per cycle basis in the high stress range decreased the lifetime, and (3) as the peak stress magnitude decreased (and the cycles to failure increased), the effects of (2) decreased; various frequency and wave form shapes produced fatigue curves which tended to converge at high cycles. From this latter observation, the conclusion was that long term fatigue was dependent primarily on the number of applied cycles.

The effects of frequency may also be an issue where thermal degradation of the matrix material might occur due to heat generation of high frequencies or stress levels. This problem tends to be more severe with glass fiber than with higher modulus reinforcement because the higher strain levels are damaging to the matrix. However, interestingly enough Hahn and Kim (Reference 19) report that thermal problems are not complicated by interruptions of a fatigue test: tests which were repeatedly stopped to allow the specimen to cool to room temperature, then restarted, showed that the test specimen temperatures fairly consistently regained their old values once the tests were restarted, and that the specimen lifetime still fell within the regular fatigue scatter bands.

When frequencies are below the range to produce thermal failures, little effect of frequency on cycles-to-failure is reported [17].

Another important issue is that since the static UTS is typically the data point placed at the one cycle failure position on an S-N curve, and that the value of the UTS depends somewhat on loading rate, the loading rate selected should correspond to that of the dynamic fatigue test [13].
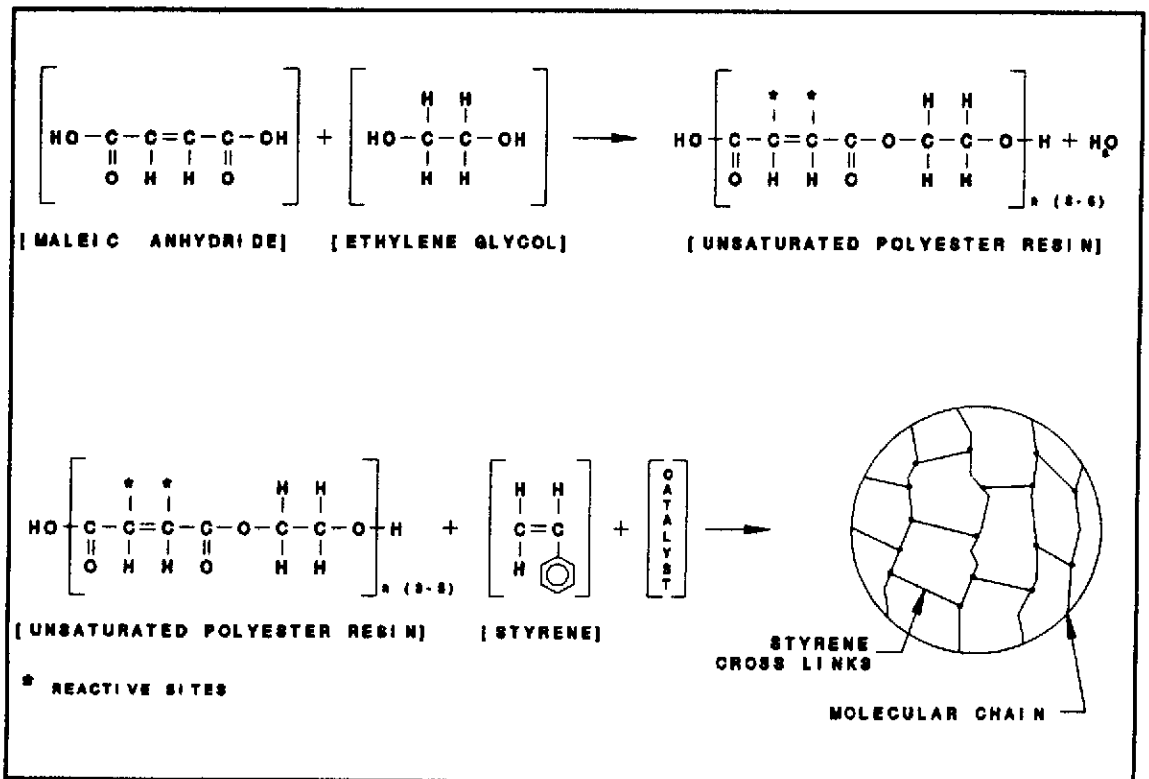
Figure 3. Unsaturated Polyester Thermoset, From Ref. 6.
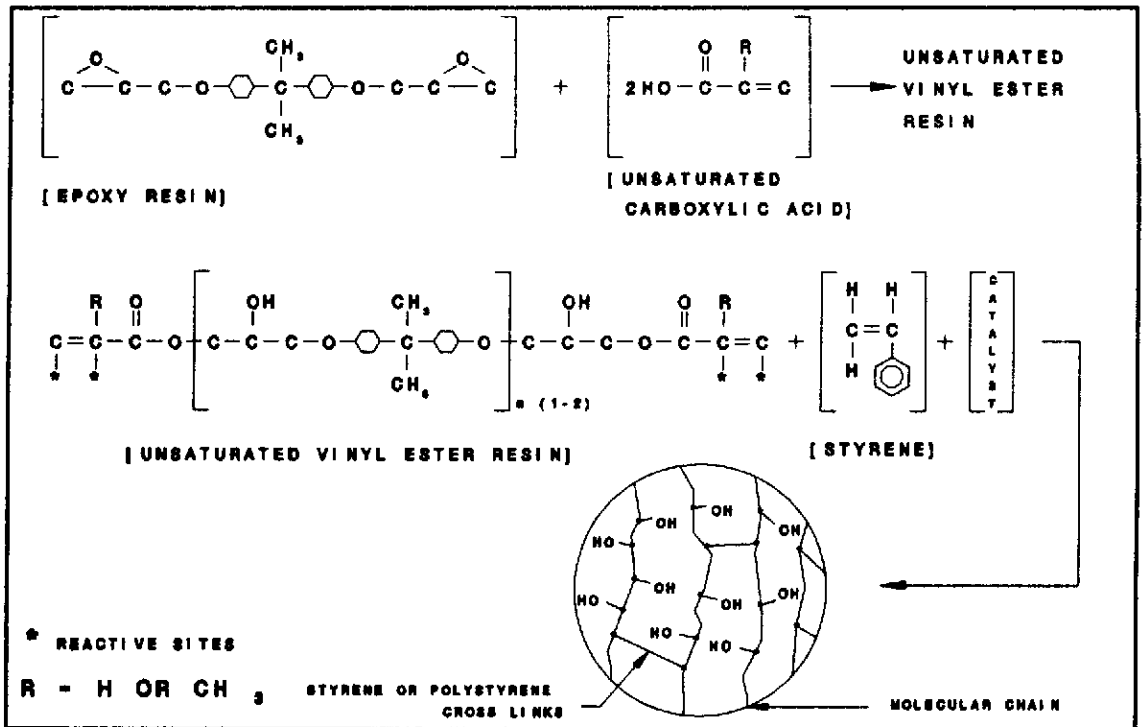
Figure 4. Unsaturated Vinyl Ester Thermoset, With Some H's Not Shown, From Ref. 6.
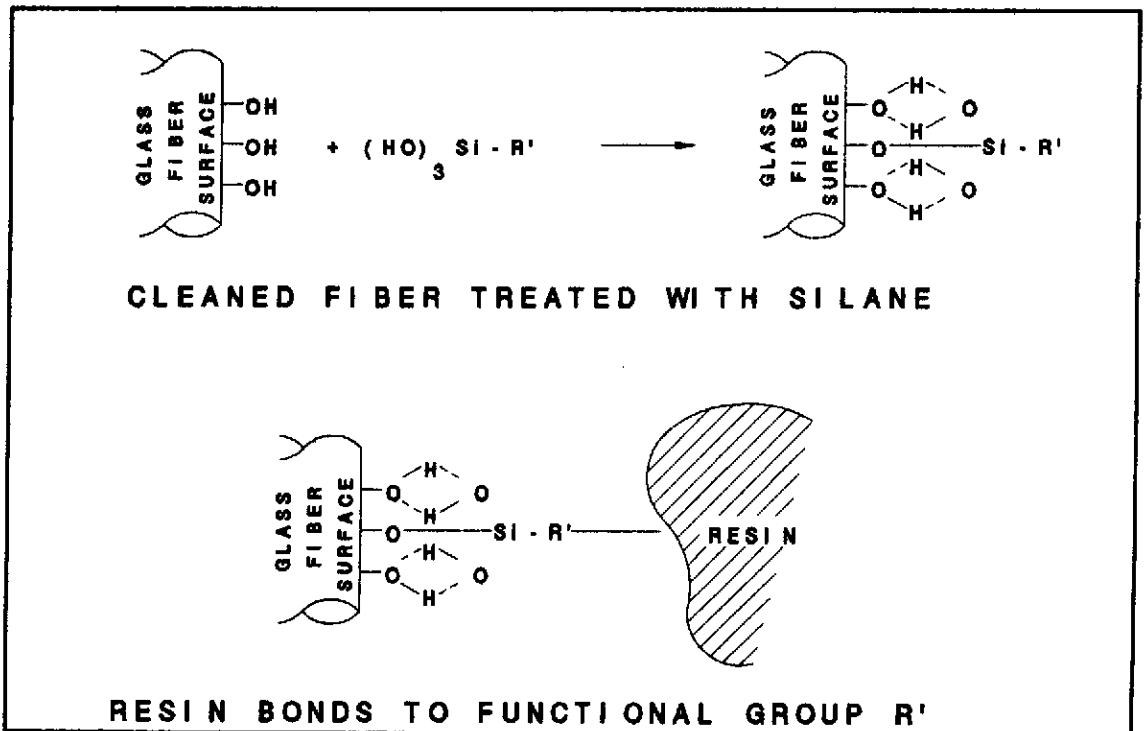
Figure 5. Interfacial Bonding Improved with Silanes, From Ref. 6.
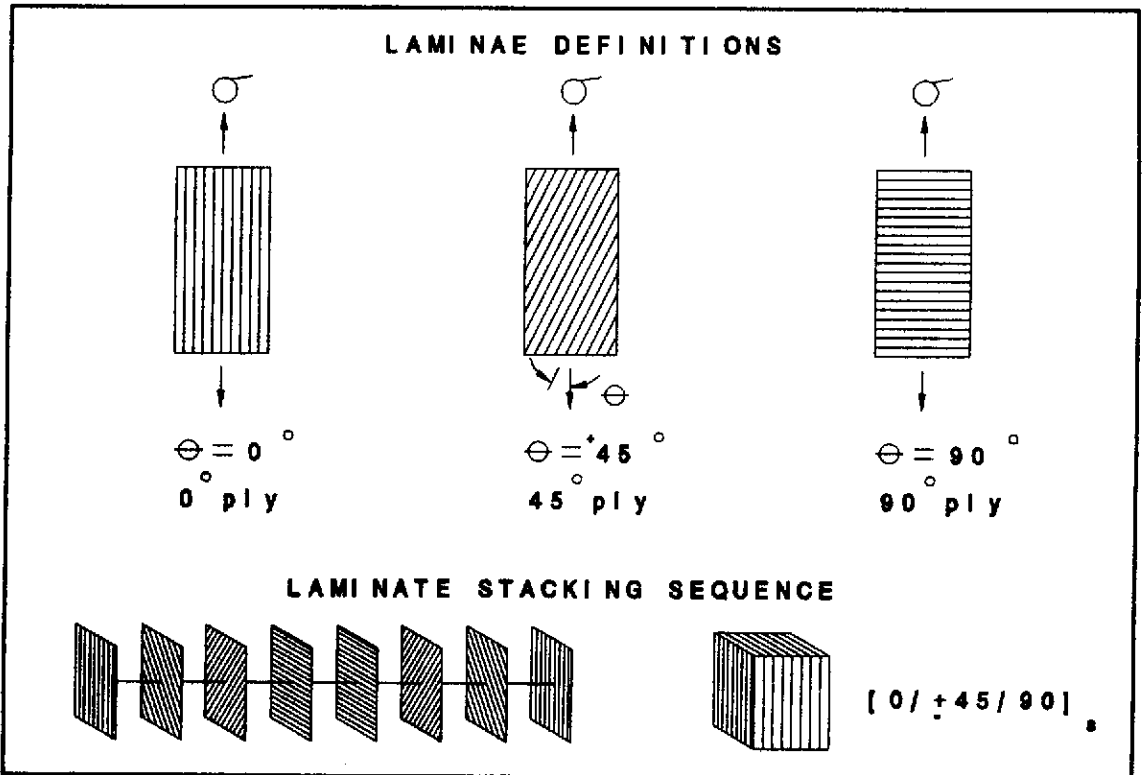
Figure 6. Laminae and Laminate descriptions.
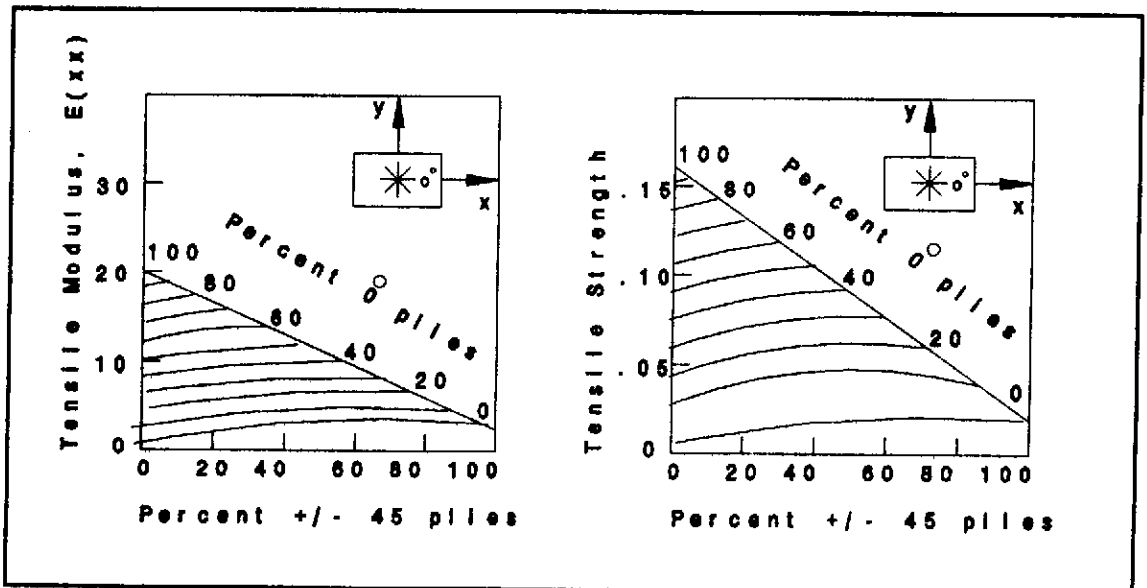
Figure 7. Design Charts For Carbon Fiber-Epoxy $[0/90/\pm45]_s$ Laminate, From Ref. 6.
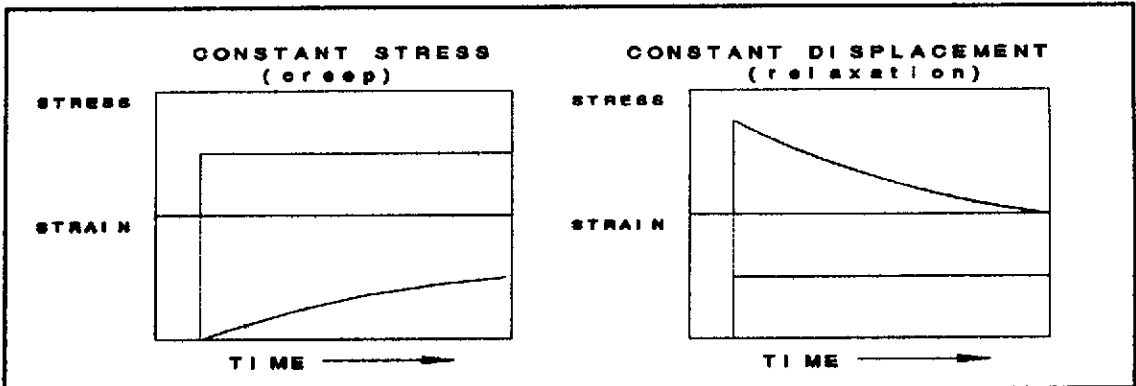
Figure 8. Response of Polymeric Material, From Ref. 10.
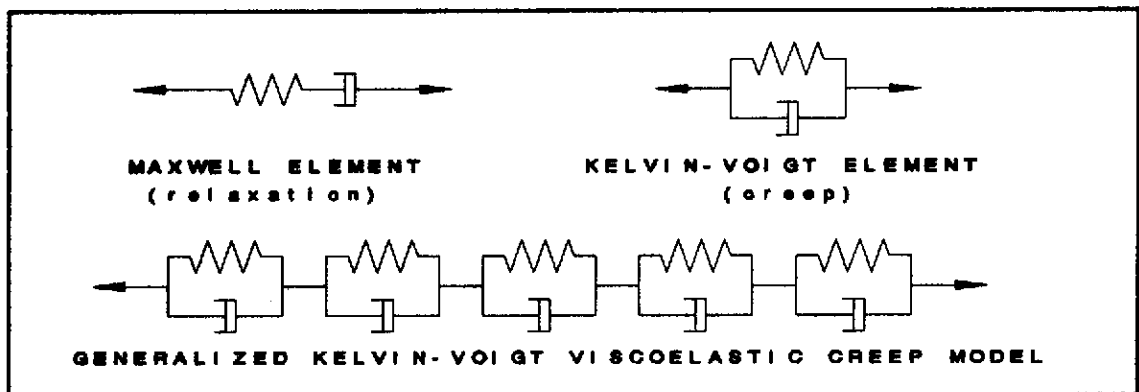
Figure 9. Modeling of Polymeric Responses, From Ref. 14.
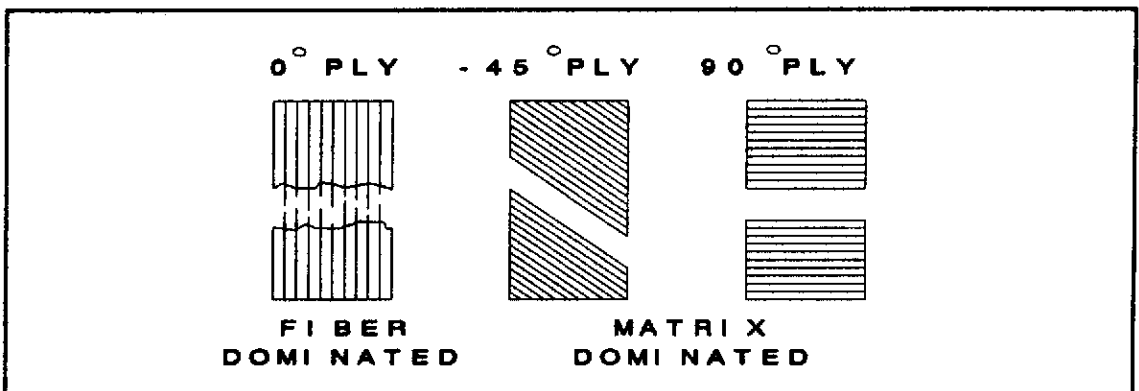
Figure 10. General Laminae Failure Trends.
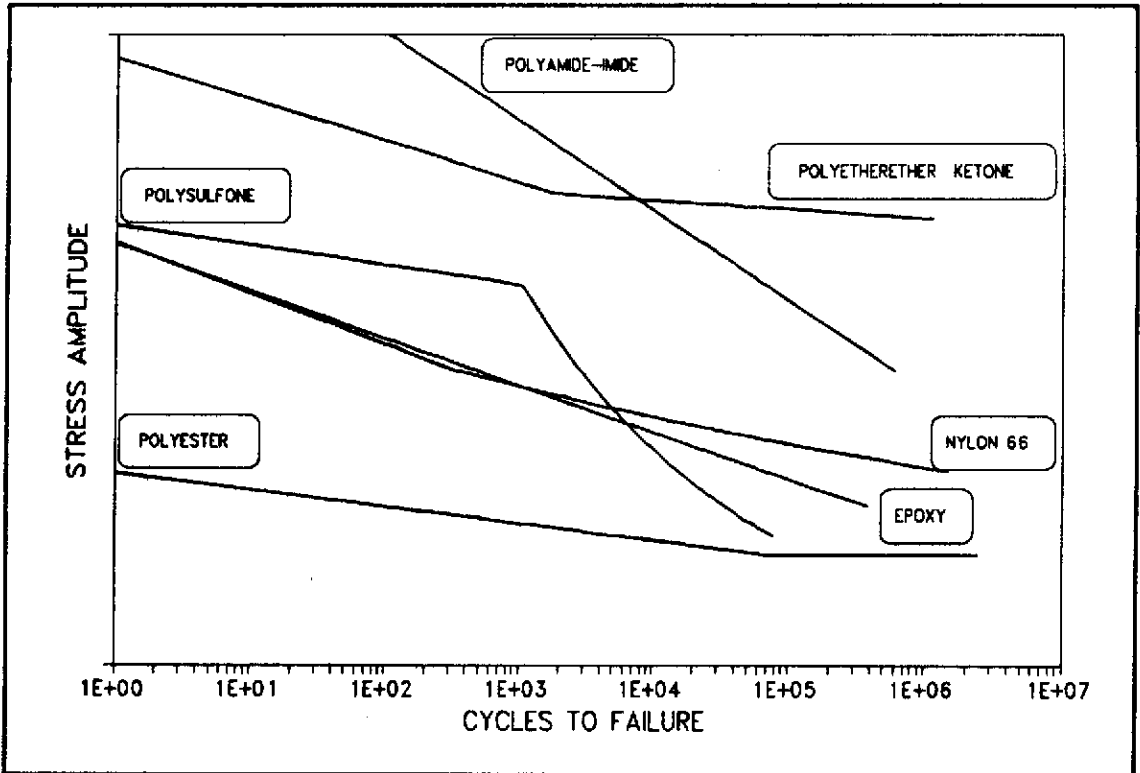
Figure 11. S-N curves for Polymeric Matrices (R=0.1, 1-10 hz.), After Ref. 9, 22.

CHAPTER FOUR

EQUIPMENT AND MATERIALS

Test Facility

A typical procedure used to evaluate the fatigue behavior of a material places a specimen of the material under a specific cyclic load condition for numerous cycles. Various machines have been developed for this type of testing, and are able to accurately maintain maximum and minimum peak loadings and wave forms while counting the number of applied cycles. The machine used for this research was a Material Testing System (MTS) 880 machine (see Appendix A and Figure 12). The specimens were clamped into the load train by hydraulic grips. An extensometer unit was attached to the specimen to measure local surface strain (change in length/ original length), while built-in force and displacement transducers measured applied load and overall piston deflection.

Materials

The test materials were supplied by wind turbine blade manufacturers in the form of cured composite sheets (24 inch x 24 inch x .125 inch). These materials are described below and summarized in Figure 13.

Material A is a 12 oz/yd^2 unidirectional E-glass reinforced polyester thermoset laminate. Each of the five reinforcement plies has a woven scrim to hold the fibers in alignment. As this material has been discontinued by the fabric supplier and is no longer used by the blade fabricator, specifications were not available for the fiber material. However, they have switched to a 10 oz/yd^2 fiber sheet, and the specifications provided for the new material state that for a 10 oz/yd^2 reinforcement in a general purpose orthopthalic polyester at 45% fiber by weight (room cured) the properties are 56.1 ± 2% ksi UTS with a modulus of 3.05 ± 0.1% msi at a crosshead speed of 0.0003 inches/second. The polyester manufacturer provided the following properties for their low exotherm isophthalic polyester thermoset: 0.68 msi modulus, 8.5 ksi UTS, and 1.10 gm/cm^3 specific gravity.

Material B was an unidirectional E-glass fiber reinforced vinylester composite. The glass reinforcement of Material B was identical to that of Material A, 100% 0° fibers. The matrix material was a bisphenol A unsaturated vinyl ester resin with additives designed for hand lay-up and room temperature cure. Matrix material specifications were given as 11 ksi UTS and .46 msi modulus.

Materials F and G were triaxial glass fiber reinforced polyester composites. The triaxial sheet is comprised of layers of unidirectional [0/±45] fibers with the layers tightly stitched together. Triaxial sheets thus exhibit a

better balance of properties in different directions as compared with pure unidirectional sheets. The triaxially reinforced composites of Materials F and G were designed to examine the behavior at ply terminations. Ply terminations allow the overall tapering of laminate thickness: in this case, six-ply laminates were reduced down to four plies via the termination of the center two plies (see Figure 13). Materials F and G had opposite layup orientations where the triaxial fiber reinforcement of the thicker section was $6[\pm 45/0]_s$ for Material F and $6[0/\pm 45]_s$ for Material G. For both F and G materials, the 0° fibers comprised 15.8 oz/yd^2 of the triaxial reinforcement sheet, while each 45° ply comprised 8.5 oz/yd^2 (± 45 totaled to 17.0 oz/yd^2). In terms of percentage, the triaxial sheets had 48% 0° and 52% ± 45° fiber reinforcement. The same unsaturated polyester matrix as in Material A was used here.

Materials H and J were also triaxial E-glass reinforced polyester materials, but were more structural in nature with more 0° material. Materials H and J were developed to study the damage effects on a composite joint as might be found in actual commercial construction. The joint was created in a 6 ply laminate by cutting the two center laminae along the width of the supplied sheets during fabrication (see Figure 13). This is also representative of a thickness tapering technique. The triaxial fiber arrangement was $6[\pm 45/0]_s$ for Material H and $6[0/\pm 45]_s$ for Material J. The same polyester resin as

used in Material A was used here. For both Materials H and J, the relative amount of 0° fibers was 21.88 oz/yd^2 as compared to 4.83 oz/yd^2 for each the +45° and -45° plies (±45 totaled 9.66 oz/yd^2). In terms of percentage, both of these materials had 69% 0° and 31% ±45° fiber reinforcement.

Material L was a unidirectional E-glass reinforced polyester composite. The reinforcement and layup technique allowed significant variations in the thickness. Material N was a [0/±45] triaxial reinforced polyester material which was tested both in the 0° direction and transversely, in the 90° direction.   Details of the polyester and triaxial reinforcement are not yet available.

Specimen Geometry

Test specimens were sectioned from the larger sheets of parent material. The original sheets were prepared by procedures representative of the fabrication methods and materials of the actual application. Standard specimen geometries allow comparison of test data from many different sources. The general geometries used for GFR composites consist of a long, thin, flat specimen with a uniform, symmetric cross section, termed a coupon (see Figure 14). The coupon usually has additional material bonded at the ends where it is clamped by the hydraulic grips. The special tab material in this area reduces stress concentrations which would otherwise induce premature failure. The guidelines for

the standard geometry are defined by the ASTM D 3039-76 standard test method for tensile properties of fiber-resin composites (see Figure 15).

Test Development

Excessive gripping pressure encouraged failure within the tab regions due to crushing. Hydraulic grip pressures of 1800 psi caused many transverse tab failures. Subsequently, settings of 600 psi were found to be adequate for low stresses, but allowed tab slippage at higher stresses. Finally, a grip pressure of 1200 psi was selected as adequate for subsequent tests. Details of the physical compressive pressure which is exerted on the tab face as a function of the hydraulic grip pressure are not entirely clear, and are currently being studied.

Initially, accepted standards set in ASTM D 3039-76 for coupon tab materials and geometries were followed. However, tabs made from the parent unidirectional material A easily cracked under the lowest grip pressure, which prevented transfer of a uniform distribution of stress to the gage section. Vector board, or electrical circuit board, was then tried. This type of board is thin enough to not require a tapered inboard edge for good stress transfer to the gage section. Additionally, the small perforated holes through the board allow a good mechanical bond with the adhesive. Although most subsequent tests utilized this configuration,

two other tab arrangements should be noted.

The hydraulic grip faces were found to chafe the vector board tabs during high cycle fatigue tests ($>10^7$ cycles). As this degradation of the outer tab surfaces might have become a problem, early efforts were made to investigate alternative approaches. Aluminum tabs with machined 15° tapered tips were used in conjunction with vector board and glass mat to provide protection. The 5 oz/yd^2 glass mat was soaked in Hysol EA9396 epoxy resin and applied over the specimen in the tab region. The vector board was then applied, followed by the aluminum tab. The effects of this configuration remain unclear as the few specimens tested have typically failed in the tab regions, even though tab chafing was not a problem. For simple initial static tests, the effort of preparing and bonding tabs may be avoided. By using double sided grit sand paper between the vector board tabs and the specimen shaft, the grip pressure can be used to prevent tab slippage. With all of the various tab configurations possible, a chart was designed for easier identification (see Figure 16).

A second area of concern was the location site for the extensometer. Depending upon the relative location of the extensometer to any damage zone, various strain readings would be observed. The calculation of the modulus would thus depend upon the local or far field strains. Thus, the extensometer was located primarily on the upper right side edge of the coupon with damage initiation referenced accordingly. Also,

specimen thicknesses have been noted to vary as much as 18%
for a given coupon. In such extreme cases, the specific cross
sectional area at the extensometer location was used in the
stress calculations. This procedure allowed a more accurate
analysis of the modulus behavior than would have been obtained
by using the average cross sectional area.
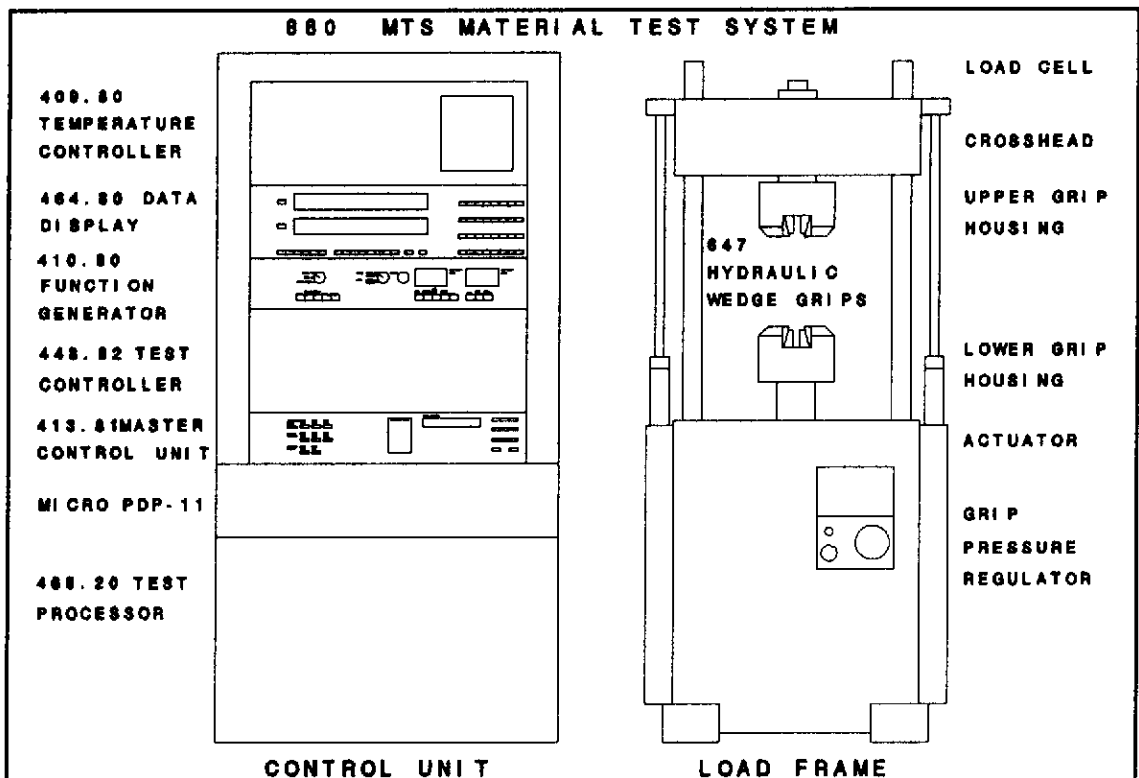
FIGURE 12. MTS TEST FACILITY
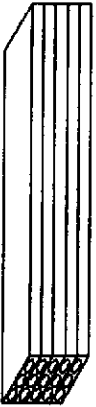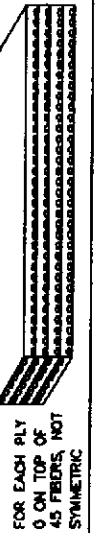
TEST MATERIAL	SUPPLIERS DESCRIPTION	DESCRIPTION OF GEOMETRY TESTED (LOADING DIRECTION)
A	12 oz. UNIDIRECTIONAL 488241, POLYESTER 63-AX-050 5 PLIES OF SCRIM ALIGNED FIBER SHEETS	
B	12 oz. UNIDIRECTIONAL D84-065, VINYLESTER 922-L-25 5 PLIES OF SCRIM ALIGNED FIBER SHEETS	
F	33oz/yd TRIAX: 15.8oz (48%) 0 FIBERS 8.5oz (26%)+45, 8.5oz (26%)-45 FIBERS. PE MATRIX. 6 PLIES REDUCED TO 4 VIA CENTERAL TWO PLIES BEING TERMINATED.	FOR EACH PLY 0 SIDE IN 45 SIDE OUT
G	33oz/yd TRIAX: 15.8oz (48%) 0 FIBERS 8.5oz (26%)+45, 8.5oz (26%)-45 FIBERS. PE MATRIX. 6 PLIES REDUCED TO 4 VIA CENTERAL TWO PLIES BEING TERMINATED.	FOR EACH PLY 0 SIDE OUT 45 SIDE IN
H	32oz/yd TRIAX: 21.9oz (70%) 0 FIBERS 4.8oz (15%)+45, 4.8oz (15%)-45 FIBERS. PE MATRIX. 6 PLY LAY UP WITH THE CENTERAL TWO PLIES DISCONTINUOUS.	FOR EACH PLY 0 SIDE IN 45 SIDE OUT
J	32oz/yd TRIAX: 21.9oz (70%) 0 FIBERS 4.8oz (15%)+45, 4.8oz (15%)-45 FIBERS. PE MATRIX. 6 PLY LAY UP WITH THE CENTERAL TWO PLIES DISCONTINUOUS.	FOR EACH PLY 0 SIDE OUT 45 SIDE IN
L	NON-WOVEN UNIAXIAL, .125" THICK POLYESTER RESIN	
N	TRIAXIAL (WEFT) 0.125" THICK POLYESTER RESIN	FOR EACH PLY 0 ON TOP OF 45 FIBERS, NOT SYMMETRIC

Figure 13. Test Material Chart.

48
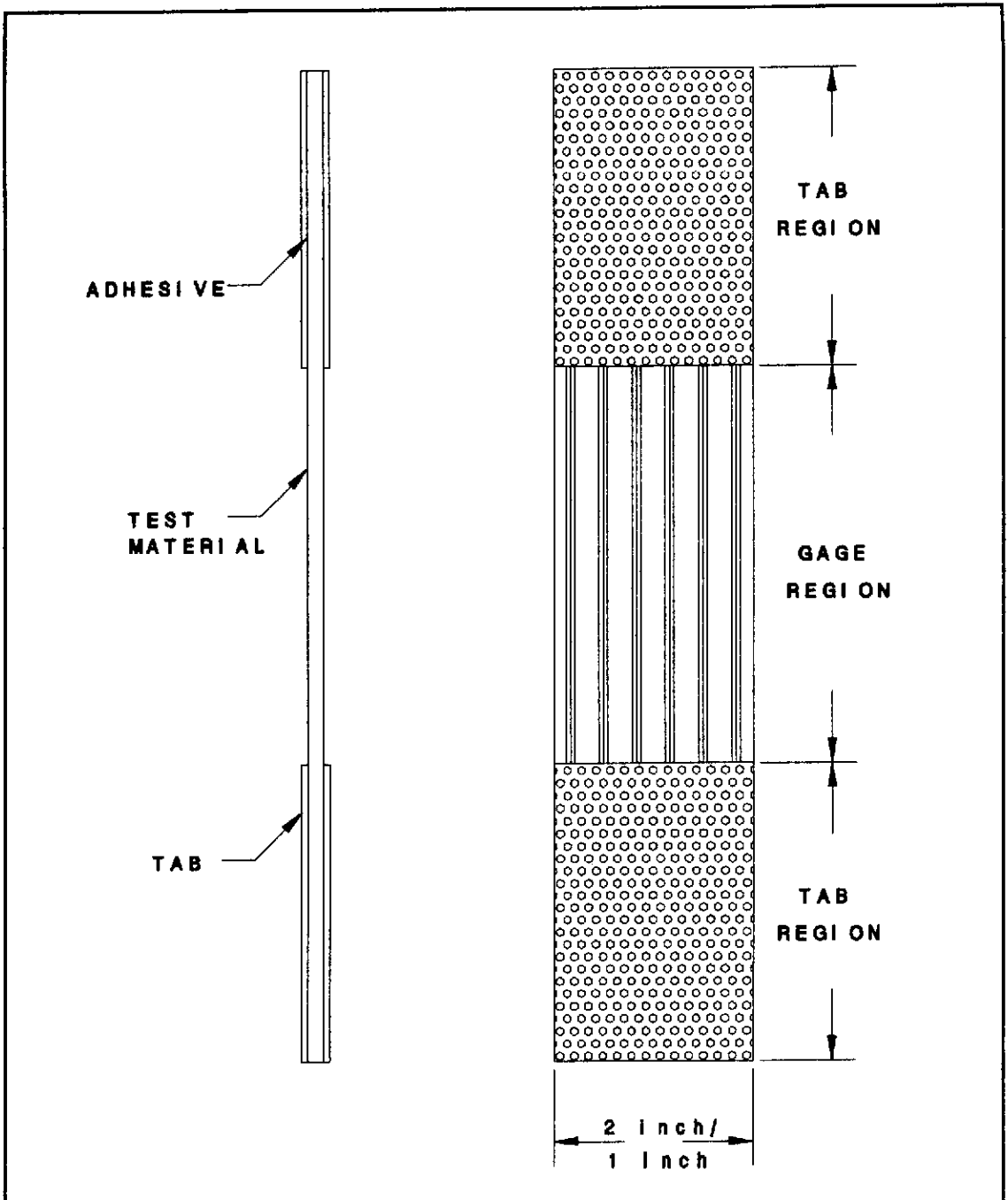
Figure 14. Coupon Geometry

49

Figure 15. Coupon Drawing Specifications of ASTM D 3039-76.
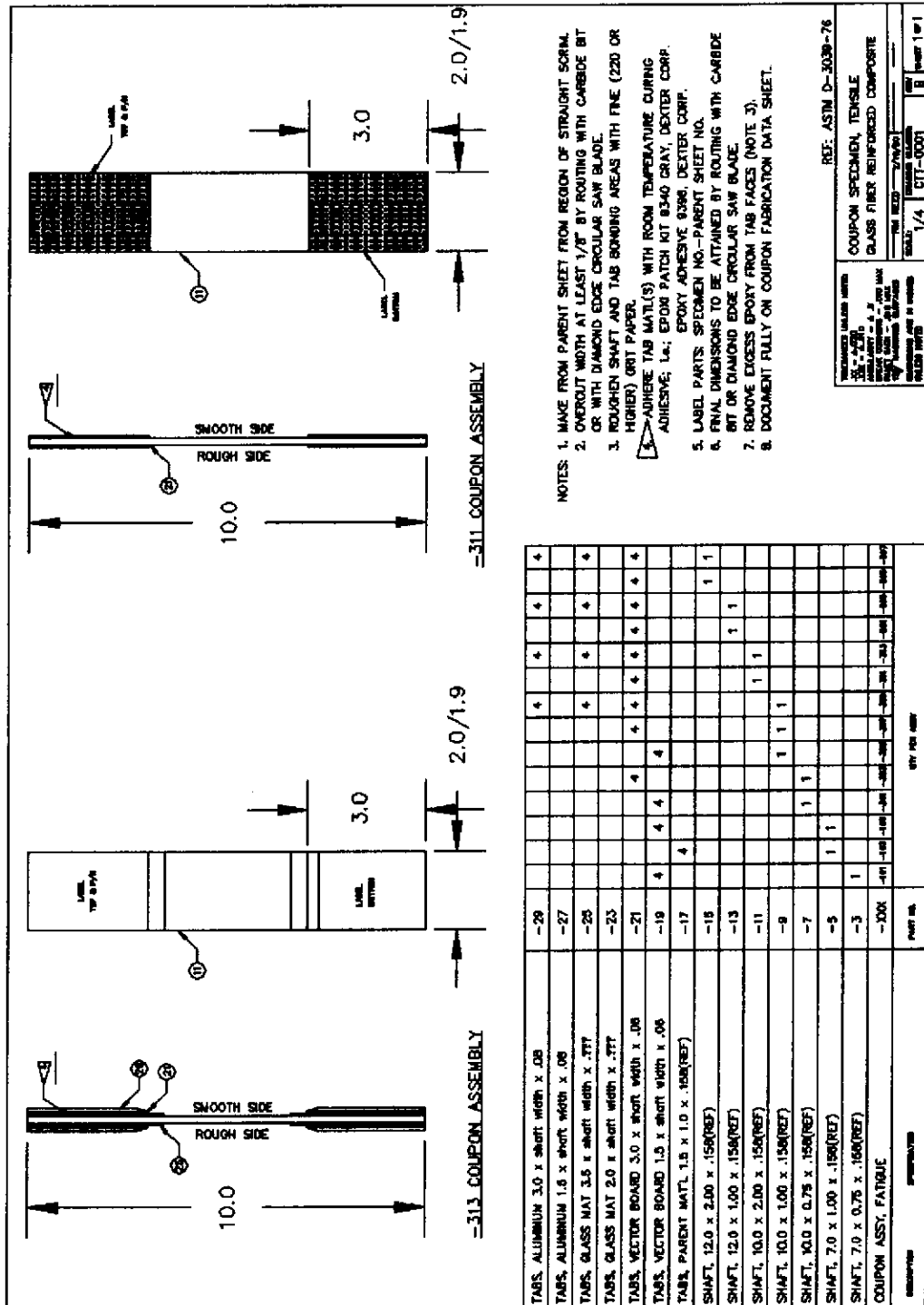
Figure 16. Modified Coupon Fabrication Specifications.

CHAPTER FIVE

RESULTS AND DISCUSSION

This chapter first presents the overall test results in summary, followed by a detailed description of test results for each material.

Overall Test Results

Table 1 lists the overall results obtained in this study for fatigue lifetime, static strength, failure mode, initial modulus, and initial elastic strain. The first column on the left gives the chronological test number (1 through 128) followed by the coupon identification number. As the first few tests were for procedure development only, they were not given test numbers. The maximum stress in the second column is either the static (single cycle ramp) ultimate tensile strength (indicated by both the * as the R value in column 3, and by 1 cycle in column 7), or else the maximum stress on each cycle, held constant during the test. The R value in column three is the ratio of the minimum to maximum stress on each cycle (cyclic tests only), again held constant during the duration of the fatigue test. All fatigue tests were operated under a sine-wave function with load control: the test frequency in hertz (cycles/second) is given in column four.

Initial values for elastic modulus and maximum strain on the first cycle are given in columns five and six. These were based on an initial loading prior to full scale cyclic loading, if initial cyclic data were not recorded. Column seven gives the total cycles to complete failure (separation into two pieces). One cycle indicates a static test which is operated at a constant displacement rate to failure at a speed given in the frequency column, but with units of inches/second as derived in Appendix A. The initial strain column for the static tests gives the total strain to failure. The eighth column contains the observed failure mode and location, as defined at the end of the table. The last column provides comments such as XX which, as explained at the bottom of the table, indicates data which are not used for analysis due to discrepancies or uncertainties in the testing process or in data gathering or reporting.

Table 1. Summary of Fatigue Test Results.

TEST & COUPON ID #	MAXIMUM STRESS psi	R VALUE	TEST FREQ. Hz.	ELASTIC MODULUS Msi	INITIAL STRAIN %	CYCLES TO FAIL	FAILURE LOC./ MODE	COMMENTS
. 102A	65790	*	0.0008	-----	----	1	RO	XX
. 102A	60150	*	0.0008	-----	----	1	UT S	XX
. 101A	61330	*	0.0008	-----	----	1	MG B	XX
. 103A	50330	*	0.0008	-----	----	1	MG B	XX
. 306B	49000	*	0.0008	-----	----	1	UG	XX
1 104A	26700	.5	----	-----	----	1400	LT J	XX
2 105A	18200	.1	10.0	-----	----	155000	RO	XX
3 106A	48300	.1	0.5	-----	----	210	LTSJ	XX
4 107A	41800	.1	1.0	-----	----	870	LTSJ	XX
5 105A	18200	.1	10.0	-----	----	2.0e6	LTSC	XX
6 108A	27600	.1	5.0	-----	----	590000	LTSC	XX
7 110A	48610	.1	0.5	-----	----	670	MG B	XX
8 101B	52300	.1	0.5	-----	----	1860	LTSJ	XX
9 103B	53600	.1	1.0	-----	----	2500	LTSJ	
10 104B	59200	.1	0.1	-----	----	40	LT S	XX
11 105B	61000	.1	0.1	-----	----	190	MG J	XX
12 108B	38700	.1	5.0	-----	----	9170	LTSC	
13 109B	47500	.1	5.0	-----	----	2640	LTSJ	
14 110B	51600	.1	0.1	-----	----	480	LTSJ	XX
15 111B	56130	.1	----	-----	----	7	LG B	
16 112B	37200	.1	5.0	2.92	1.29	38100	LT J	
17 113B	48100	.1	5.0	3.11	----	2840	LT J	
18 114B	53900	.1	1.0	2.83	----	400	LG J	
19 115B	57900	.1	0.1	2.66	----	180	LG J	XX
20 116B	46600	.1	5.0	2.79	1.6	3000	LTSJ	
21 107B	46500	.1	4.0	3.28	1.4	32600	LT C	
22 117B	33200	.1	10.0	-----	----	655100	LTSJ	
23 111A	40480	.1	5.0	2.90	1.4	17700	LT C	
24 118B	49700	.1	1.0	2.34	----	980	UT J	
25 112A	30800	.1	10.0	3.24	----	138600	LT C	
26 119B	82800	*	0.5	3.23	2.36	1	UG J	
27 123B	90200	*	0.5	3.11	2.73	1	GBJ	
28 124B	82800	*	0.5	3.07	2.76	1	UT J	
29 125B	84500	*	0.5	3.31	2.77	1	UG J	
30 121A	85670	*	0.5	3.25	2.83	1	MG B	
31 120A	82170	*	0.5	2.89	2.82	1	MG B	
32 119A	78945	*	0.5	2.96	2.64	1	MG B	
33 120B	33200	.1	10.0	3.08	-----	16150	LT C	
34 121B	34400	.1	5.0	2.78	-----	206800	UT C	
35 122B	33200	.1	10.0	3.35	-----	671300	ULTJ	
36 114A	27430	.1	10.0	3.04	-----	1.613e6	LTSC	
37 113A	27785	.1	10.0	3.28	-----	920100	LT J	
38 126B	27585	.1	10.0	3.01	0.90	2.31e6	UTSC	
39 129B	22290	.1	15.0	2.89	0.76	40.0e6	RO	
40 130B	27250	.1	10.0	3.27	0.79	7.48e6	LTSC	
41 105F	53700	*	0.5	2.58	-----	1	MGDB	
42 105G	57530	*	0.5	2.31	-----	1	MGDB	
43 106G	53095	*	0.5	2.38	3.51	1	MGDB	
44 106F	52600	*	0.5	2.12	3.55	1	MGDB	
45 108F	49130	*	----	2.78	-----	1	MGDB	

Table 1. - <u>Continued</u>

TEST & COUPON ID #	MAXIMUM STRESS psi	R VALUE	TEST FREQ. Hz.	ELASTIC MODULUS Msi	INITIAL STRAIN %	CYCLES TO FAIL	FAILURE LOC./ MODE	COMMENTS
46 108G	48180	*	1.0	----	----	1	MGDB	
47 109F	28225	.1	5.0	----	----	2690	MGDB	
48 107G	27550	.1	5.0	----	----	2630	LGDB	
49 101F	14830	.1	5.0	N/A	N/A	95100	LGDB	
50 101G	14900	.1	10.0	N/A	N/A	69000	LGDB	
51 104F	11250	.1	10.0	N/A	N/A	1.62e6	LG A	
52 102G	11155	.1	10.0	N/A	N/A	1.67e6	LG A	
53 103F	11250	.1	10.0	N/A	N/A	2.49e6	MG C	
54 109G	14970	.1	10.0	N/A	N/A	65370	LG C	
55 111F	14750	.1	10.0	N/A	N/A	108000	UG C	
56 135B	27130	.1	10.0	3.24	0.84	2.72e6	UT C	
57 133B	21985	.1	15.0	3.15	0.70	37.9e6	RO	
58 127B	89730	*	----	3.25	2.90	1	MG J	
59 101H	62218	*	----	3.74	3.24	1	MGDB	
60 102H	57680	*	----	2.72	----	1	MGDB	
61 137B	82330	*	----	2.95	----	1	MGB	
62 101J	63590	*	----	3.56	>3.23	1	MGDB	
63 102J	54235	*	----	3.44	----	1	MGDB	
64 138B	N/A	*	----	N/A	N/A	1	MGDB	
65 103J	N/A	*	----	N/A	N/A	1	MGDB	
66 138B	49700	.1	1.0	3.03	----	6085	UG J	
67 110G	11250	.1	10.0	2.58	0.43	11.2e6	LG J	
68 104J	25050	.1	5.0	3.45	0.77	17880	MGDB	
69 104H	25015	.1	5.0	3.65	0.68	45360	LG J	
70 105J	12500	.1	10.0	3.80	0.31	11.0e6	RO	
71 106H	70370	*	3000	3.56	>2.10	1	MGDB	
72 107H	85025	*	0.25	----	----	1	MGB	
73 108H	77120	*	0.25	----	----	1	MGB	
74 109H	86400	*	0.25	----	----	1	LT J	
75 110H	6440	*	0.25	----	----	1	LG C	TRANSVERSE
76 105H	12560	.1	10.0	4.13	0.30	10.0e6	RO	
77 101L	59480	.1	1.0	5.13	1.18	2580	UG B	
78 103L	58820	.1	1.0	4.48	1.32	590	UG B	
79 102L	40000	.1	5.0	4.57	0.87	59000	MG B	
80 104L	38550	.1	5.0	4.21	0.97	45800	UG B	
81 106J	10770	.1	15.0	3.28	0.26	18.0e6	RO	
82 107J	10910	.1	15.0	3.96	0.28	30.3e6	RO	
83 109L	47120	.1	10.0	5.00	0.91	153000	UT J	
84 127L	41500	.1	10.0	4.70	0.93	450000	RO	
85 111N	12410	*	0.25	N/A	N/A	1	UG C	TRANSVERSE
86 101N	7785	.1	1.0	1.25	1.34	6465	LG C	TRANSVERSE
87 102N	9800	.1	1.0	----	1.7	470	MG C	TRANSVERSE
88 104N	5000	.1	5.0	----	0.45	511000	UG C	TRANSVERSE
89 111H	12550	.1	15.0	3.40	0.43	20.5E6	MGDA	
90 112H	-----	--	----	3.52	----	------	WENT INTO COMPRESSION	
91 113H	30020	.1	1.0	3.85	0.73	16100	MGDB	
92 114H	21810	.1	10.0	3.48	0.60	69425	MGDA	
93 108J	18000	.1	----	3.35	0.54	-----	RO DELAMINATION TEST	
94 109J	27230	.1	----	3.27	0.82	-----	RO STATIC DELAMINATION	
95 115H	23590	.1	10.0	2.99	0.76	11400	MGDA	

Table 1. - <u>Continued</u>

TEST & COUPON ID #		MAXIMUM STRESS psi	R VALUE	TEST FREQ. Hz.	ELASTIC MODULUS Msi	INITIAL STRAIN %	CYCLES TO FAIL	FAILURE LOC./ MODE	COMMENTS
96	003N	3000	.1	15.0	3.35	0.28	34e6	RO	TRANSVERSE
97	037A	79500	*	0.25	3.19	----	1	MG B	
98	036A	84040	*	0.25	3.36	----	1	MG B	
99	128B	81150	*	0.25	2.88	----	1	MGJB	
100	131B	81085	*	0.25	3.54	----	1	MGJB	
101	017L	107260	*	0.25	4.47	----	1	MG B	
102	019L	108053	*	0.25	5.31	2.21	1	MG B	
103	011N	69850	*	0.25	3.03	2.97	1	MG B	
104	012N	67850	*	0.25	3.03	2.84	1	MG B	
105	013N	12600	*	0.25	1.00	3.82	1	UG B	TRANSVERSE
106	014N	13050	*	0.25	1.33	2.29	1	MG B	TRANSVERSE
107	104G	51070	*	0.25	2.85	----	1	MG B	
108	105G	51850	*	0.25	2.96	----	1	MG B	
109	111N	7785	.1	1.0	1.28	1.15	7950	UG B	TRANSVERSE
110	112N	9800	.1	1.0	----	1.42	710	UG B	TRANSVERSE
111	117N	56270	.1	1.0	2.47	2.74	20	UG B	
112	116N	40000	.1	1.0	----	1.60	620	UG B	
113	120N	40000	.1	5.0	2.51	1.70	810	LG B	
114	114N	5000	.1	15.0	1.19	0.42	1.63E6	LGCB	TRANSVERSE
115	118N	30000	.1	15-5	2.78	1.08	5680	MGJDB	
116	119N	30000	.1	5.0	2.85	1.05	4870	UGDB	
117	010N	20000	.1	10.0	2.92	0.69	25370	LG A	
118	009N	20000	.1	10.0	2.83	0.71	25780	LGCB	
119	129N	20000	.1	10.0	2.96	0.68	37595	UGJDB	
120	128N	20000	.1	10.0	2.78	0.72	29230	LGDB	
121	131N	15000	.1	15.0	2.67	0.56	231825	MG A	
122	130N	12500	.1	15.0	2.87	0.42	1.34E6	UG A	
123	006N	50000	.1	1.0	2.78	1.82	150	MG B	
124	126N	11000	.1	15.0	2.85	0.39	1.65E6	MGDB	
125	008N	10000	.1	15.0	2.89	0.34	7.83E6	MG A	
126	121N	15000	.1	15.0	2.75	0.54	166000	MGDB	
127	110J	15000	.1	15.0	3.51	0.42	1.46E6	MGDB	
128	127N	10000	.1	15.0	2.80	0.35	4.0E6	UGCB	

FAILURE LOCATION AND MODE DESCRIPTION MNEMONICS

RO - RUN OUT; NO FAILURE YET C - CLEAN TRANSVERSE FRACTURE
UG - UPPER GAGE LOCATION   J - JAGGED TRANSVERSE FRACTURE
MG - MID   GAGE LOCATION   S - DEBONDING OF TAB FROM COUPON SHAFT
LG - LOWER GAGE LOCATION   B - SEPARATION OF FIBERS/MATRIX INTO BROOM
UT - UPPER TAB REGION   LIKE APPEARANCE; USUALLY 2 HALVES
LT - LOWER TAB REGION   D - DEBONDING OF PLY LAYERS
                               A - STOPPED FEW CYCLES BEFORE FAILURE
* STATIC TEST ["TEST Hz." value replaced by "Ramp rate (inches/second)"
      INITIAL TEST STRAIN LEVEL replaced by STRAIN TO FAILURE]
   MAXIMUM STRESS VALUE FOLLOWED BY XX means data not acceptable:
      1.grip pressure induced failure(initial tests)
      2.test frequency too low (initial tests)

Specific Test Results

Material A

Material A is a unidirectionally reinforced polyester matrix system. The static characterization information shows material A with a fiber content of V_f = 0.3 (weight fraction, W_f = 0.49) and, a UTS of 82 ± 4% ksi (for a 0.20-0.25 inch/second ramp rate) and a modulus of 3.13 ± 7% msi. Figure 17 gives a static stress-strain curve to failure. The static tests induced a brooming type of a failure as shown in the 1-inch-wide specimen of Figure 18. Due to random splintering of the material, which will be discussed later, and the relative speed of data acquisition, the point at which the stress-strain curve becomes non-linear will vary slightly, as will the values of the UTS and strain to failure. The reported UTS values in Table 1 use a force taken from a peak readout which is more accurate.

Figure 19 presents the fatigue results for Material A on a traditional S-N curve. Only relatively low and moderate cycle data were obtained for this material. The fatigue data therein are compared with two trend lines. The linear trend follows the 10% static strength loss per decade of cycles anticipated for well aligned unidirectional glass fiber composites, as discussed in Chapter 3. The data fall slightly below this line. The nonlinear curve is fit to the data with a least squares routine to fit Equation 3.3. This Equation fit the data well with an exponent, m, of 12.5. The curve fit

procedure used for this and succeeding data sets presented in this chapter was to vary m in increments of 0.5 to obtain the best fit to the data. For the summary trends in Chapter 6, SIGMAPLOT, a computer software package was used to generate the best fit solutions. As noted in Chapter 3, a fit to Equation 3.3 implies a lifetime determined by a crack growth mechanism. The 0.63% initial strain, as indicated on the right side of Figure 19, is the value associated with a maximum stress of 20 ksi; similar strains are shown for comparison on following figures.

The origin of the trends for these and subsequent unidirectional data may lie in the detailed mode of damage in these materials. Inherent to many types of fiber reinforced composites are high matrix/interface stress areas around fiber ends, where the load is transferred into the surrounding matrix material. These matrix stress concentration sites may initiate matrix and/or interfacial damage. Material A and other unidirectional materials in this study showed significant fiber misalignment so that fibers were frequently cut at the machined edges. As the number of fibers which are cut along the edge of a composite structure may be extreme, fiber end edge effects may be of considerable concern. Such edge effects within a one or two inch wide coupon may lead to a failure mode which is not representative of the full scale structure.

Fatigue testing of unidirectional laminates does not

employ dumbbell shaped coupon geometries which are used in more homogeneous materials to encourage failure within the gage section. Tapering of a unidirectional reinforced coupon would merely create fiber-end edge-effects which would lead to more complex and premature (low stress) failures. As such, the unidirectional material is typically tested in a rectangular geometry. As this geometry does not include a reduced width gage section, fatigue failures in the tab regions cannot be prevented (see the 2- inch-wide specimen in Figure 18).

Due to the fabrication technique, poor fiber alignment existed within Material A; the fibers in the top surface and bottom surface plies did not lie in a straight line, but curved in a random, wavy pattern. Although the degree of this waviness varied throughout the entire sheet of material, the thickness of the sheet remained consistent. However, this fiber waviness created fiber-end edge-effects in a majority of the test coupons. This resulted in the majority of Material A coupon fatigue failures being dominated by edge splintering induced tab failures (discussed in Chapter 6). Tests designed with a wider gage section (1-inch-wide increased to 2- inch-wide) to reduce this problem did not succeed, and width had little effect on the results.

Although the typical unidirectional brooming failure mode was eventually achieved by the tab region material, the initial mode of damage at lower cycles was splintering. The splinters, in effectively reducing the cross-sectional area at

the tab region, increased the stress within the tab region. Thus, the actual final stress at the failure site was higher than the initially recorded (and plotted) stress. Although it may be possible to monitor the reduction of area for each cycle, and integrate the stress level over the lifetime of the coupon to achieve a more accurate effective stress, this has not been done here. Thus, the stress is the traditional engineering stress, based on the initial cross-sectional area. In a few tests, actual width measurements in the tab area prior to failure were recorded. These data indicate that the stress in the tab region is closer to the order predicted by the 10%/decade fiber dominated fatigue trend curve than is apparent in Figure 19. This will be discussed in Chapter 6.

The results in Figure 19 are fit well by the Paris power law, and the exponent is reasonable for crack growth parallel to the fibers due to edge splintering. As discussed later, it appears that the growth of cracks forming the splinters, as well as tab delaminations, dominate the lifetime of Material A. Thus, the data trend follows the prediction based on matrix dominated crack growth, even for this unidirectional material. This is contrary to findings for most fiber dominated composites, as discussed in Chapter 3. Whether cross-over of the two trend lines in Figure 19 would actually occur is uncertain at this time, and requires further testing.
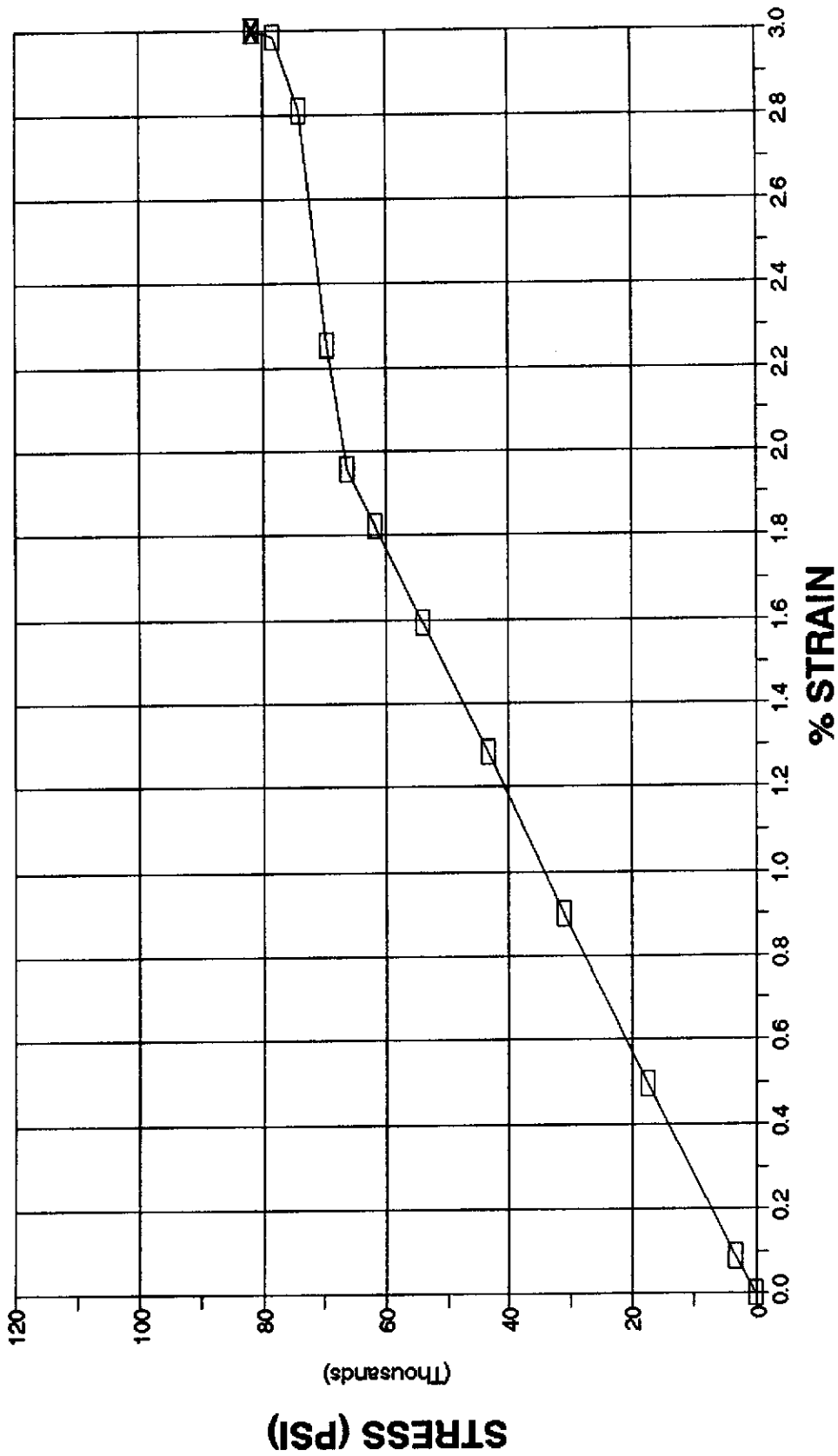
Figure 17. Stress-Strain Curve for Material A, Unidirectional E-Glass/Polyester, 4 inch Gage Length, 0.25 inch/sec Ramp Rate.
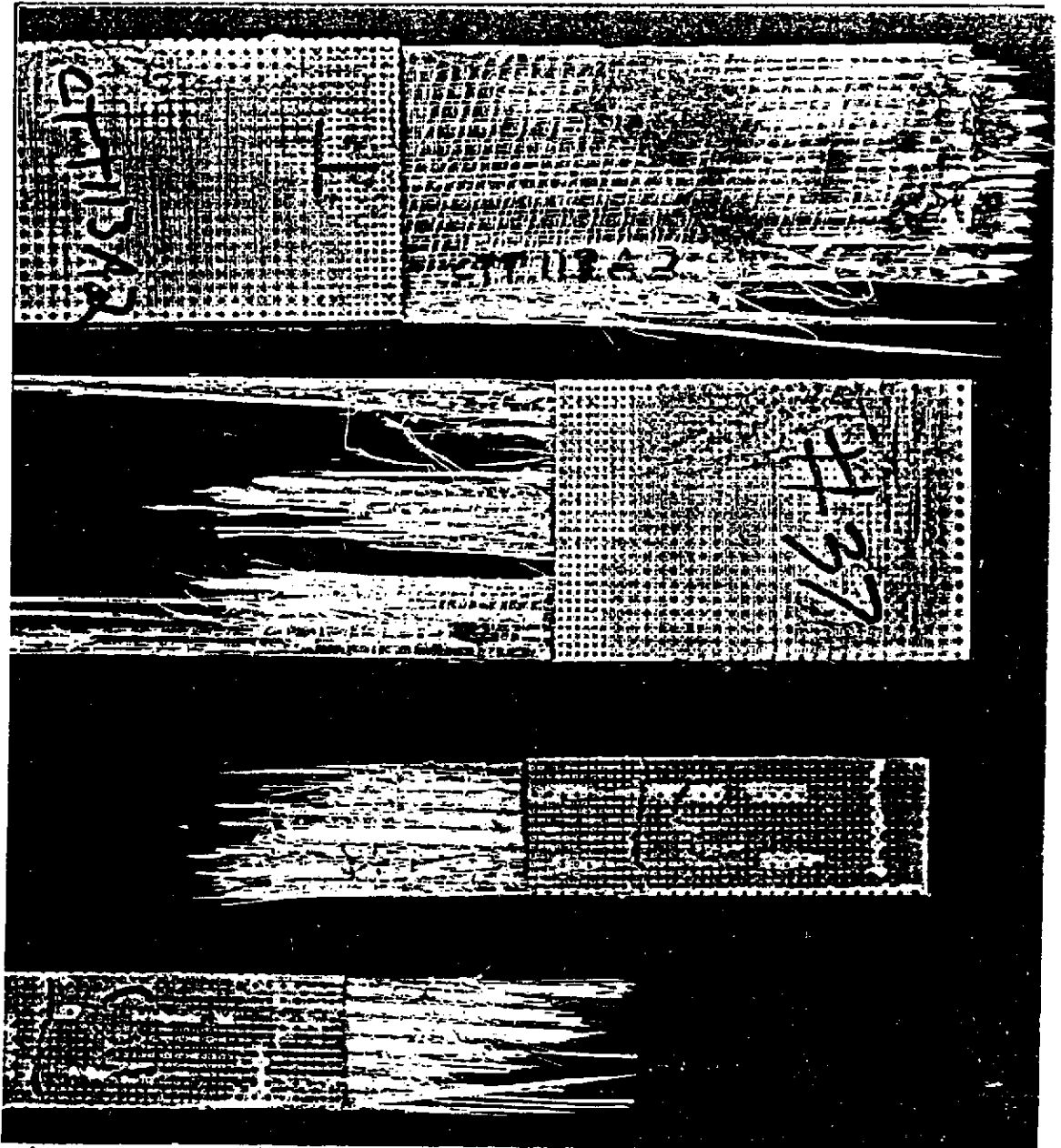
Figure 18. Typical Failure of Material A, 1 and 2 inch wide Test Specimens.
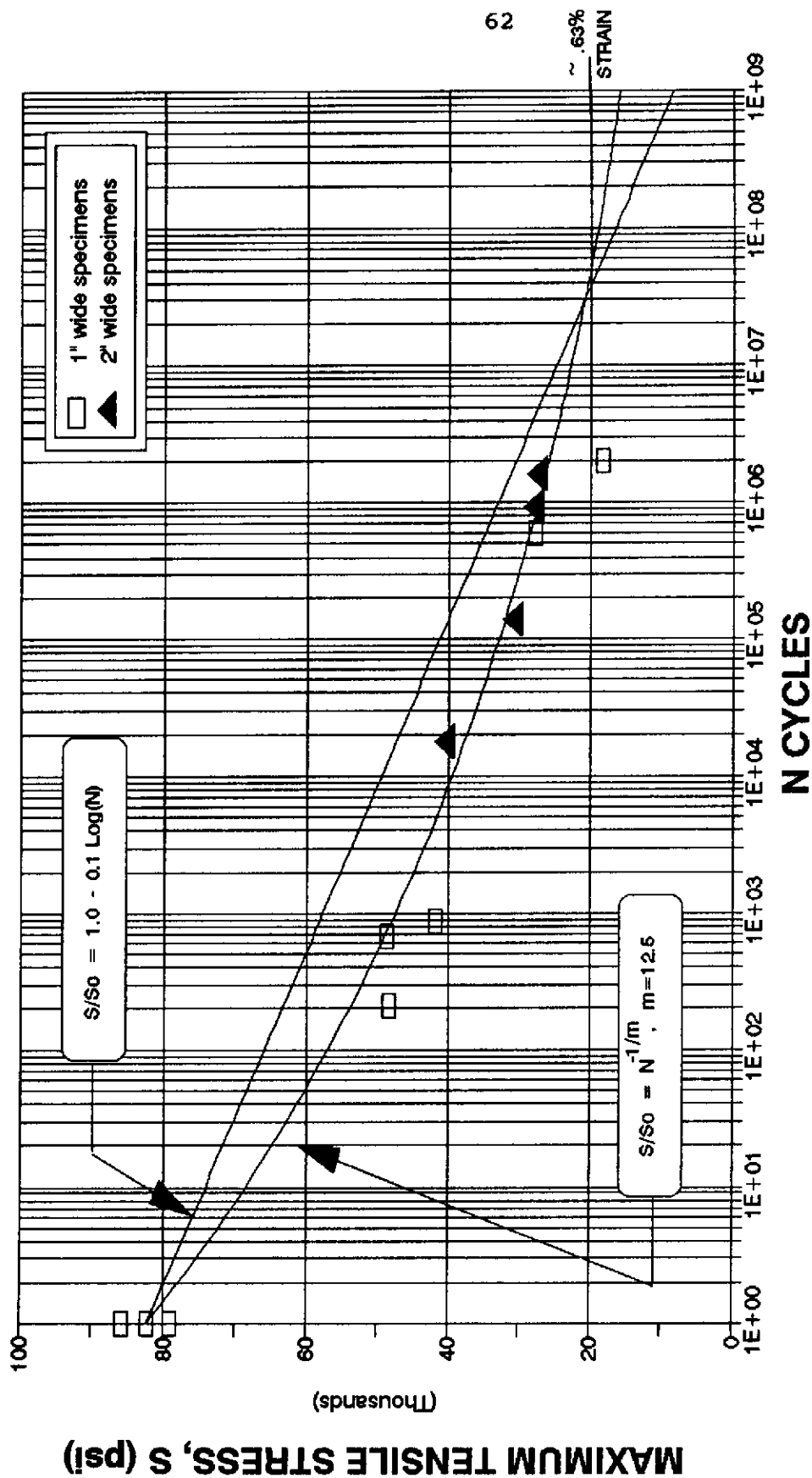
Figure 19. S-N Curve for Material A, Unidirectional E-Glass/Polyester, R = 0.1, 0.1 to 10 Hz.

Material B

Material B is also unidirectional with a fiber volume $V_f = 0.3$, but has a vinyl ester matrix. The UTS and modulus checks of Material B have average values of 86 ± 5% ksi for UTS, and 2.94 ± 20% msi for modulus. A stress-strain curve is shown in Figure 20. As the same fiber end edge effects noted for Material A also created tab problems here, only 19 of the 33 total tests performed on Material B resulted in gage failures (see Figure 21). As with Material A, the tab region which remained after splintering eventually failed in a typical brooming mode. Failures were then plotted at the initial stress levels, as was done for normal-failure data.

The fatigue curve of Figure 22 contains many more results than for Material A, with some tests reaching 40 million cycles. The data again fall slightly below the 10%/decade line, and are fit well with Equation 3.3 with a slightly higher value of m = 13.5. Again, the data fit agrees with the Paris law model, which suggests that the lifetime may be determined by the growth of the matrix/ interface dominated edge splits. The exponent difference from Material A is insignificant, and reflects a much greater data base for Material B. The longest tests of this study were stopped after 40 million cycles as no major damage was observed in the gage section; the fatigue levels were 22.3 ksi (0.76% initial strain) and 22 ksi (0.70% initial strain). Assuming that the scatter which would exist at the lower stress levels is

comparable to that of the higher stress levels, it remains unclear which trend the run out (undamaged) data follow, since the two trend lines cross in this range of stress.

One possibly important observation was noted after a comparison among various failed coupons of both Materials A and B. Areas of the initial translucent green color of the vinyl ester matrix remained between the white, cloudy damaged regions on the failed coupon. The failed coupons with the polyester matrix material, though, seemed entirely whitened: there typically remained no areas of the initial translucent yellow color. Thus, damage may be more widespread and uniform with the polyester matrix.

The tests of Material B resulted in more strain data with a higher percentage of accurate data (no splinter induced edge problems) than in Material A tests. These data were used to obtain a cyclic modulus value as a function of cycles. Figure 23 gives the normalized modulus as a function of n/N, cycles normalized by cycles to failure of that particular test. The minor reduction of elastic modulus due to fatigue, as presented in Figure 23, is representative of the expected stiffness decrease for an axially loaded, fiber dominated composite. Figure 24 shows the normalized change in overall specimen displacement (stroke) measured at the piston. This shows a more severe softening, probably associated with tab delamination and minor grip slippage. Figure 25 shows similar stroke data for Material A.

Although the stroke data show less scatter and seem to follow the modulus trend shape based on extensometer strain fairly well, the change is still greater than expected, with stiffness reduction values around 20% to 30%. For a given test, the difference between these two methods of analysis can be extreme. When lacking the proper initial data (when the operator fails to record the initial strain or stroke values during the first few dynamic loading cycles), the analysis must be based on a linear extrapolation of the measured data. Such incomplete tests require the normalization using a calculated initial strain and stroke. The calculated strain and stroke may cause the trend data to shift slightly higher or lower than they might normally (see Figure 24). Also, depending upon the extensometer location (extensometer is located above, below, or straddles a damage zone), various strain outputs would be recorded for a given overall displacement (see Figure 23). Thus, the strain based modulus curve (E/Eo) could be interpreted as a local modulus reduction, whereas the stroke based modulus reduction (Do/D) could be examined as an overall specimen stiffness reduction including grip effects, which were sometimes obvious (minor tab delamination will cause the displacement to increase because the effective length of the specimen increases, while the strain measured by the extensometer remains unaffected).
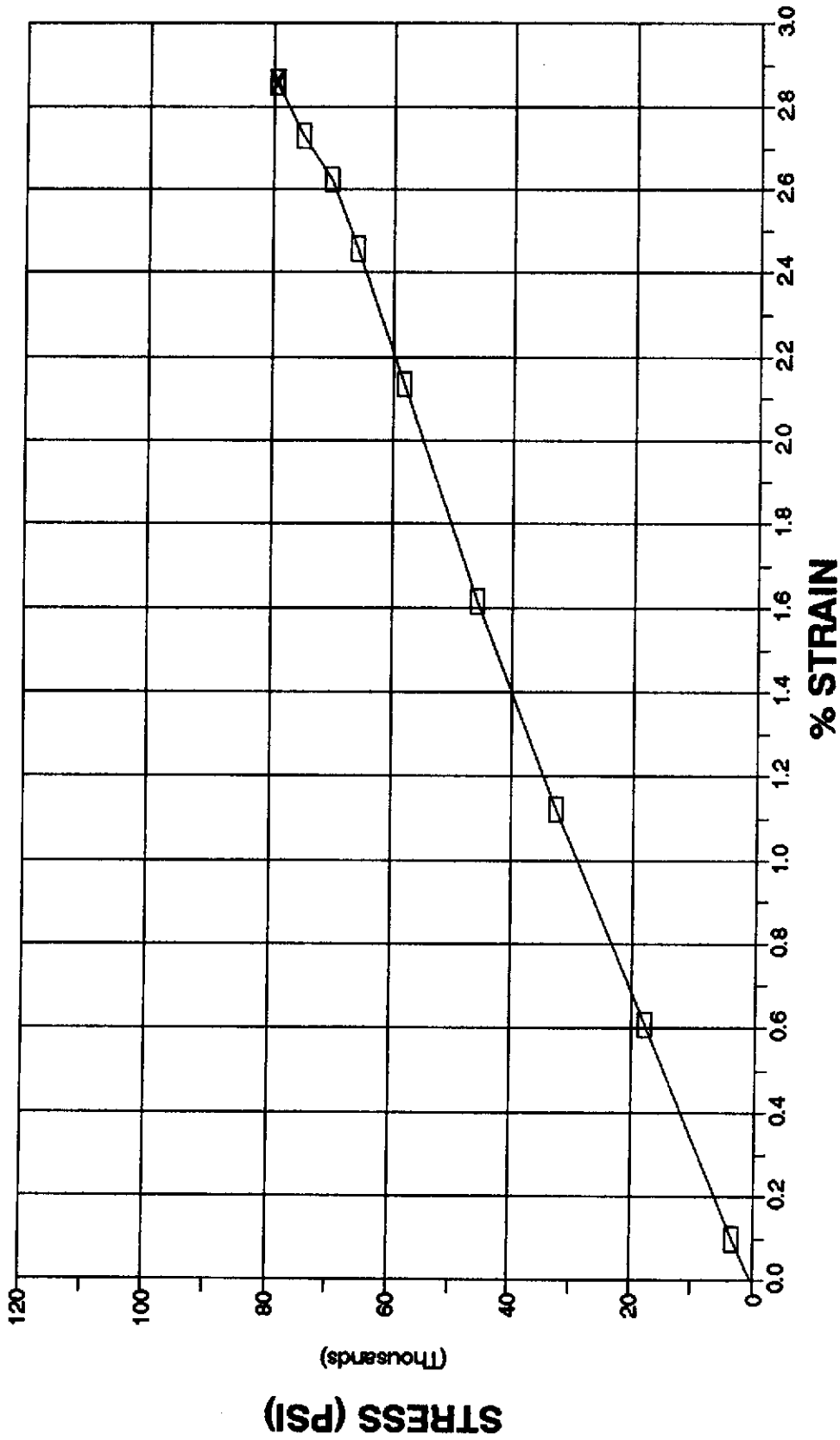
Figure 20. Stress-Strain Curve for Material B, Unidirectional E-Glass/
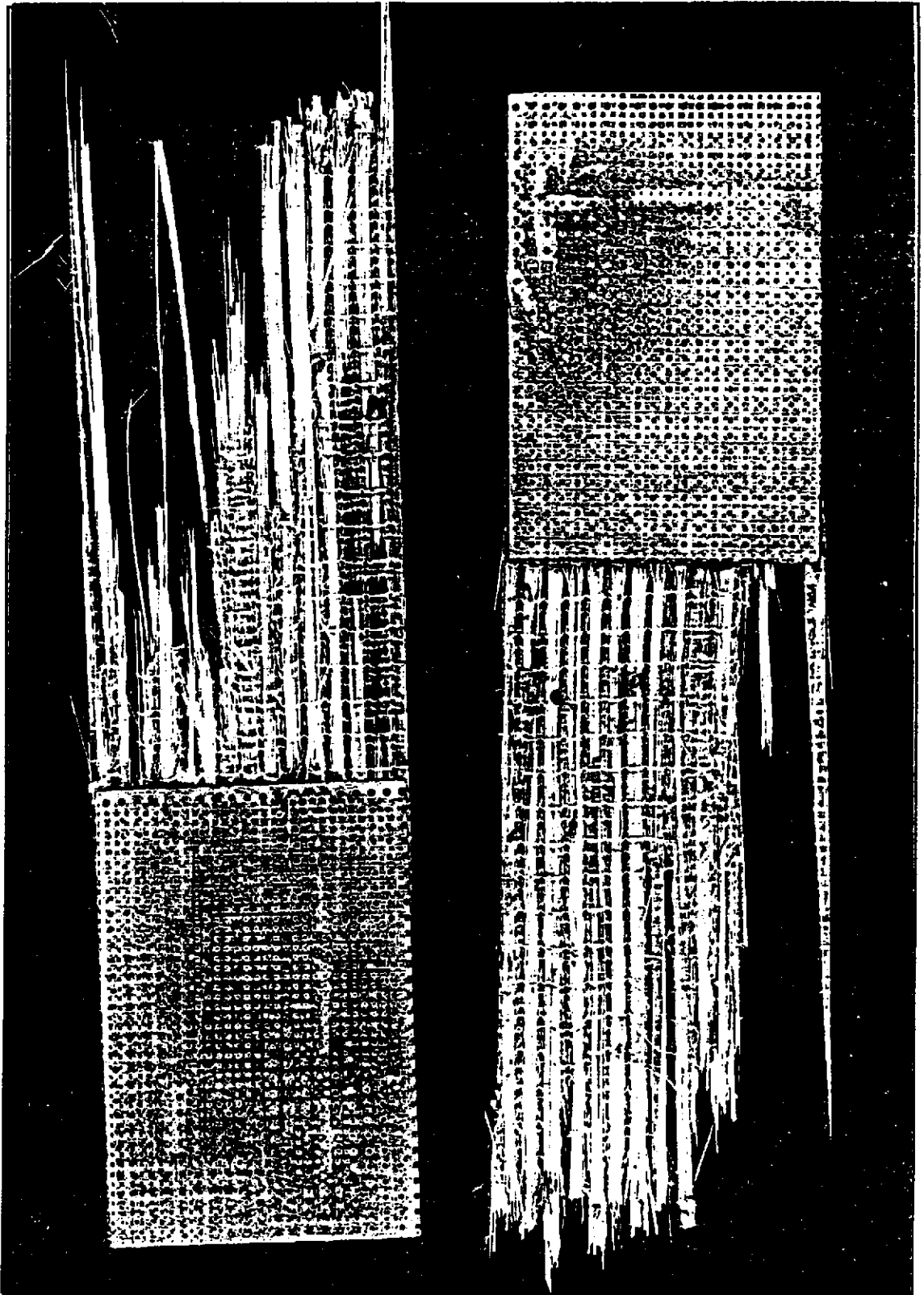Vinyl Ester, 4 inch Gage Length, 0.25 inch/sec Ramp Rate.

Figure 21. Typical Tab Failure of Material B Specimens.
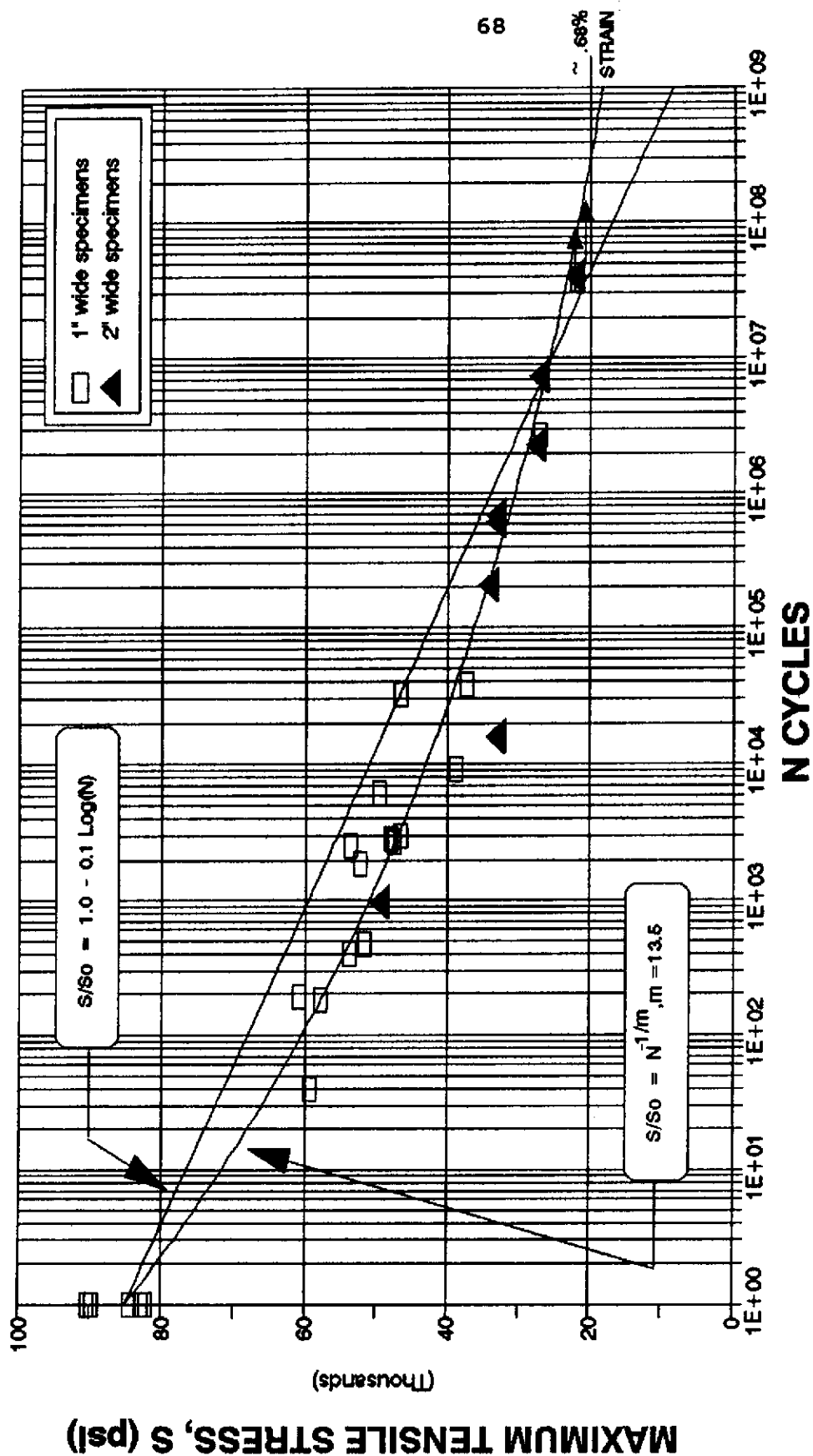
Figure 22. S-N Curve for Material B, Unidirectional E-Glass/Vinyl Ester,
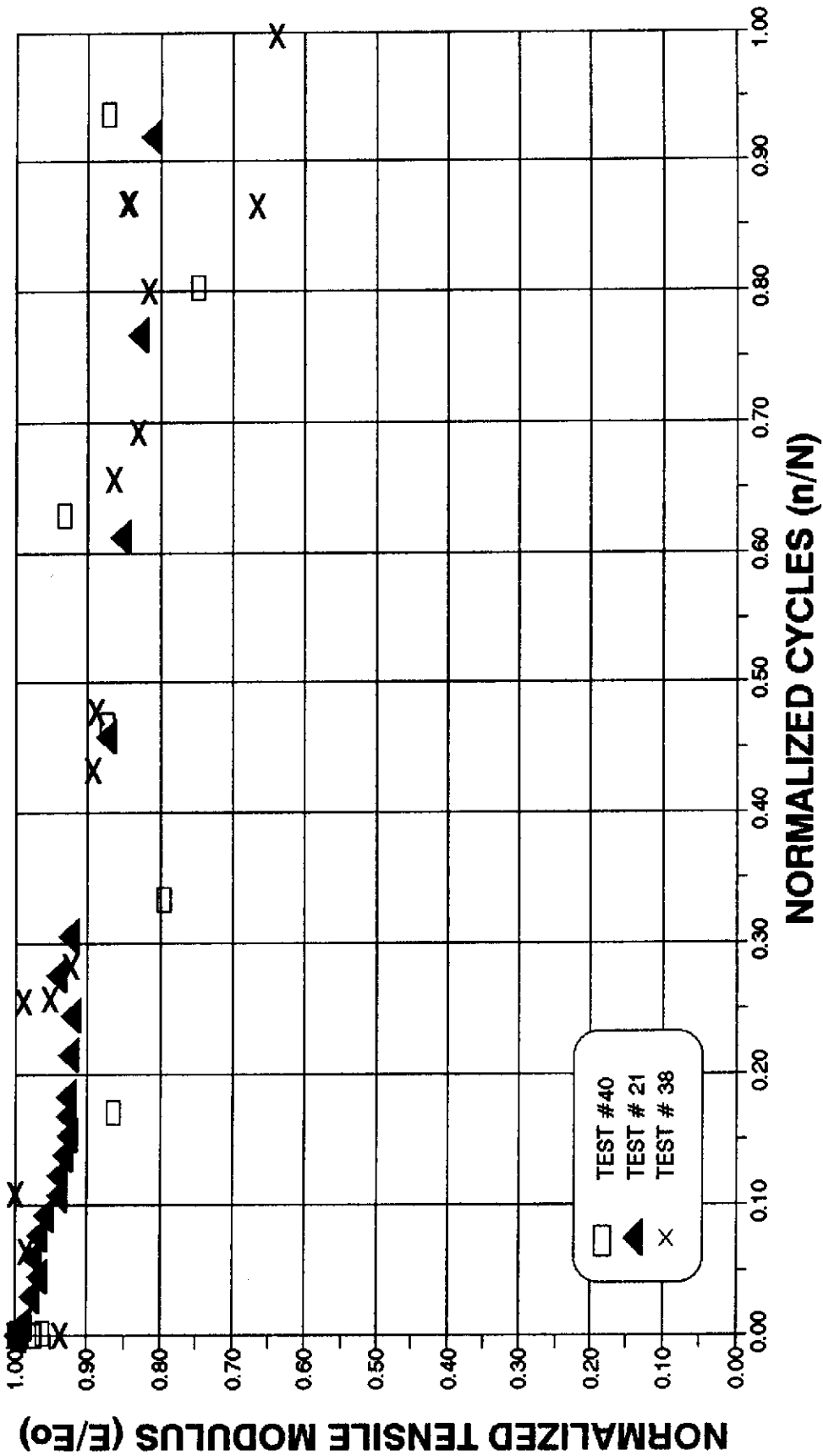R = 0.1, 0.5 to 15 Hz.

Figure 23. Elastic Modulus Trend for Material B, Unidirectional E-Glass/
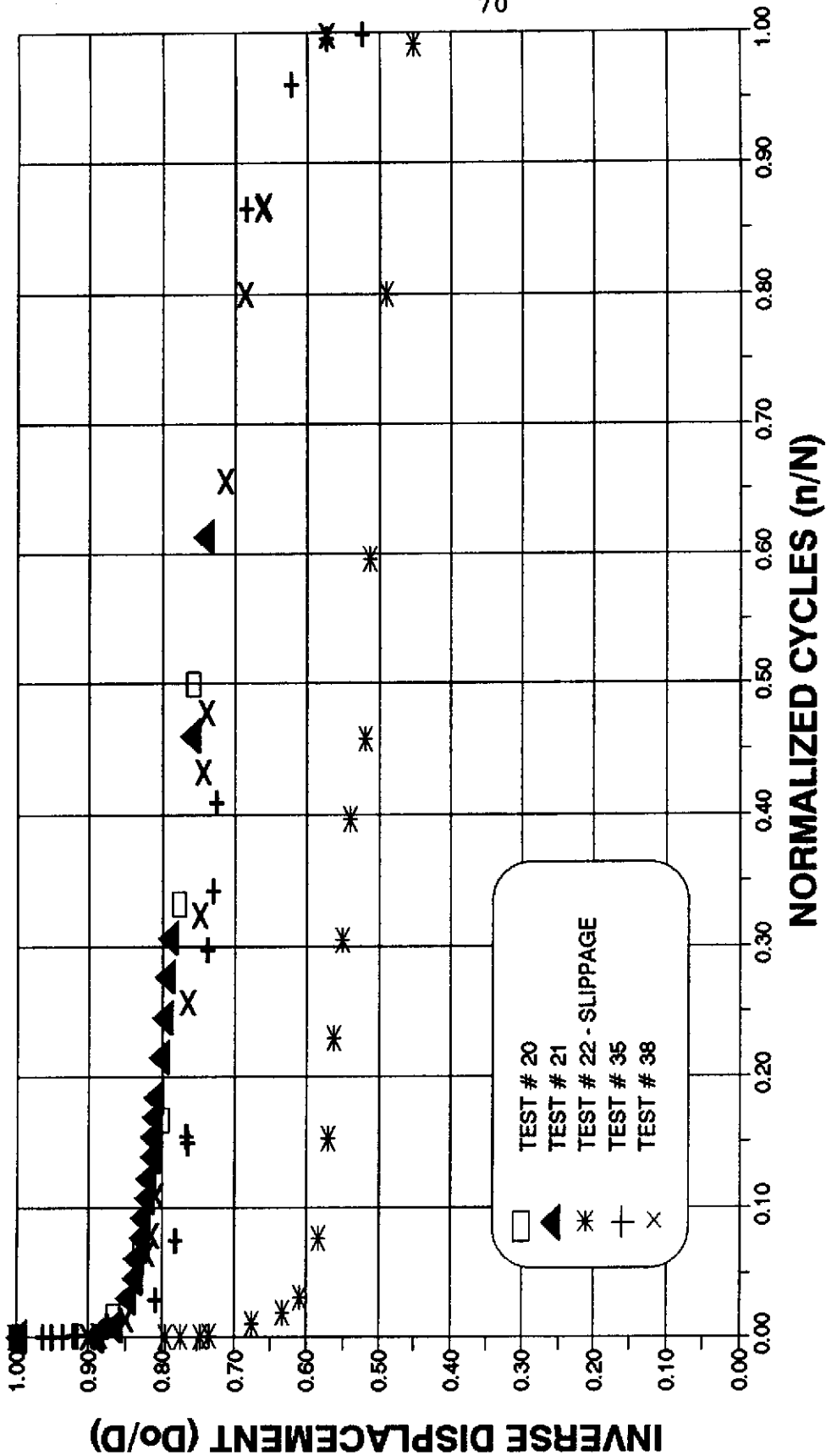Vinyl Ester, R = 0.1, 4 to 10 Hz.

Figure 24. Normalized Inverse Displacement Trend for Material B, Unidirectional E-Glass/Vinyl Ester, R = 0.1, 4 to 10 Hz.
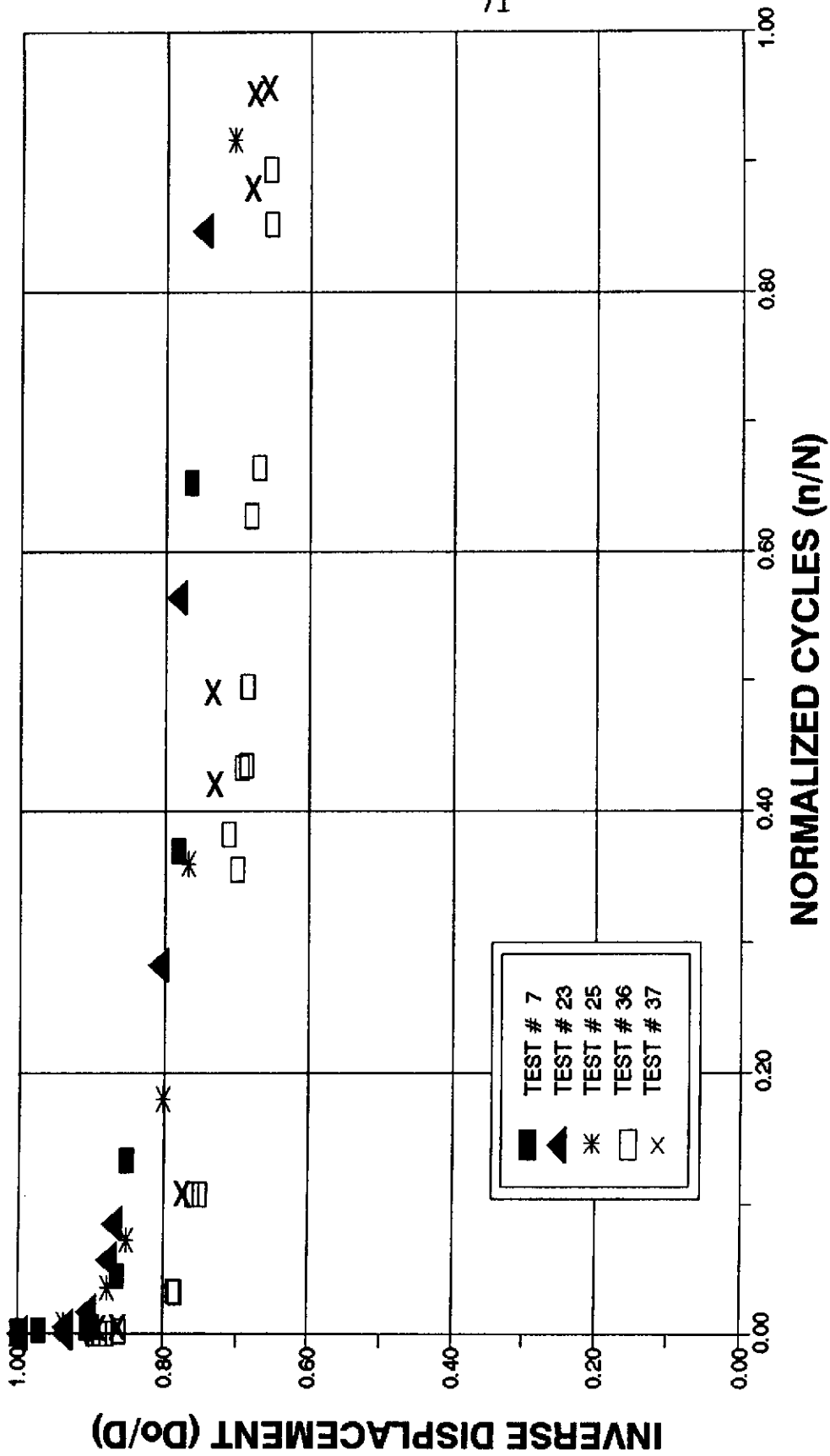
Figure 25. Normalized Inverse Displacement Trend for Material A, Unidirectional E-Glass/Polyester, R = 0.1, 0.5 to 10 Hz.

Materials F and G

Materials F and G are [0/±45] triax reinforced
polyester. They have exhibited UTS values in the 4 ply
section of 54 ± 6% ksi with a modulus of 2.54 ± 17% msi. A
preliminary stress-strain curve is presented in Figure 26: the
location of the knee point, where the ±45° plies fail and the
load is redistributed to the 0° fibers, depends upon the data
acquisition rate. Static failures result in a brooming
failure mode of the 0° fibers of the outer four plies, with
relatively minor damage to the two central terminated plies;
static specimens delaminated at the joint prior to failure.

The specimens appeared to generate ±45° ply damage
evident as white areas while under cyclic loading. The areas
of damage developed roughly half way between the lower tab and
the specimen center (the ply termination area), as seen in the
right most specimen of Figure 27. The cracks only developed
within the thinner section of the coupon and appeared to be
matrix and/ or interface damage. As only one specimen
developed damage at the joint, the resin rich area near the
ply termination had no effect on the overall fatigue strength
of this geometry. Tests on 4-ply material coupons with no
termination exhibited the same failure mode and fatigue
strength (see Figure 28). The difference in ply stacking
between F and G did not affect the overall fatigue resistance.

The S-N data in Figure 28 show a greater fatigue
sensitivity than for Materials A and B, with the points

falling further below the 10%/decade trend line. The initial strains at high cycles were also well below those for unidirectional materials. The nonlinear trend using Equation 3.3 does not fit the data well when forced through the static strength, and the exponent is lower at 10.0. These trends will be discussed later.
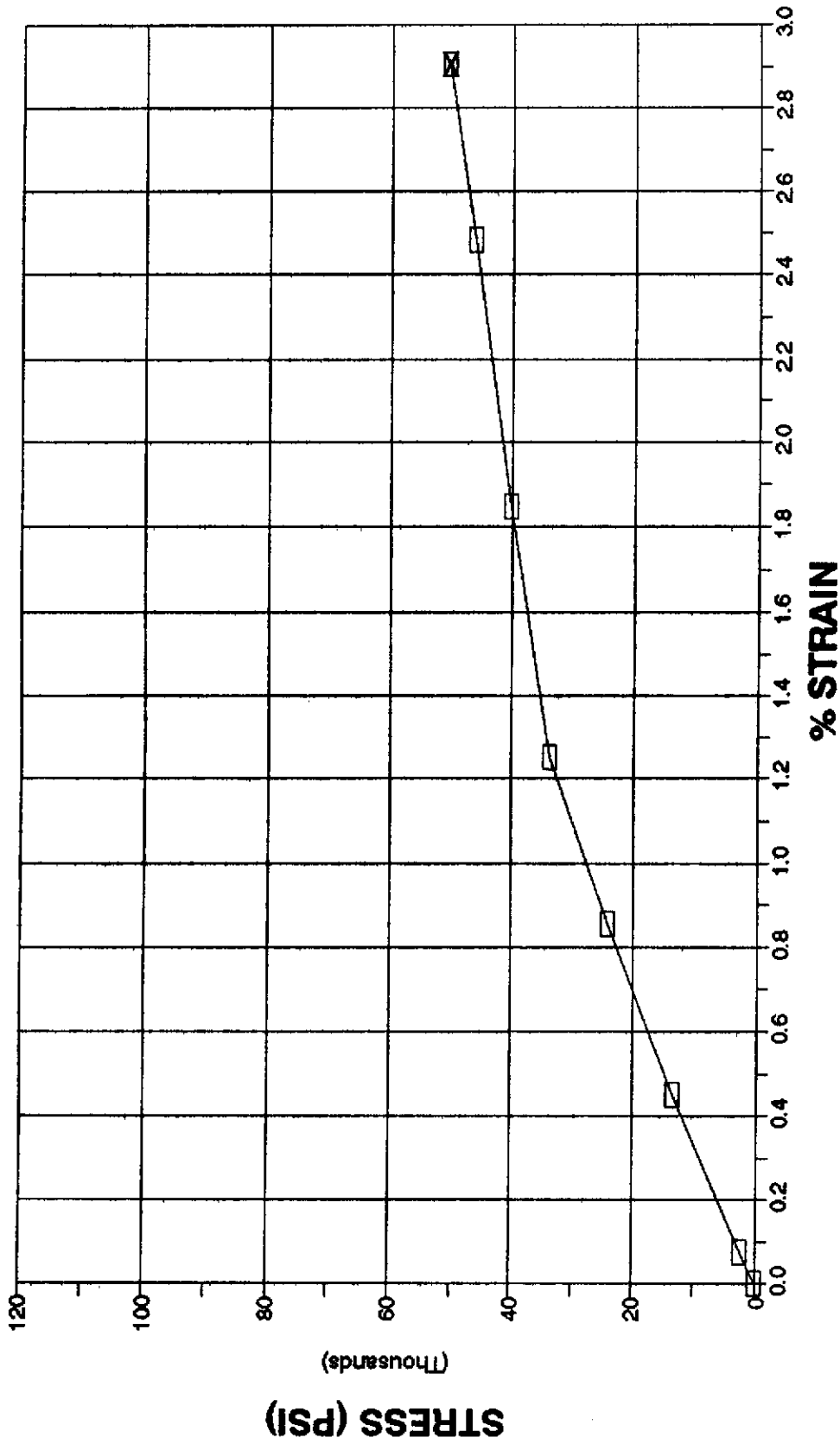
Figure 26. Stress-Strain Curve for Material G, Triaxial E-Glass/Polyester, 5 inch Gage Length, 0.25 inch/sec Ramp Rate.
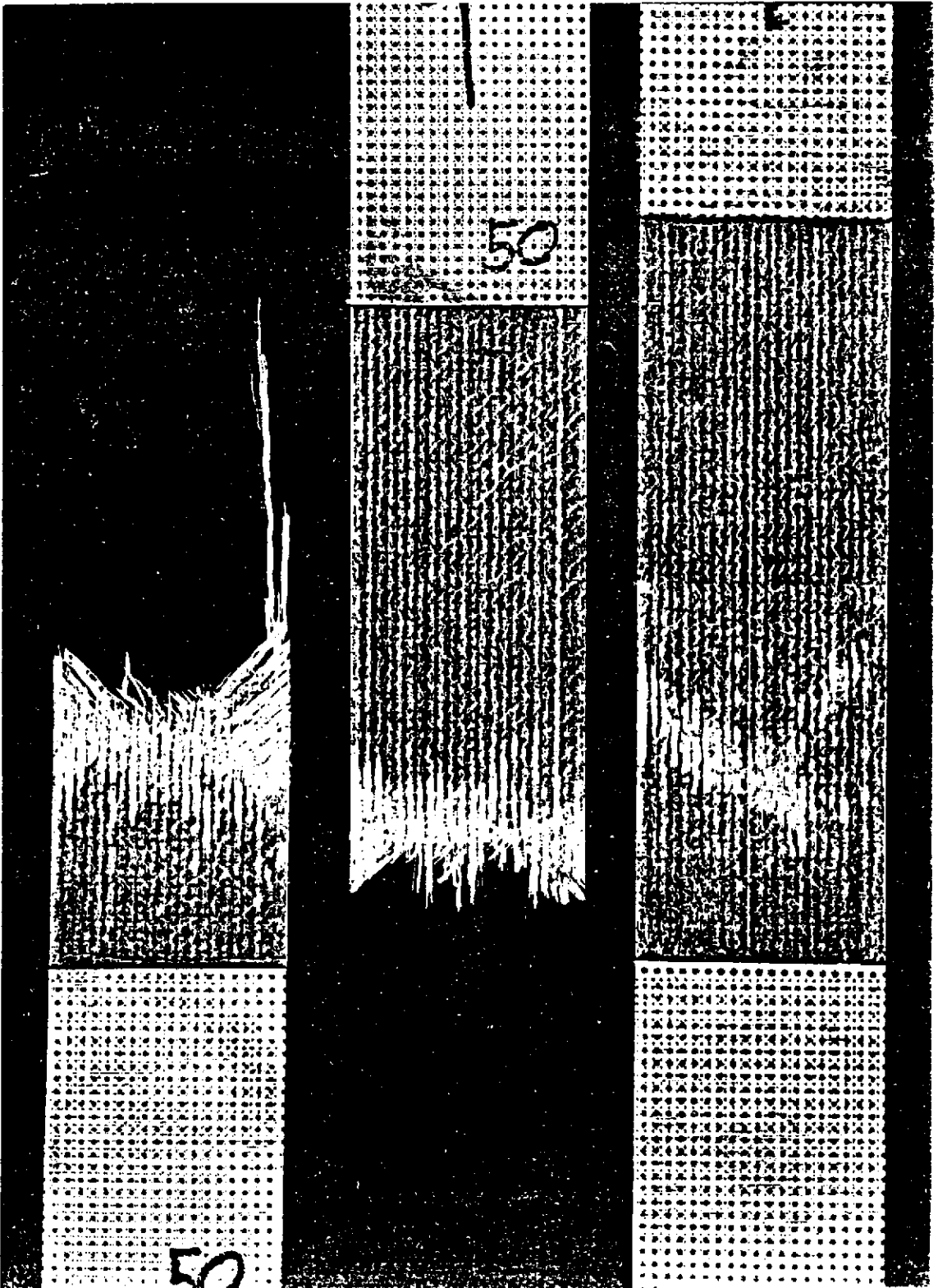
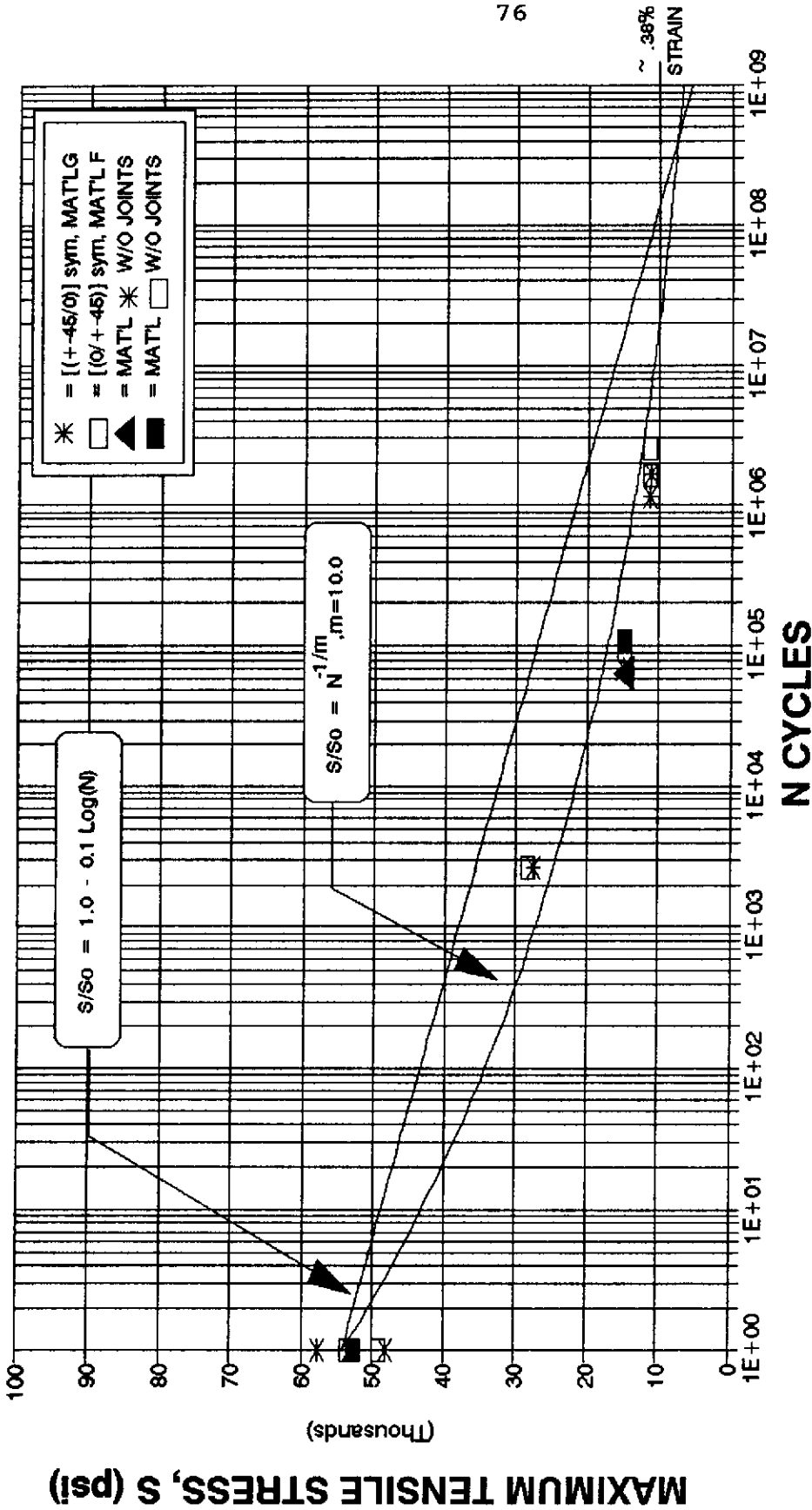**Figure 27.** Typical Damage Development in Materials F and G
Which Lead to Failure.

Figure 28. S-N Curve for Materials F and G, Triaxial E-Glass/Polyester,
R = 0.1, 5 to 10 Hz.

Materials H and J

Materials H and J were also [0/±45] triaxial reinforced polyester materials, but of higher 0° fiber content, relative to the ±45° content. As discussed earlier, they each contain a ply joint but have opposite ply stacking sequences. The UTS of Materials H and J were the same, 82 ± 6% ksi at the joint region, with tensile modulii of 3.43 ± 21% msi away from the resin-rich joint region. For both static and R=0.1 fatigue tests, Materials H and J always failed in the joint region: the outer 4 plies experienced brooming failure whereas the center 2 terminated plies delaminated and remained relatively undamaged. Figure 29, second specimen from the right, shows the intact nature of the center plies.

Under fatigue, cracks initiated in the matrix rich region between the terminated center plies, perpendicular to the load direction (see Figure 50). These cracks coalesced and grew into delaminated regions between the innermost continuous plies and the outermost discontinued plies: delamination of the second from the third ply, and of the fourth from the fifth ply. The delamination data, which were measured and documented as total coupon edge crack lengths (the sum of all lengths) versus cycles, are presented in Chapter 6. Depending on the applied load level, once the delaminations had reached significant size, chafing between the load bearing continuous plies and the unloaded discontinuous plies produced a dust which oozed from the crack faces. The relative deflection

between the unloaded inner plies and the outer plies during high stress tests resulted in a noticeable opening and closing of the matrix rich joint region. After the side edge cracks had propagated to significant lengths, lighter shaded areas became noticeable when viewing the front and rear faces through the thickness where delamination had occurred. As increased load was transferred to the outer four plies, matrix cracking developed on the smooth front face as seen in the left most specimen in Figure 29, and white fiber debonding regions appeared on the rough rear face as ply damage initiated (see Figure 29). Finally, brooming failures of the $0°$ fibers led to total coupon failure.

The S-N plot for this triaxial material with a joint is presented in Figure 30. As expected, the fatigue data lie below the 10%/decade trend. With the combined effects of triaxial material fatigue and the joint induced concentration of load into the outer 4 plies, fatigue resistance becomes more complex. Under one long term test, the delaminated regions appeared to arrest, and after further cycling, the test was stopped with no major signs of damage to the adjacent continuous ply regions. So, whether the failure mode was one of a delamination-affected triax-fatigue failure or simply normal triax fatigue is not certain. One possible trend curve, utilizing the Paris power law, was drawn through the average short term strengths and the one high cycle failure point of 20 million cycles. This curve required a power law

exponent (m) of 10. Although four other high cycle tests were performed, they all were considered runouts (no gross failure). Thus, there is insufficient data at present to establish a long term fatigue mode of failure of the joint.

Strain, stroke, and temperature data proved useful in establishing fatigue behavior trends for the coupons (see Figures 31 - 33). The fatigue trend for stiffness reduction based on the far-field strain (away from the joint) followed the same shape as for the previous materials, with the thick 6 ply region decreasing a significant amount, to 40% - 50% of the initial modulus. Interestingly, the stroke data in Figure 32, which gives the overall jointed specimen modulus, indicates a reduction in overall modulus of only 20% to 50%. Although the data for test# 69 correlate closely in both plots, it would seem unlikely that a stiffer 6 ply region would decrease in modulus at the same rate as a less stiff 4 ply matrix rich region at the joint. Generating additional strain data may add clarity to this topic. The wide degree of scatter for the Do/D plot, which is greater than for previous materials, may be due to inadequate initial stroke data, possible grip slippage, and joint region delamination.

Temperature readings were taken on the surface using an Omega micro-processor thermometer (Model #HH23) with a Type T thermocouple. Typically, coupon surface temperatures would slowly increase as internal damage increased. Then suddenly, around 90% of the coupon fatigue life, the temperature would

rapidly rise, as with Test# 89 in Figure 33. However, there was an instance where temperature readings around a localized damage zone gave false indications of nearness to failure: test# 92 experienced a dramatic temperature increase at a hot spot of damage at 40% of the total fatigue life. Thus, caution should be used in associating coupon surface temperature with total coupon nearness to failure.

Modulus data varied in magnitude with the location along the specimen. Strain readings showed only minor variation as long as cross-sectional areas remained uniform. However, in one test which has not been included herein, a thinner undocumented cross section at the extensometer location led to higher strain readings which correlate to significantly lower modulus readings. Thus, the actual cross-sectional area for the extensometer location should become a documented parameter.
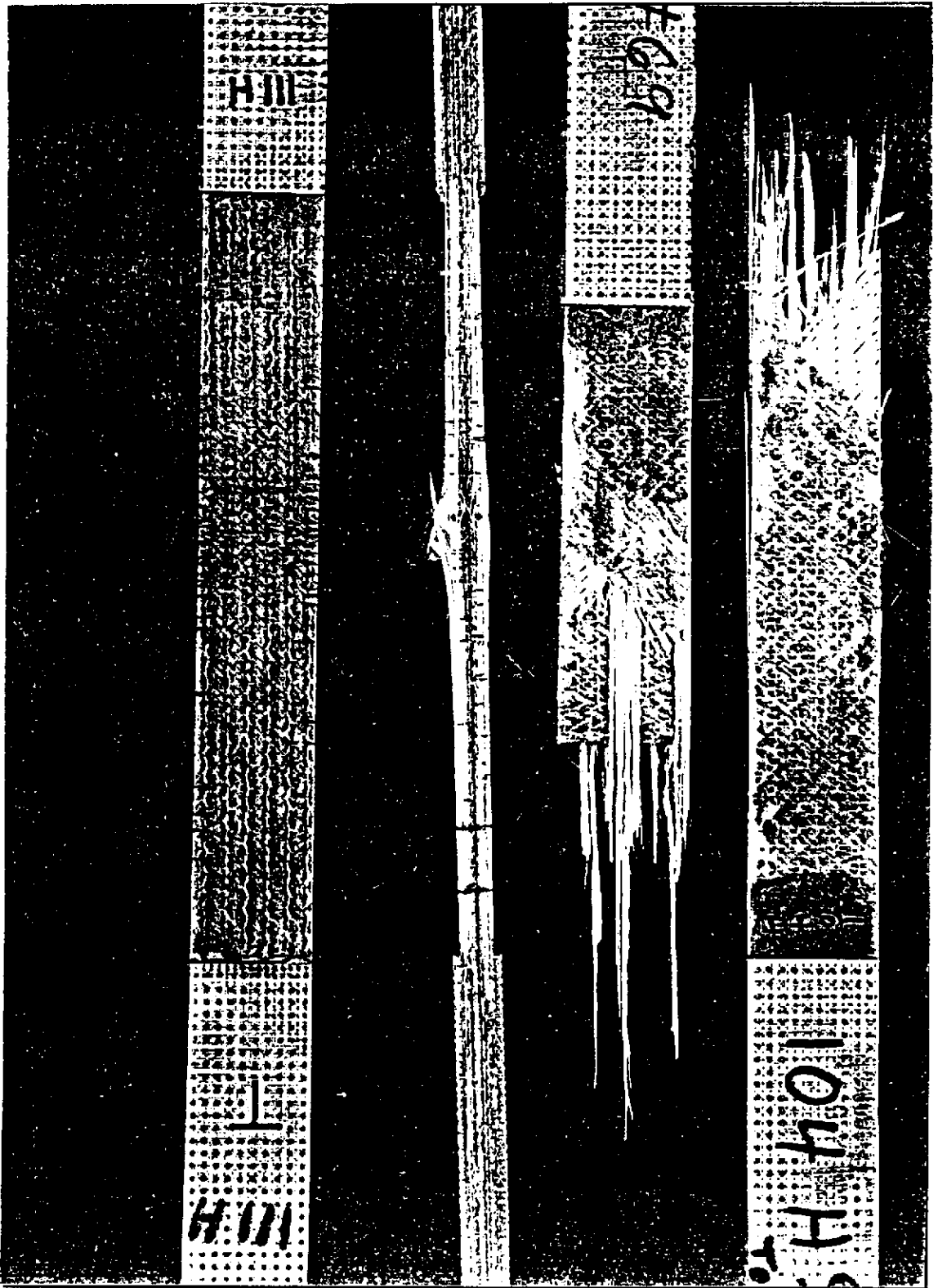
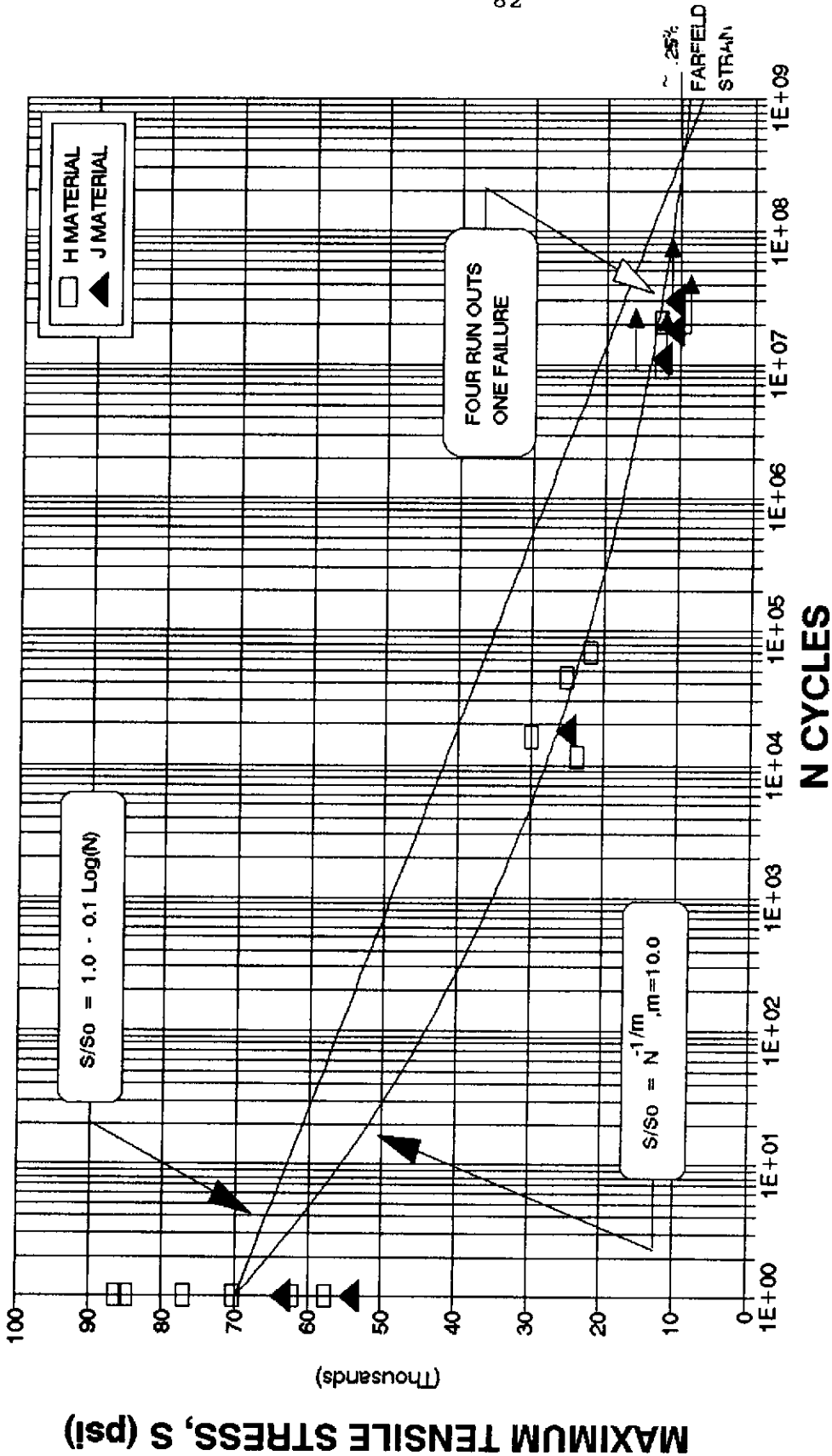**Figure 29.** Material H and J Typical Matrix Cracking, Initial Fiber Damage, and Brooming Failure.

Figure 30. S-N Curve for Materials H and J, Triaxial E-Glass/Polyester With a Joint, R = 0.1, 1 to 15 Hz.
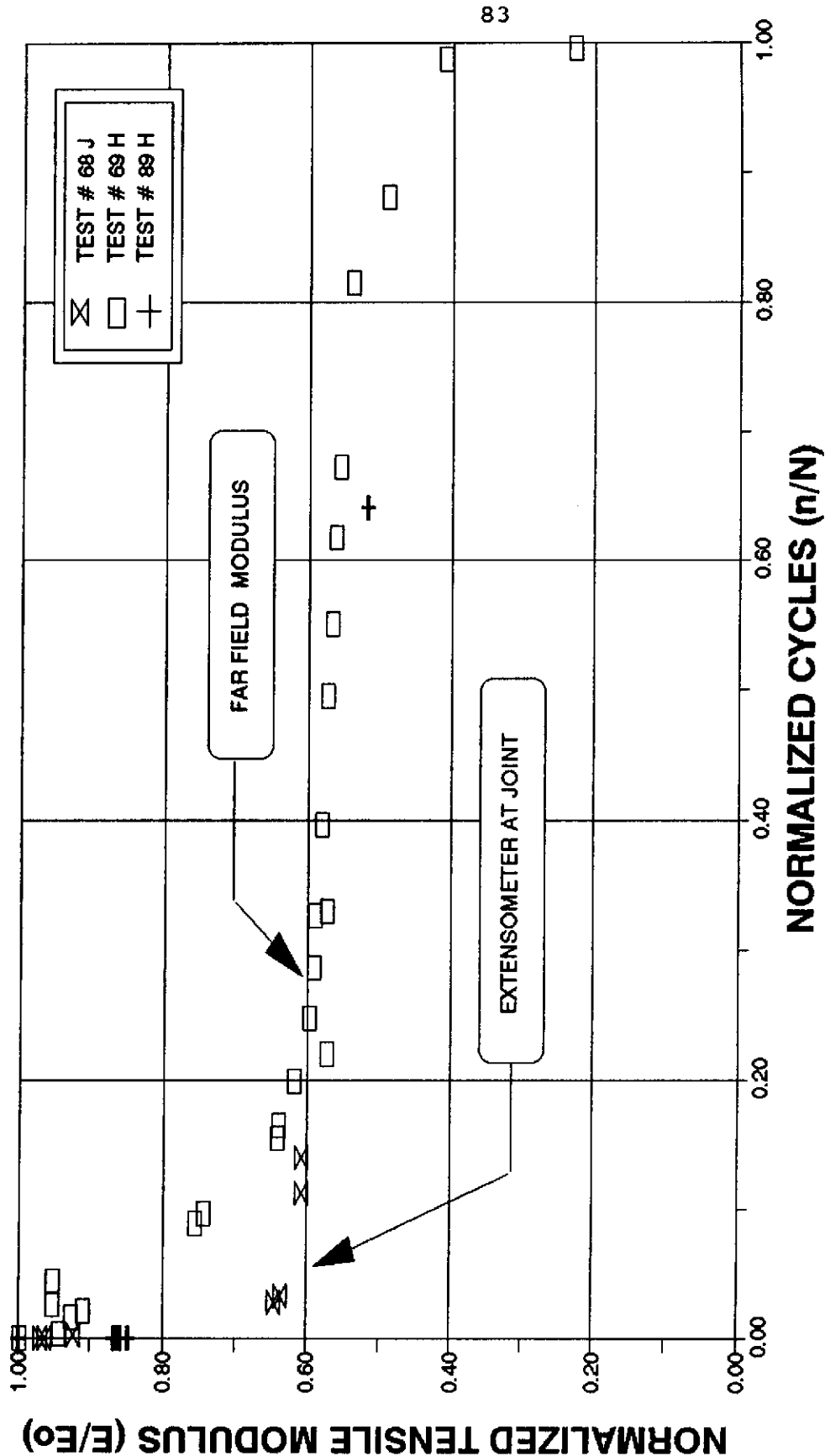
Figure 31. Elastic Modulus Trend for Materials H and J, Triaxial E-Glass/
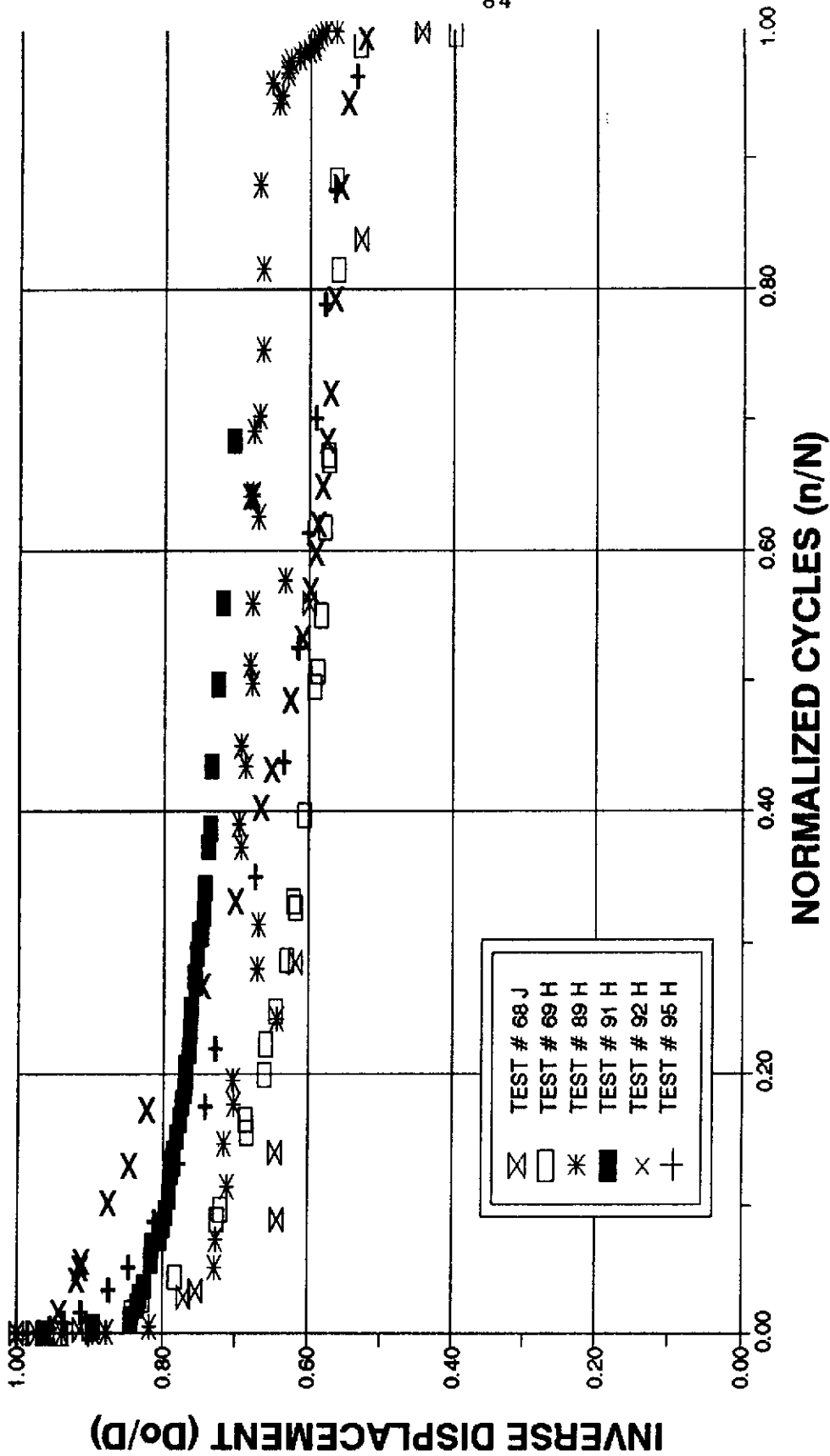Polyester with a Joint, R = 0.1, 5 to 15 Hz.

84

Figure 32. Normalized Inverse Displacement Trend for Materials H and J,
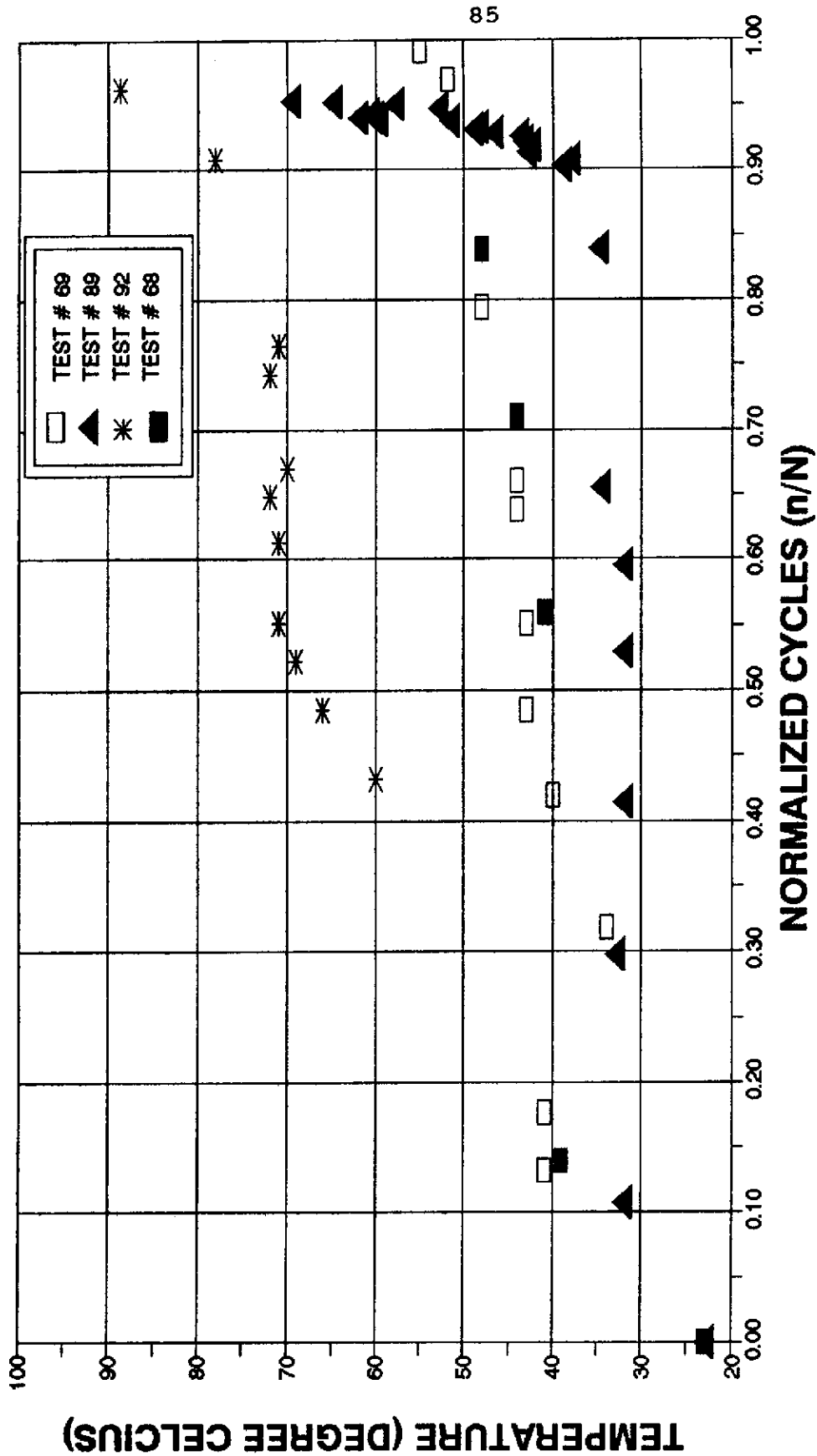Triaxial E-Glass/Polyester with a Joint, R = 0.1, 1 to 15 Hz.

Figure 33. Temperature Increase Trend for Materials H and J, Triaxial E-Glass/ Polyester, with a Joint, R = 0.1, 5 to 15 Hz.

Material L

Even with the significant waviness in the fibers of Material L, the higher V_f of 0.5 resulted in a UTS of 108 ksi with a modulus of 4.76 ± 12% msi (see Figure 34). The static mode of failure was typically extreme brooming of the fibers.

Although Material L is classified as unidirectional, the individual fibers appeared to wind and curve relative to each other to form a complex three dimensional interwoven unidirectional. Thus, although one face was cured on a flat smooth surface, the back face contained many rises and troughs. This geometric anomaly induced a wide range of stress and strain variations. Only the average cross-sectional areas could be measured and thus considered in calculations with the stress and modulus. In addition, the fiber-end edge-effects due to the fiber waviness created a high degree of splintering.

The splintering effects were typically different in shape than were previously experienced by Materials A and B. For Material L, the splinters typically started in the mid-gage region and developed along both edges, top and bottom. Thus, where Materials A and B experienced one or two well defined splinters, Material L typically had a complex array of up to four major corner splinters which left a diamond shaped section to carry the load. The remaining load bearing fibers then failed in a brooming fashion (see Figure 35).

The S-N data of Figure 36 exhibit a slight curve which

suggests that reducing the amount of splintering could possibly increase the lifetime to follow the 10%/ decade trend of uniaxial reinforced glass fiber dominated composites. Perhaps an applied edge coating of glass mat and epoxy could preserve the edge from splintering. As more data are collected, the curve will become better defined.

The limited research thus far on Material L has encountered great difficulty in measuring local surface strain due to the edge effects. More tests are expected to be performed for this material during the next stage of this research project.
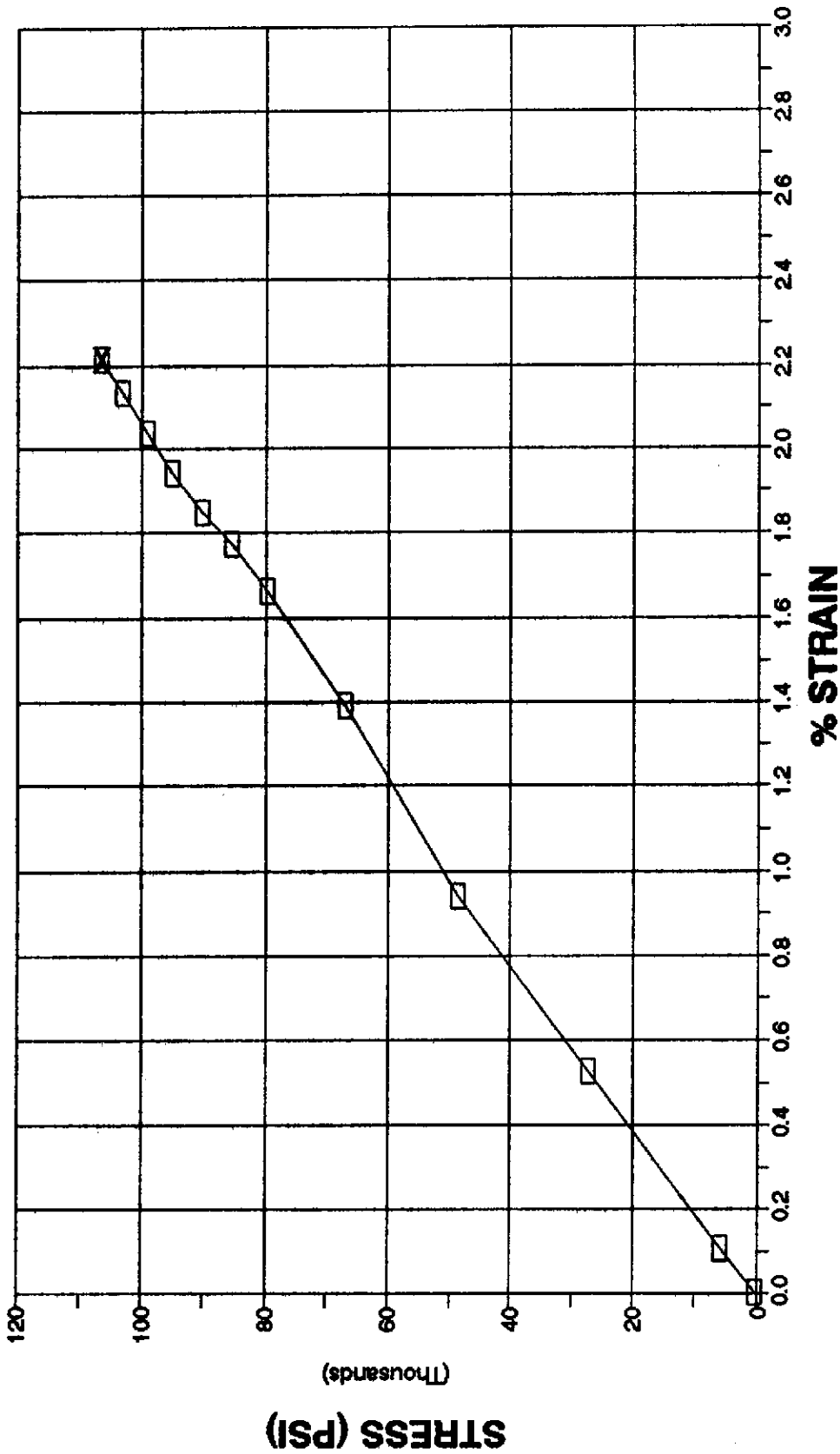
Figure 34. Stress-Strain Curve for Material L, Unidirectional E-Glass/ Polyester, 4 inch Gage Length, 0.25 inch/sec Ramp Rate.
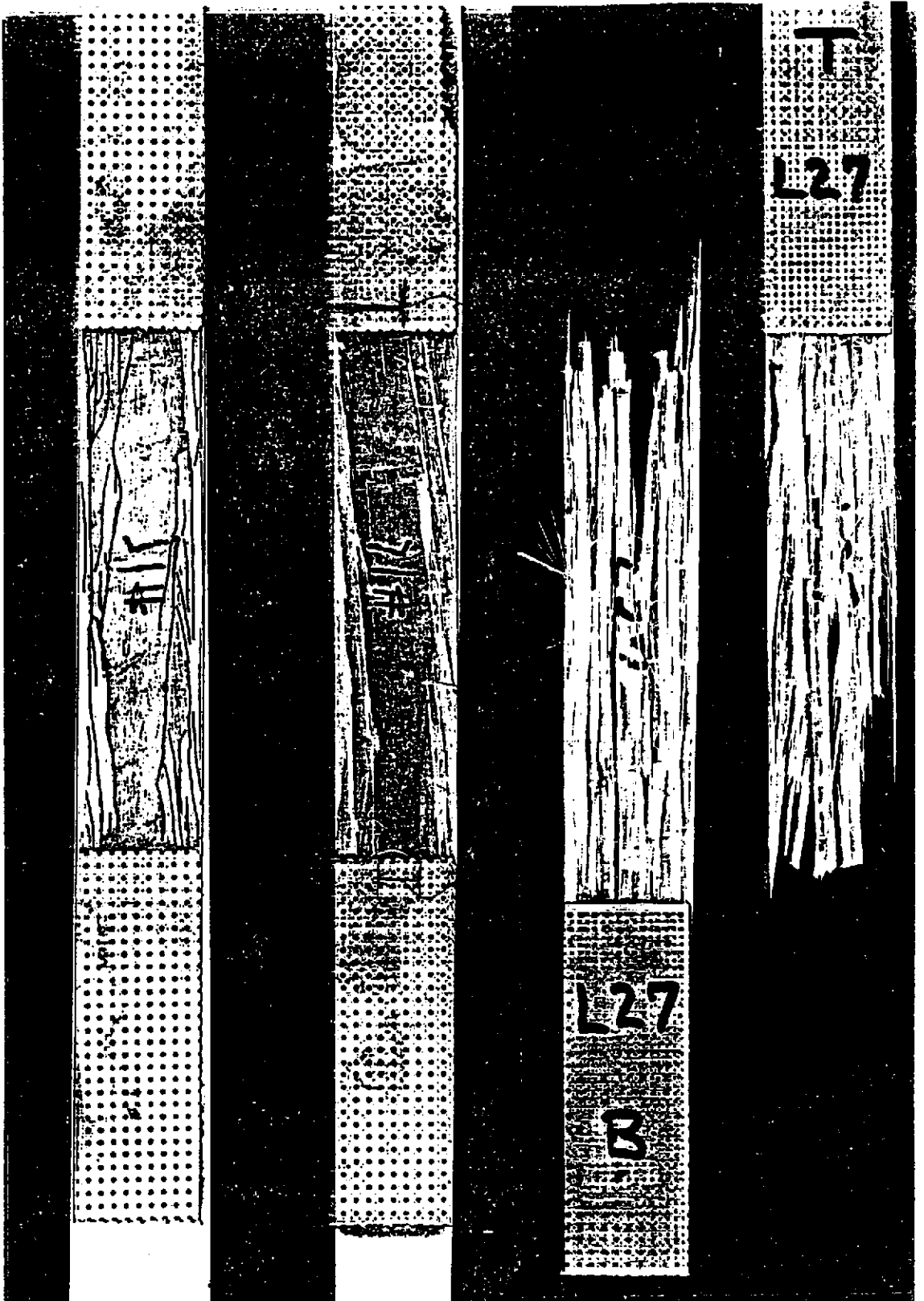
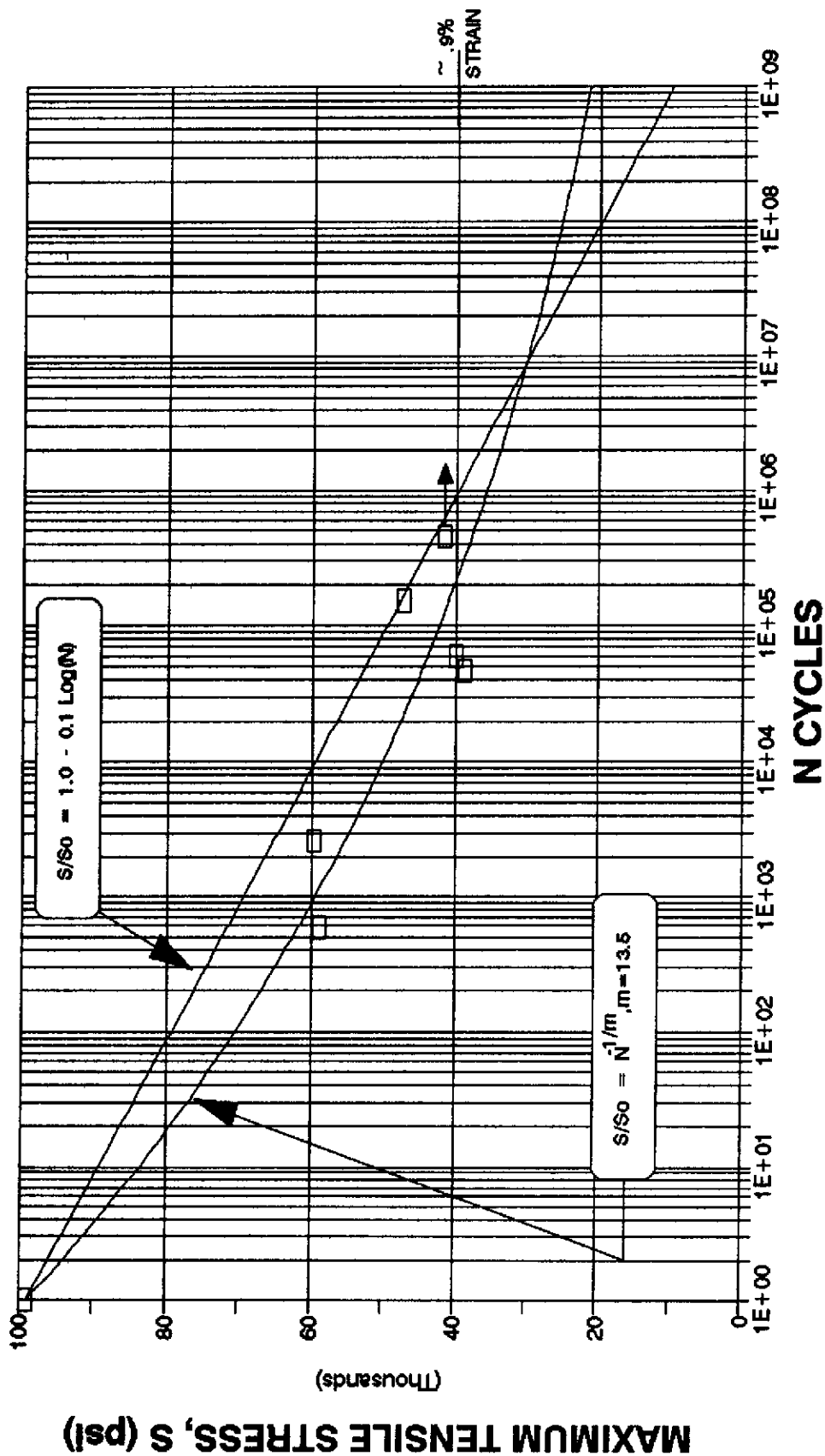**Figure 35.** Damage Development and Failure of Material L.

Figure 36. S-N Curve For Material L, Unidirectional E-Glass/Polyester,
R = 0.1, 5 to 15 Hz.

Material N

Material N is a triaxial reinforced polyester with a fiber volume fraction of $V_f = 0.5$, with roughly 50% 0° fibers and 50% ±45° fibers. This Material has been tested both in the [0/±45] direction and the transverse [±45/90] direction (relative to the force) to provide directional properties. The UTS of the [0/±45], herein termed 0° triaxial, is 69 ksi with a tensile modulus of 3.03 msi; a static stress-strain curve is presented in Figure 37. The UTS of the [±45/90], herein termed 90° triaxial, is 13 ± 3% ksi with a tensile modulus of 1.17 ± 15% msi; a static stress-strain curve is presented in Figure 38. Even though the data acquisition rate was low for these static tests, the data show the strongly directional properties even for the triaxial type reinforcements.

The static mode of failure for the 0° triaxial material was a brooming failure of the 0° and center ±45° fibers, with an associated debonding of some ±45° fibers. The static mode of failure for the 90° triaxial material was dominated by the breakage of the center-most ±45° fibers, with an associated debonding of the edge-most ±45°, as well as the 90° fibers (see 1-inch-wide specimen, Figure 39).

The fatigue failure mode for the 0° triaxial material sometimes appeared as a transverse scrim dominated failure mode. Specimens were noted to develop thin linear damage regions along a transverse scrim fiber as shown by the left-

most specimen in Figure 40. This damage zone would then develop a single crack which would propagate across the specimen, leading to total failure (second specimen from left Figure 40). Also, a second typical mode of failure often developed as a result of multiple large matrix/interface damage regions. A single crack would develop from one of the damage zones closer to an edge. This crack would then typically proceed across the specimen width (see the two right-most specimens, Figure 40).

In contrast to the 0° triaxial material, the 90° triaxial material appeared to develop small, fine matrix/interfacial damage extensively through out the gage section. Multiple cracks would then typically develop at the edges of the coupon and propagate straight across, through the finer damage, perpendicular to the load (see Figure 39). The high-cycle run-out specimen (34 million cycles) had developed only a minor degree of the fine matrix cracking when the test was terminated.

The S-N curve of Figure 41 and the enlargement (Figure 42) establish that, although the initial strengths are highly sensitive to the direction of the triax, the long term fatigue resistance (at R=0.1) is less sensitive: the trends converge from a strength ratio factor of 5 to about 2. On the other hand, the material stiffness does appear to be extremely sensitive to the presence of 0° fibers. The 0° triaxial material shows only a slight 10% to 20% reduction from the

initial stiffness due to the fatigue loading, whereas the 90°
triaxial material exhibits a tremendous decrease in the range
of 60% to 70% (see Figures 43 and 44). In this case, the
modulus trend is well supported by the normalized inverse
displacement data of Figures 45 and 46.
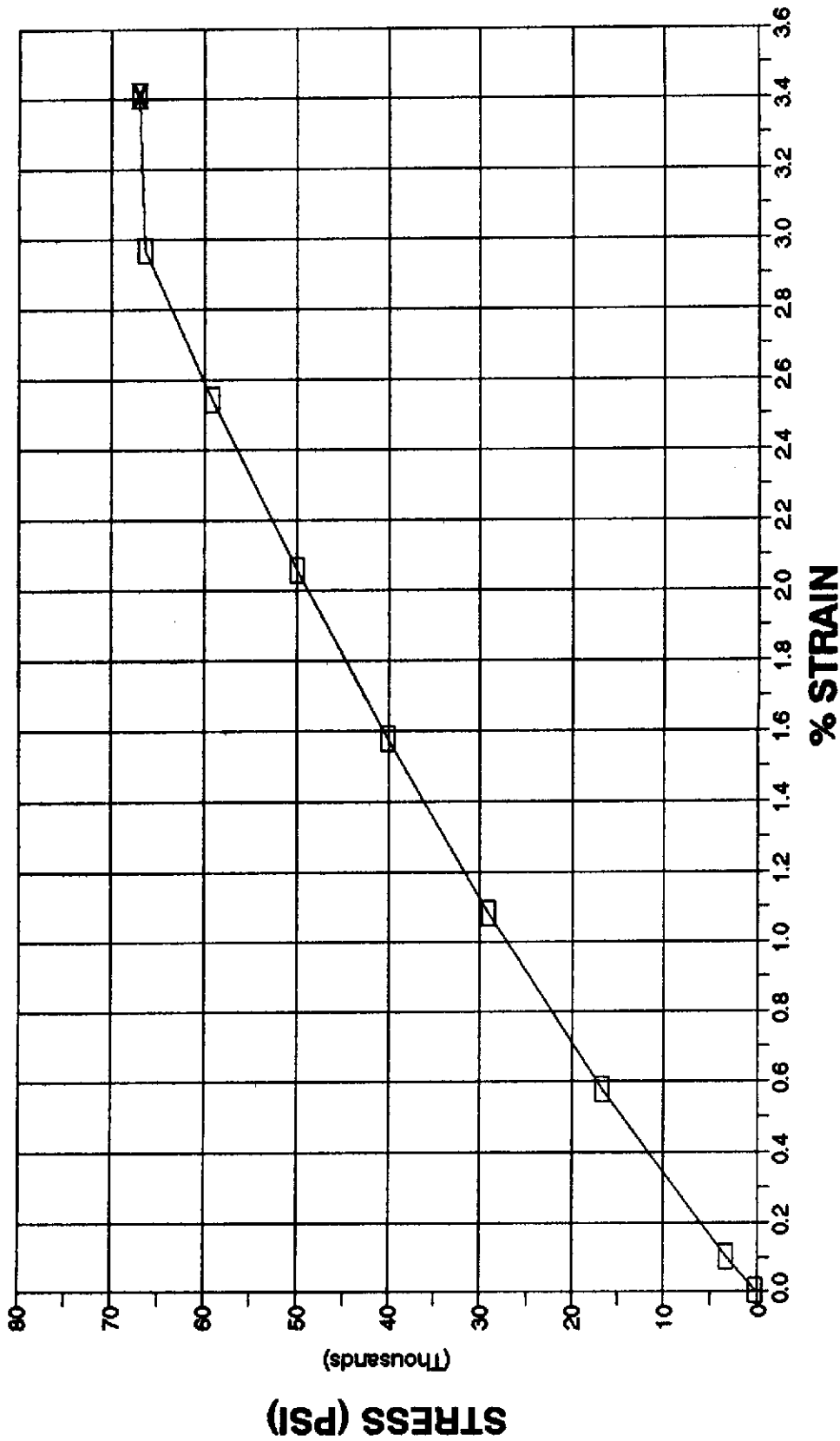
Figure 37. Stress-Strain Curve for Material N, [0/±45] Triaxial E-Glass/
Polyester, 4 inch Gage Length, 0.25 inch/sec Ramp Rate.
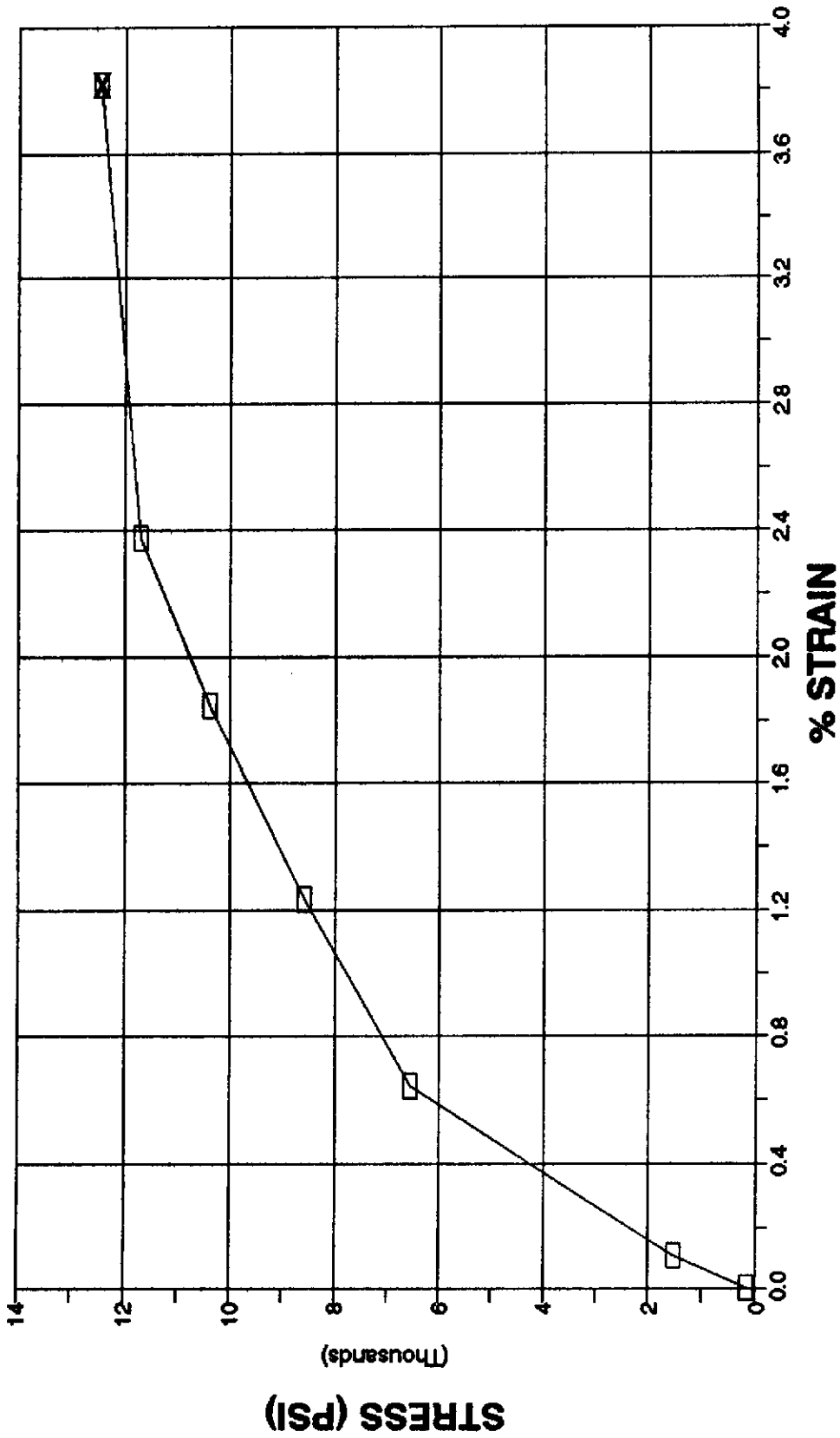
Figure 38. Stress-Strain Curve for Material N, [90/±45] Triaxial E-Glass/ Polyester, 4 inch Gage Length, 0.25 inch/sec Ramp Rate.

Figure 39. Typical [90/±45] Material N Matrix Cracking,
Edge Fiber Pullout, and Center Fiber Failures.
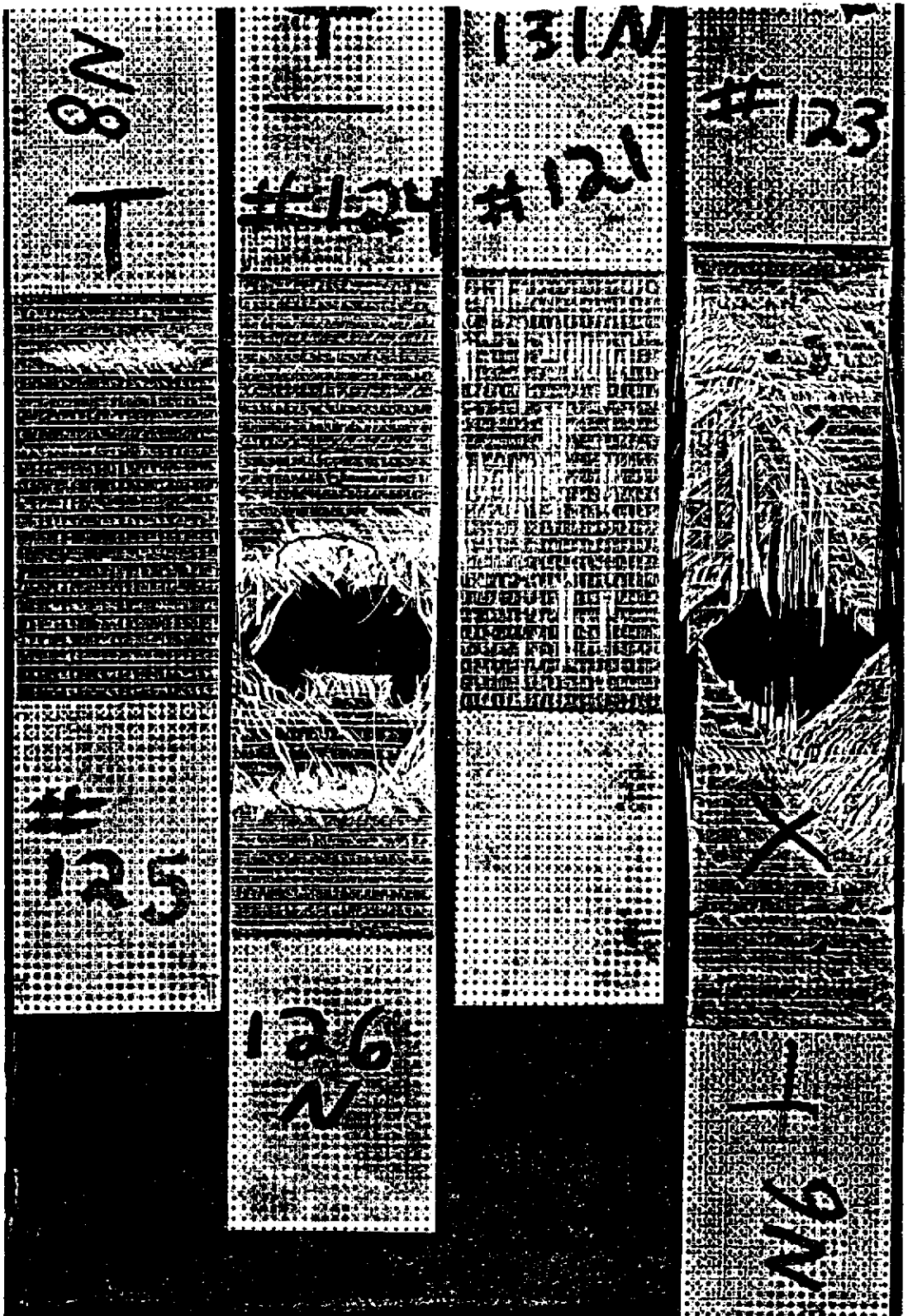
Figure 40. Typical [0/±45] Material N Scrim Cracking, and ±45 Damage Region Failure Modes.
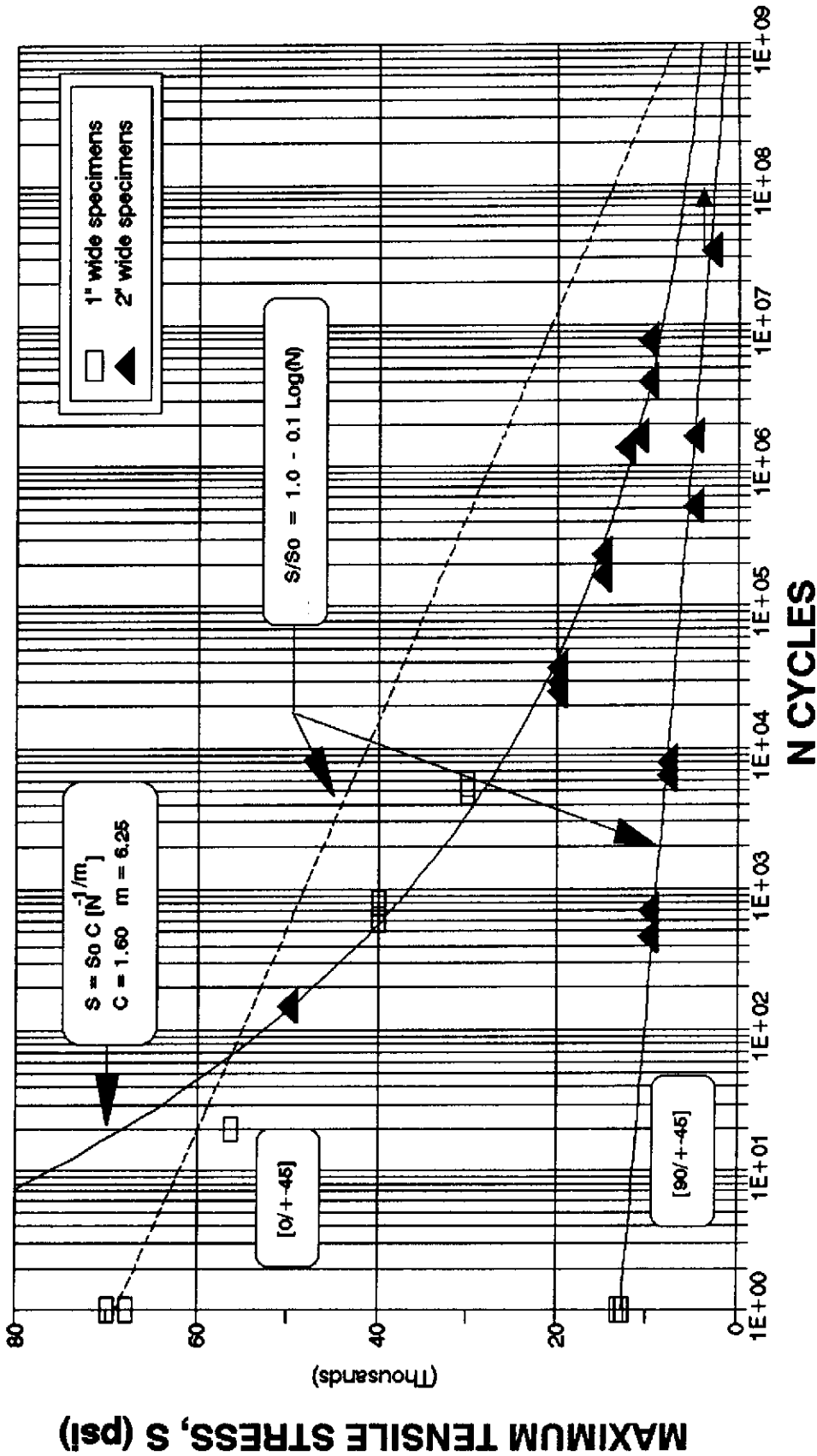
Figure 41. S-N Curve for Material N, Triaxial E-Glass/Polyester,
R = 0.1, 1 to 15 Hz.
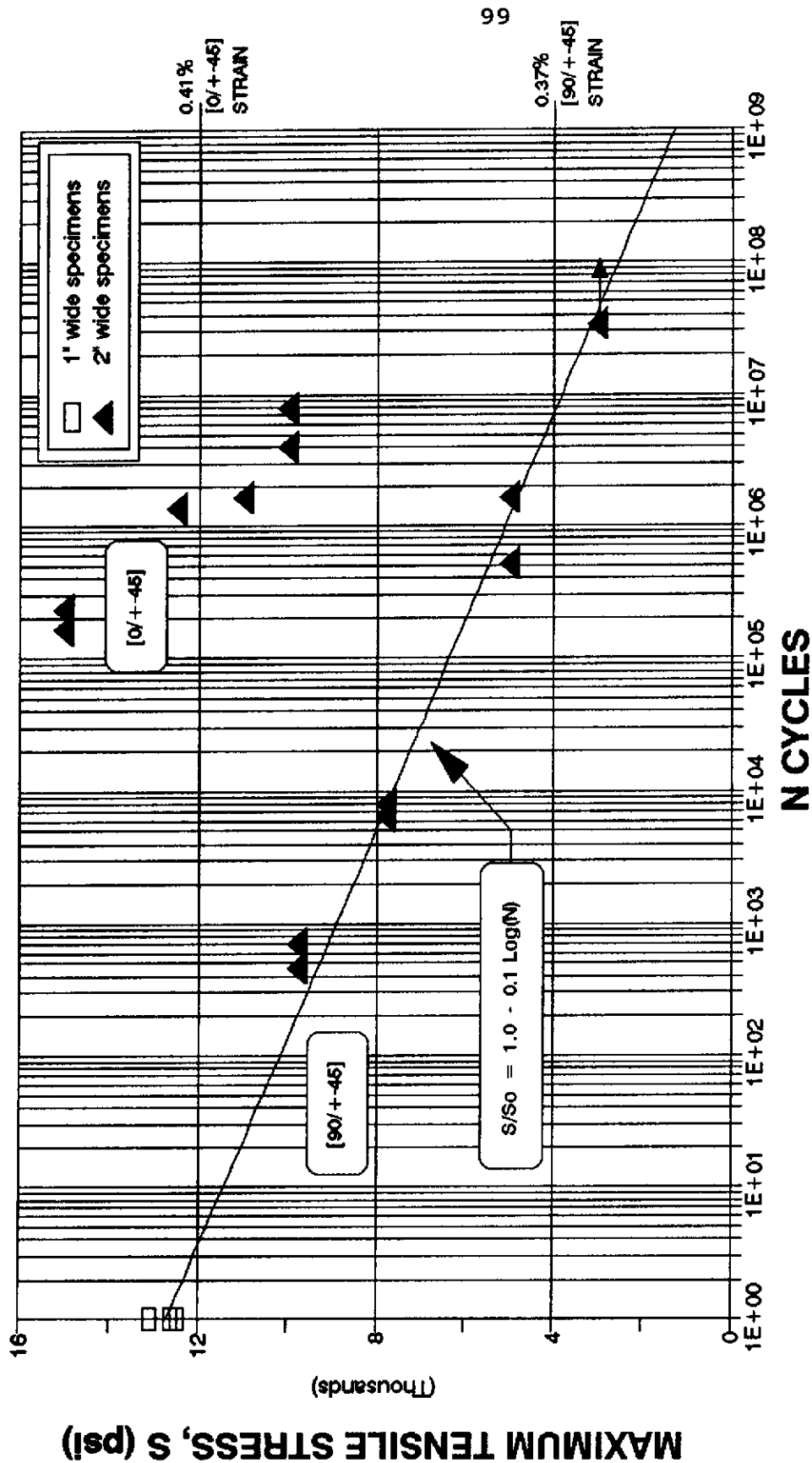
Figure 42. S-N Curve for Material N, Triaxial E-Glass/Polyester, R = 0.1, 1 to 15 Hz.
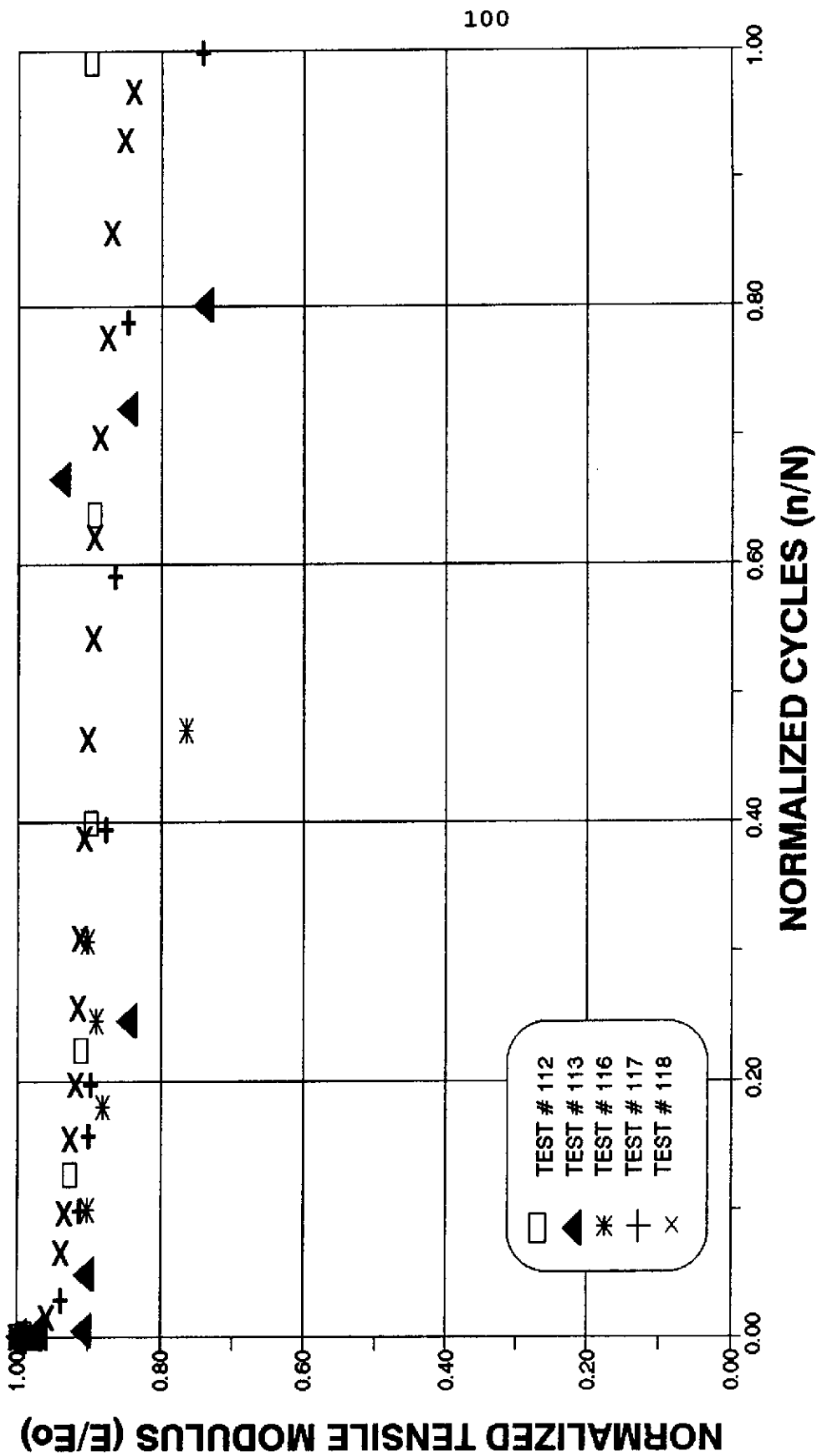
Figure 43. Elastic Modulus Trend for Material N, [0/±45] Triaxial E-Glass/ Polyester, R = 0.1, 1 to 10 Hz.
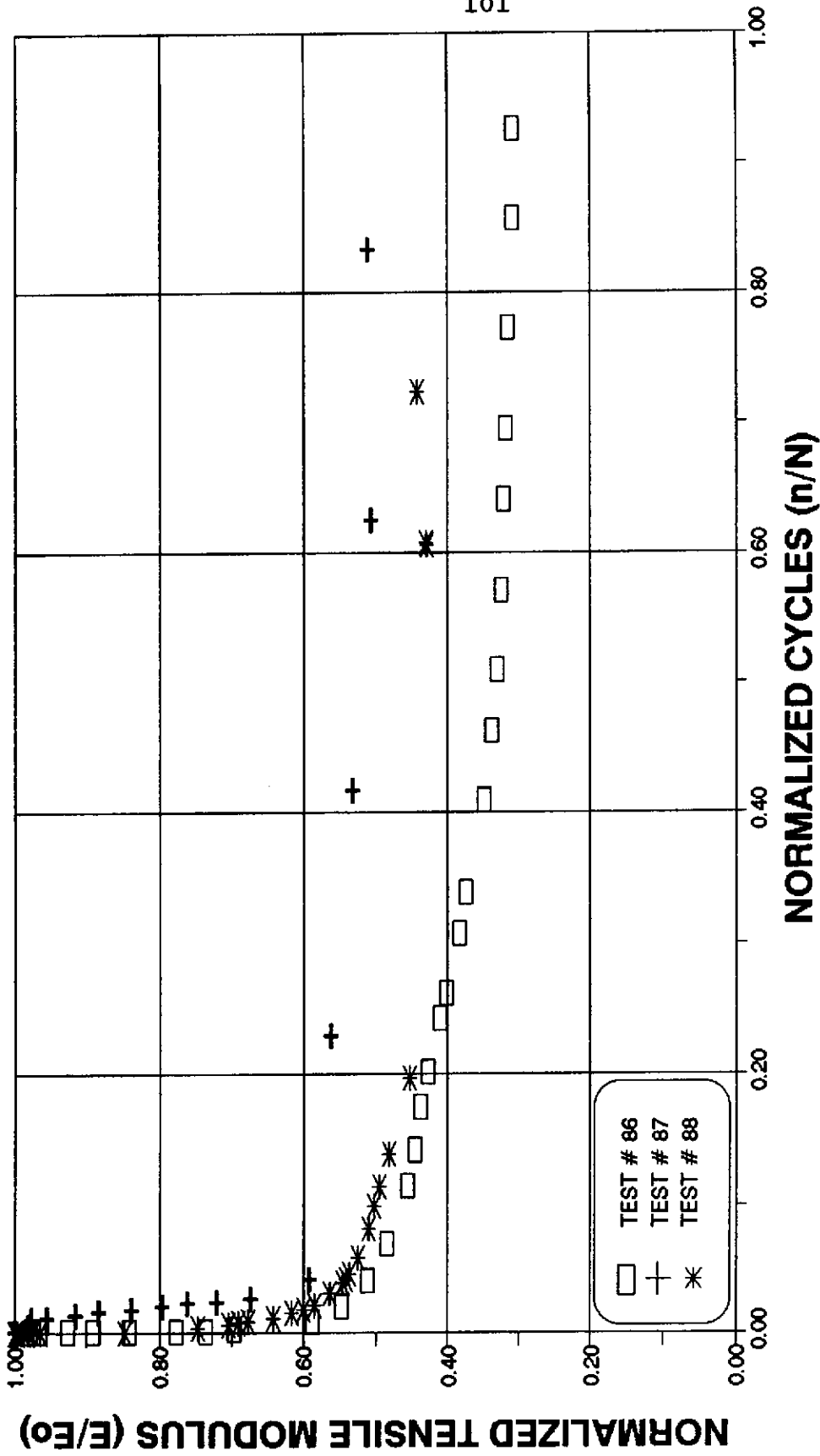
Figure 44. Elastic Modulus Trend for Material N, [90/±45] Triaxial E-Glass/
Polyester, R = 0.1, 1 to 10 Hz.
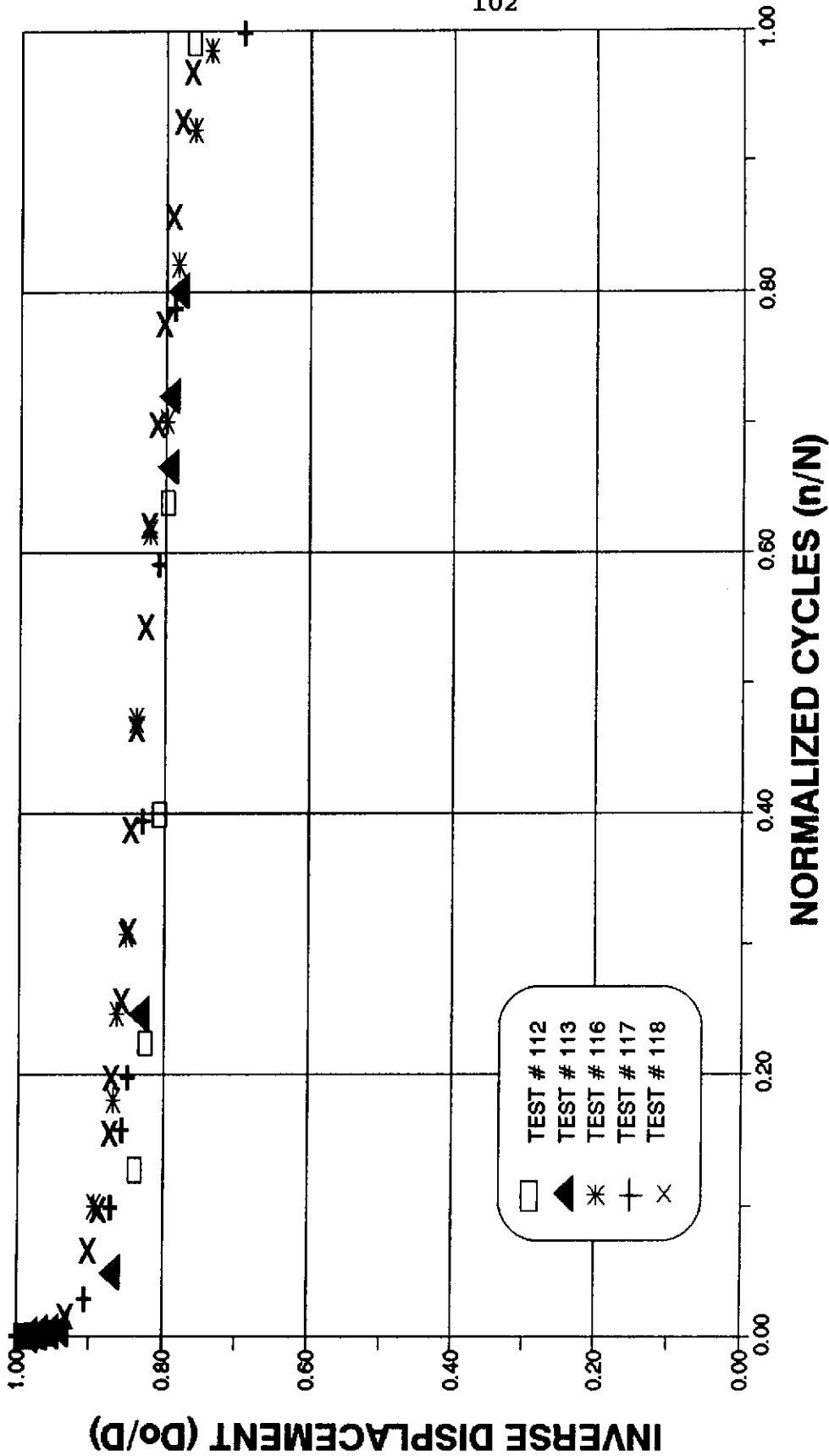
Figure 45. Normalized Inverse Displacement Trend for Material N, [0/±45]
Triaxial E-Glass/Polyester, R = 0.1, 1 to 10 Hz.
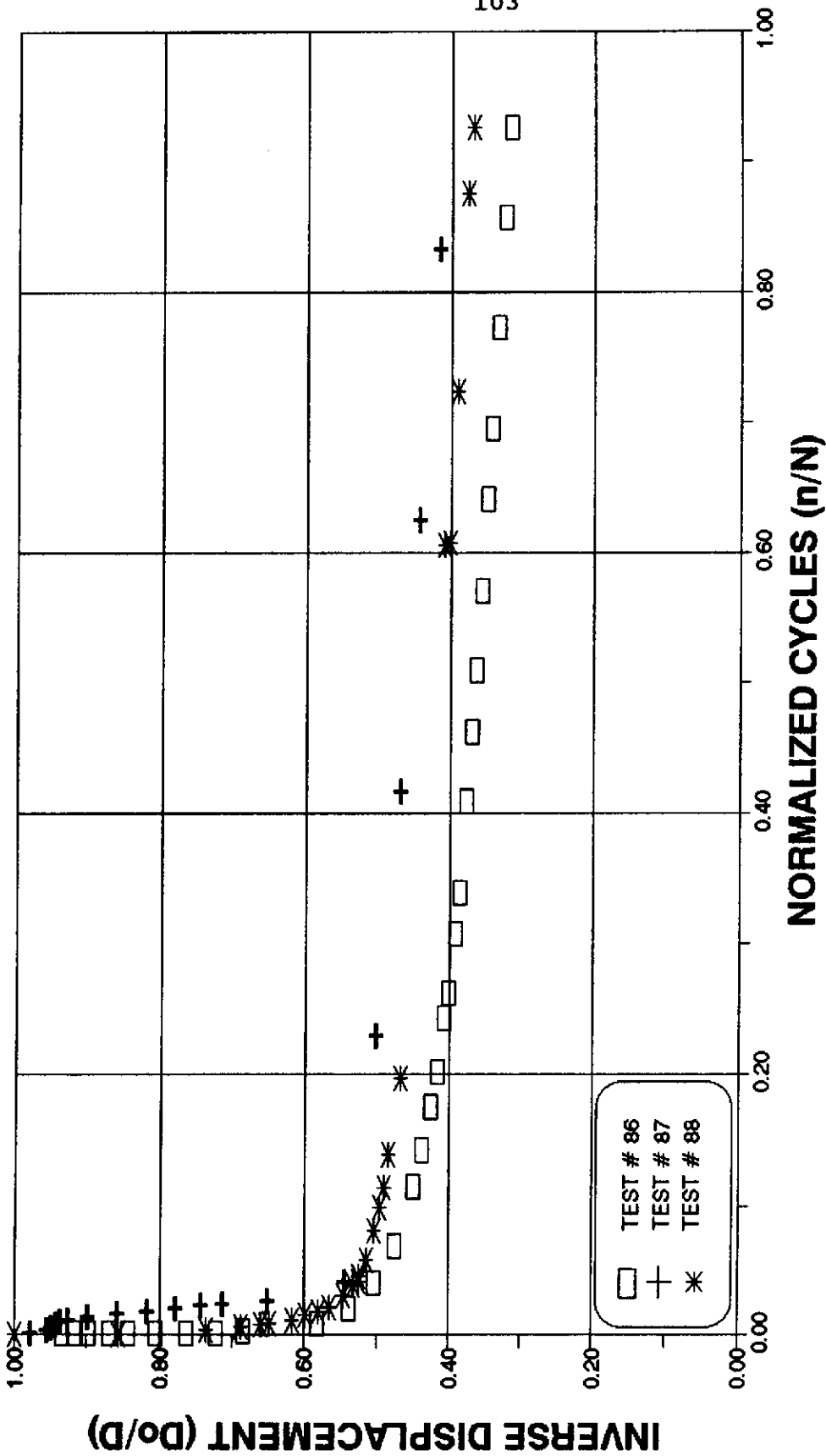
Figure 46. Normalized Inverse Displacement Trend for Material N, [90/±45]
Triaxial E-Glass/Polyester, R = 0.1, 1 to 10 Hz.

CHAPTER SIX

ANALYSIS

Unidirectional Reinforcement

The fatigue data generated for the unidirectional materials (A, B, and L) are compared in Figure 47 by normalizing the test maximum stress levels against the respective static strengths. As noted earlier, data for these unidirectional materials fall below the 10%/decade line which has been extensively reported for E-glass fiber dominated composites. Instead, the data agree well with the Paris power law trend of Equation 3.3 with exponents between 10 and 14 (see Figure 47).

The majority of unidirectional specimens developed early edge damage due to poor fiber alignment. As indicated earlier, fibers which were not well aligned in the lengthwise direction were typically cut at the edges during the coupon fabrication process. These fiber ends created points of matrix stress concentration which typically initiated damage. Once initiated, the cracks then propagated along the misaligned fibers into the tab region, creating a splinter (see Figure 48). The amount of area reduction which the splinter induced was a function of the degree of misalignment and location of initiation. The increased stress in the tab

region resulted in a more rapid failure than would have been expected for the initial test stress level. Thus, the fatigue resistance for the unidirectional materials relied both on the rate at which the splinters developed (crack growth rate) and the relative size of the splinter (relative degree of induced area reduction). Modeling of the unidirectional failure mode by the Paris power law relationship for matrix crack growth (Equation 3.3) is, therefore, appropriate. Figure 47 shows the effect of a range of values for the power law exponent m.

Although better fiber alignment, or protected edges, might increase the overall fatigue resistance, such effects might only be noticeable for the low to medium cycle data. The 10%/decade and the power law model trends cross at high cycles. Thus, better fiber alignment might be less noticeable on the long term fatigue plots in the cycle range where the curves cross. Even so, a reduction in splintering would probably reduce the scatter band of all the stress levels, as well as enable more unambiguous definition of test stress levels. Figure 49 presents a second analysis where the effects of total fiber misalignment are examined. With the fiber alignment shifted 4° off-axis from the loading direction, the UTS is theoretically reduced about 20%. This reduction in strength, coupled with the 10%/decade fiber dominant model, shows a better fit of the high to moderate stress data. (The 4° misalignment was the maximum value found for the A and B materials).

Crack Initiation and Propagation

Delamination tests on Materials H and J (ply joint) were performed to determine the magnitude of the Paris power law exponent, m, for this mode of crack growth. Crack initiation and propagation tests were conducted via fatigue tests at a constant cyclic stress range. Total delamination length versus cycles were recorded; total delamination length is the sum of the lengths of the eight delamination edge-cracks. Typical crack growth patterns are shown in Figure 50: the crack initiated in the matrix rich region at the joint normal to the stress direction, and then propagated along the ply interface causing delamination between the inner and outer plies. Plotted as total crack length versus number of cycles (see Figure 51), a typical three-stage crack growth curve is observed: initiation, stable growth, unstable growth (not shown). The slope of the stable growth region is the growth rate da/dN, taken as the average growth rate over a period of cycling.

Multiple tests were performed at various constant stress levels to develop a plot (log-log) of da/dN versus normalized stress in Figure 52. The stresses are normalized by the static stress level (S_0) which produces delamination. The slope of the linear mid-region is the Paris power law exponent, m. The experimentally derived value of m = 13.5 is taken as representative of matrix dominated fatigue crack growth in this material system. However, these results

actually apply only to this geometry, which will produce a particular combination of Modes I and II crack growth. The particular combination of modes requires further analysis, and data are needed for a range of crack growth modes.

The measured exponent compares well with the Paris power law exponents fit to the unidirectional fatigue data: Material A (m = 12.5), Material B (m = 13.5), and Material L (possibly in the range of 13.5). Thus, it appears that the splintering and/or tab delamination trends could be represented utilizing the delamination Paris power law curve, at least for the cycle range studied to date, up to 10-40 million cycles. The measured exponent is also in the range of values reported for fatigue crack growth in neat thermoset polymers [24], as well as delamination in other composites, particularly in Mode II [25].

Triaxial Reinforcement

The fatigue failures of triaxial [0/±45] materials appeared to exhibit damage initiation and propagation as described in Chapter 3: the off-axis plies developed damage along the ±45° fibers, followed by failure of the 0° fibers. In some Material N tests, however, it appeared that the scrim played an important role in damage initiation (see Figure 40). Microscopic examination of this initiation mode will follow in future tests to determine the actual damage process.

Through normalization of all the triaxial material data, Figure 53 indicates that the same trend is followed regardless

of ply stacking sequence, fraction of orientated fibers (50%
or 30% ±45° fibers), inner ply termination, or inner ply
joint. The data fit the Paris power law prediction well,
except at the extremes: the low (static) and high cycle
ranges. The power law trend does not pass through the static
ultimate strength, which may be due to a shift from a mode of
failure with instantaneous matrix damage to one where initial
cycling is required to produce initial matrix/ interface
damage. Also, the conservative prediction for the high cycle
data tends to suggest another possible mode of failure shift,
which will be discussed later under the initial strain-to-
failure section.

Temperature

Coupon surface temperatures were monitored on selected
tests as a plausible test parameter for failure prediction, as
well as a control on frequency to prevent overheating.
Correlation of the available data suggests that temperature
may indeed indicate relative closeness to failure, or at least
the presence of a damage zone. As Figure 33 shows, false
failure indications may be brought on by localized damage
zones. Also, the plateau temperature which a specimen
typically exhibits (from .2 to .8 percent of its lifetime)
depends upon the level of stress and frequency; higher
stresses and frequencies induce higher temperatures. At
higher cycles, tests have typically shown an increased
localized temperature within a damage zone, and a localized

rapid temperature surge which forewarned specimen failure. The increase in temperature associated with damage is generated by the rubbing of various crack surfaces. Further research in this area may prove significant in establishing alternative methodologies for locating damage initiation areas in full scale tests.

Modulus of Elasticity

The initial modulus depends entirely on the V_f and the fiber orientation to the loading direction. Figure 54 summarizes the modulus plots for six of the materials tested. The degradation rate of the modulus during the fatigue process depends on the type of reinforcement: the lower the percent of 0° reinforcement, the more dramatic the reduction in stiffness.

As modulus calculations for these tests were based on extensometer readout, the relative location of any damage zone is critical. Damage beneath the extensometer unit resulted in larger than average strains, whereas damage immediately above or below the extensometer would produce lower than average strains. For this reason, Figures like 44 show wide scatter for the localized modulus changes.

Although slippage or tab delamination may occur within the grips in some cases, displacement may also be used to correlate the stiffness change. The total coupon displacement calculation examines the total effective specimen stiffness, rather than a localized modulus. Thus, the location of the

damage is less critical. And, as the stroke can be consistently monitored with fewer problems than with an extensometer, more data with a higher degree of accuracy can be documented, assuming only minor grip slippage. As such, Figures like 32 illustrate the smooth, steady decrease in overall tensile stiffness during the fatiguing process. However, the results of this method should not be confused with material elastic modulus fatigue: the overall coupon displacement is sensitive to all types of damage such as edge splitting and local damage zones in the triax. The modulus is viewed as a material response which only includes more uniformly distributed damage such as ±45° ply cracking.

Fatigue Endurance Limits

Thus far, there has been a general trend for the majority of the materials tested to follow a power law model. The most widely accepted curve for prediction of matrix crack growth dominated trends, the Paris power law, suggests that the fatigue resistance of the material continues to degrade at very high cycles, but that the trend gradually levels-out (Figure 53). However, within the range of 10^9 cycles no endurance limit is reached where the trend would be entirely flat.

Although the general lifetimes appear to be matrix crack dominated, in local regions, the fibers, the matrix, and interface are experiencing their own unique fatigue mechanisms. At relatively high stresses where instantaneous

matrix/interface damage shifts the load into the surrounding axially aligned (0°) fibers, the fibers immediately begin to fatigue at higher stresses. However, at medium stress levels the matrix/interface damage requires a number of cycles to initiate. This required initiation period allows the fibers to fatigue at the initial lower stress level, prior to higher levels after matrix cracking, resulting in higher cycles to failure. Two questions then arise. First, what happens when the stress levels are low enough that matrix/interface damage does not initiate at all; do the fibers fatigue and fail within an undamaged matrix? And second, when the type of loading shifts from the high to the medium to the low stress range, is there a corresponding shift in the fatigue resistance curve? One approach to answering these questions is through strain analysis.

Theoretically, the plies of a laminate may distribute an applied load but experience the same uniform strain: in a constant cyclic load fatigue test, the strain levels in each layer should be the same. As the initial strain levels have been documented for a majority of the tests, an initial-strain versus cycles-to-failure curve was plotted (see Figure 55). At high to medium strain levels, the lifetimes are similar for unidirectional and triaxial materials. At lower strain levels the curves separate, and the unidirectional material strains are roughly twice as high as the triaxial material strains for the same lifetime (see Figure 56). As the 0° and 90° triaxial

materials follow the same trend throughout, it would appear that neither the 0° nor the 90° fibers significantly affect the overall fatigue resistance, in terms of strain. When the ±45° plies fail, the associated modulus drop is apparently enough to increase the 0° ply strain to the point of failure.

Laminate theory can provide insight to the stress-strain behavior of the plies and the laminate. Appendix B provides such analysis for the various triaxial materials. This analysis indicates that when the ±45° plies in Material N [0/±45] statically fail, the 0° plies would remain intact. However, the associated 25% reduction in modulus would increase the overall strain 1.3 times, under constant load. Therefore, if such a laminate were under constant cyclic loading and suddenly lost the contribution of the ±45° plies, a similar reduction in modulus should be experienced: the E/Eo plot of Figure 43 confirms this. Analyzing the low strain region of Figure 56, ±45° ply failure would not increase the strain to a level which would cause 0° ply failure. Thus, a mechanism which degrades the strength of the 0° fibers must also be at work. The observed scrim associated damage to the 0° fibers could be such a mechanism (Figure 40, left).

Further testing is required to determine the effects of a strain level in the off-axis layers which is below a damage initiation limit for 10^9 cycles. Until then, the trends may be extrapolated to determine conservative allowable strains. The table below summarizes the intercepts of both the

10%/decade and the power law fatigue trend curves at 10^9 cycles: the % strain which the material should be able to withstand for 10^9 cycles (at R=0.1), about 25 years of wind turbine use.

The unidirectional materials typically show a higher strain-to-failure than the triaxial materials, and when analyzing the data with the power law model, the extrapolated trend shows roughly a 2:1 difference at 10^9 cycles. In contrast, when comparing the materials using the more conservative 10%/decade model, the strains to failure are roughly equivalent, with the exception of the relatively weaker 90° triax. All other material fatigue trends project a 0.2% to 0.3% initial strain to failure intercept at 10^9 cycles. A conservative approach would be to utilize the lower of the two predicted trends.

Table 2. Approximate Initial Far Field % Strain Which Would Cause Coupon Failure at 10^9 Cycles.

MATERIAL LABEL	10%/DECADE TREND	POWER LAW TREND
A	0.26	0.49
B	0.29	0.62
F & G	0.21	0.26
H & J	0.17	0.22
L	0.22	0.48
0° N (90° N)	0.24 (0.10)	0.14 (N/A)

Again, it should be pointed out that this table is based

on test data from coupon specimens, with a loading ratio of R=0.1, and that the values in the chart are extrapolations. The actual data are only available out to 40×10^6 cycles.
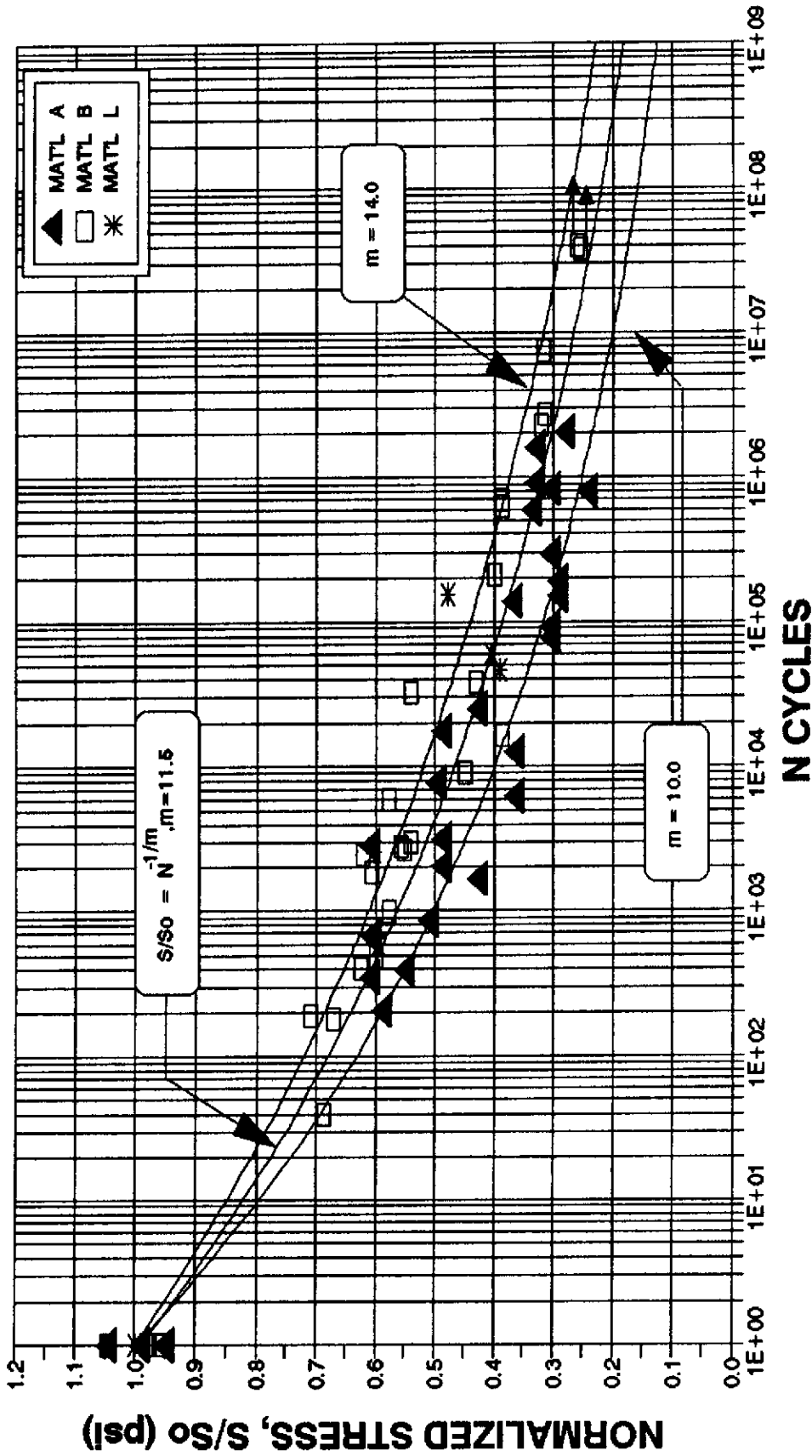
Figure 47. S-N Curve Summary of Unidirectional E-Glass Composites,
R = 0.1, 0.5 to 15 Hz.

116
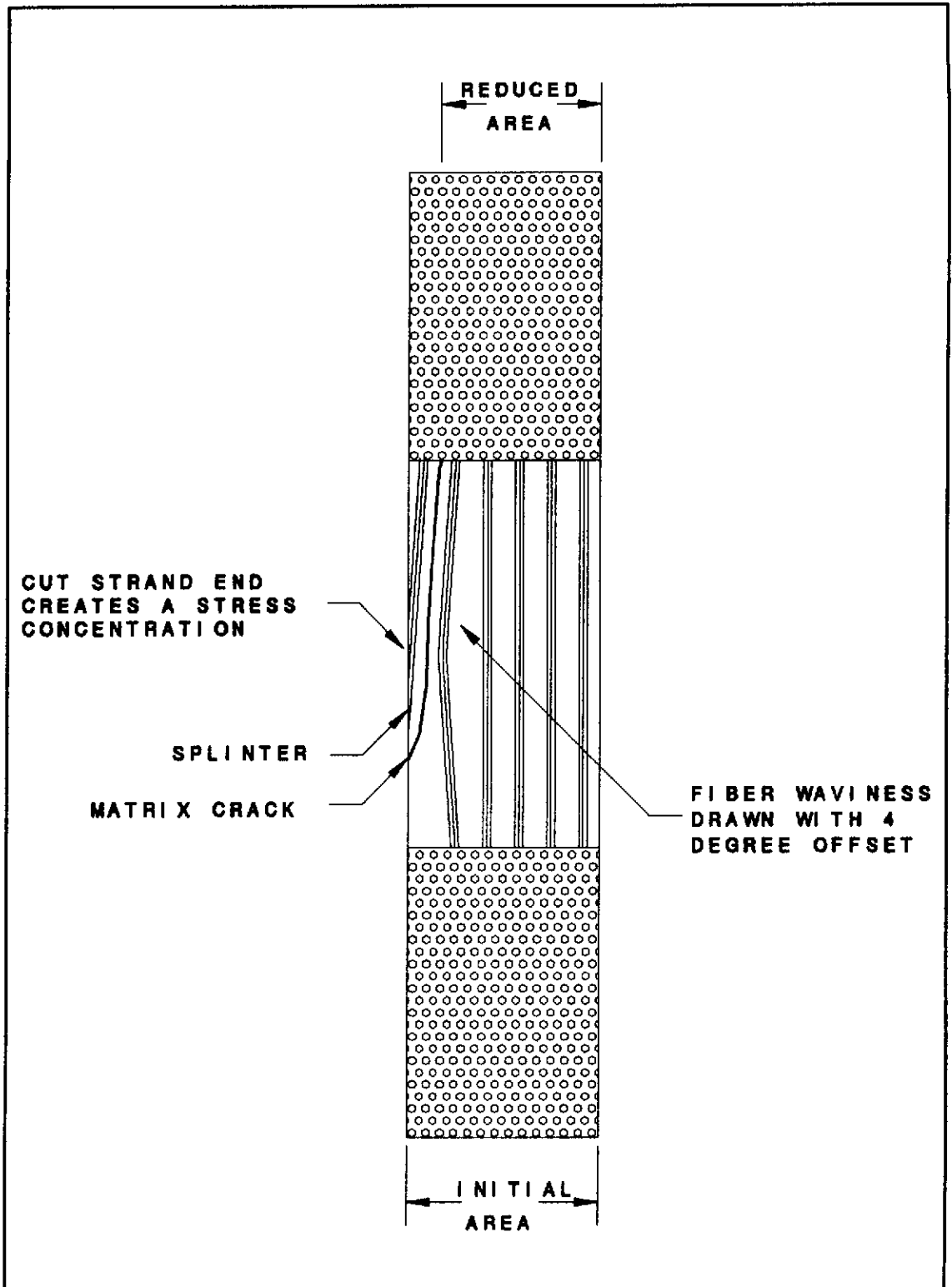
Figure 48. Splinter Geometry For Unidirectional Coupon Test.
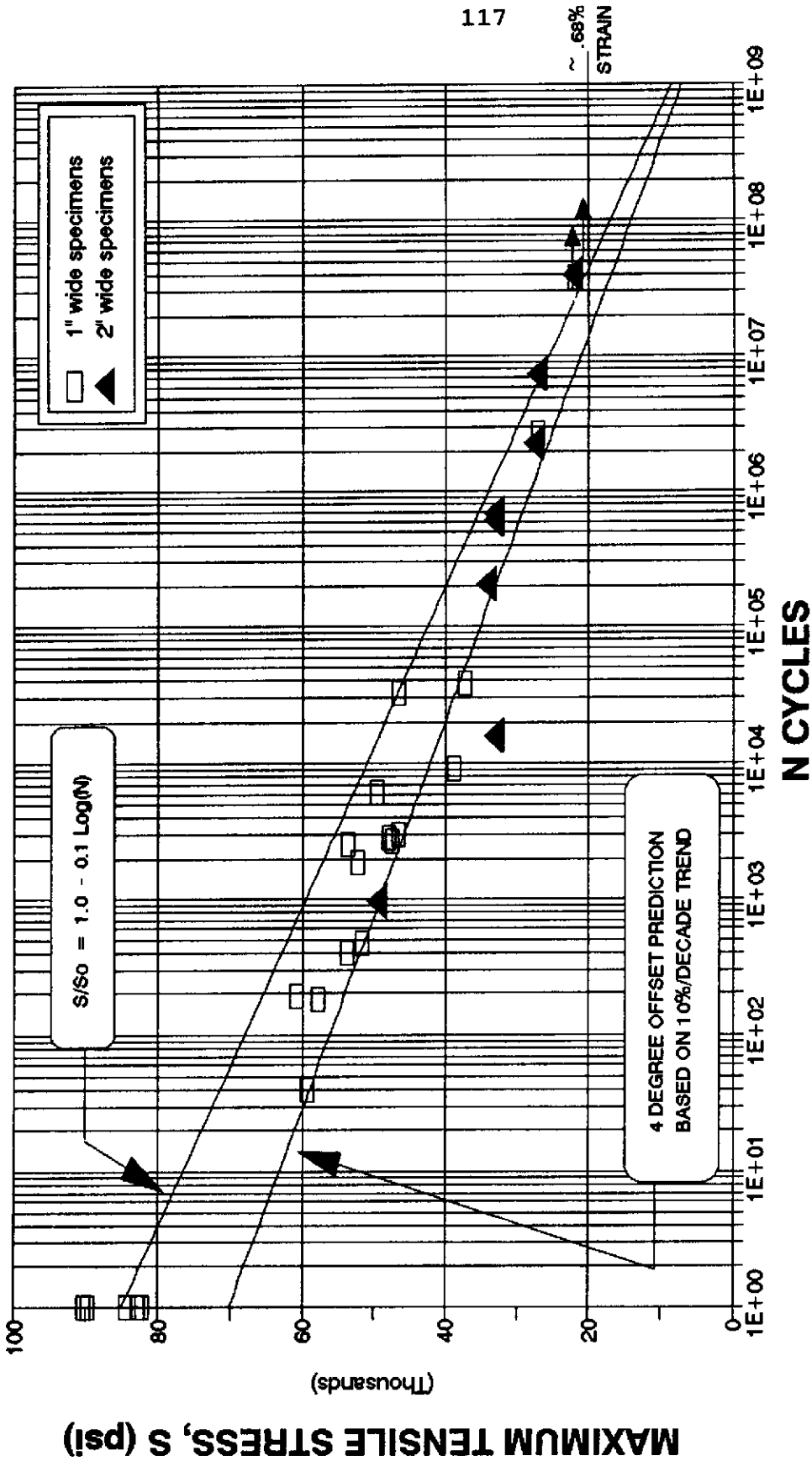
Figure 49. S-N Curve for Material B, Unidirectional E-Glass/Vinyl Ester, R = 0.1, 0.5 to 15 Hz.
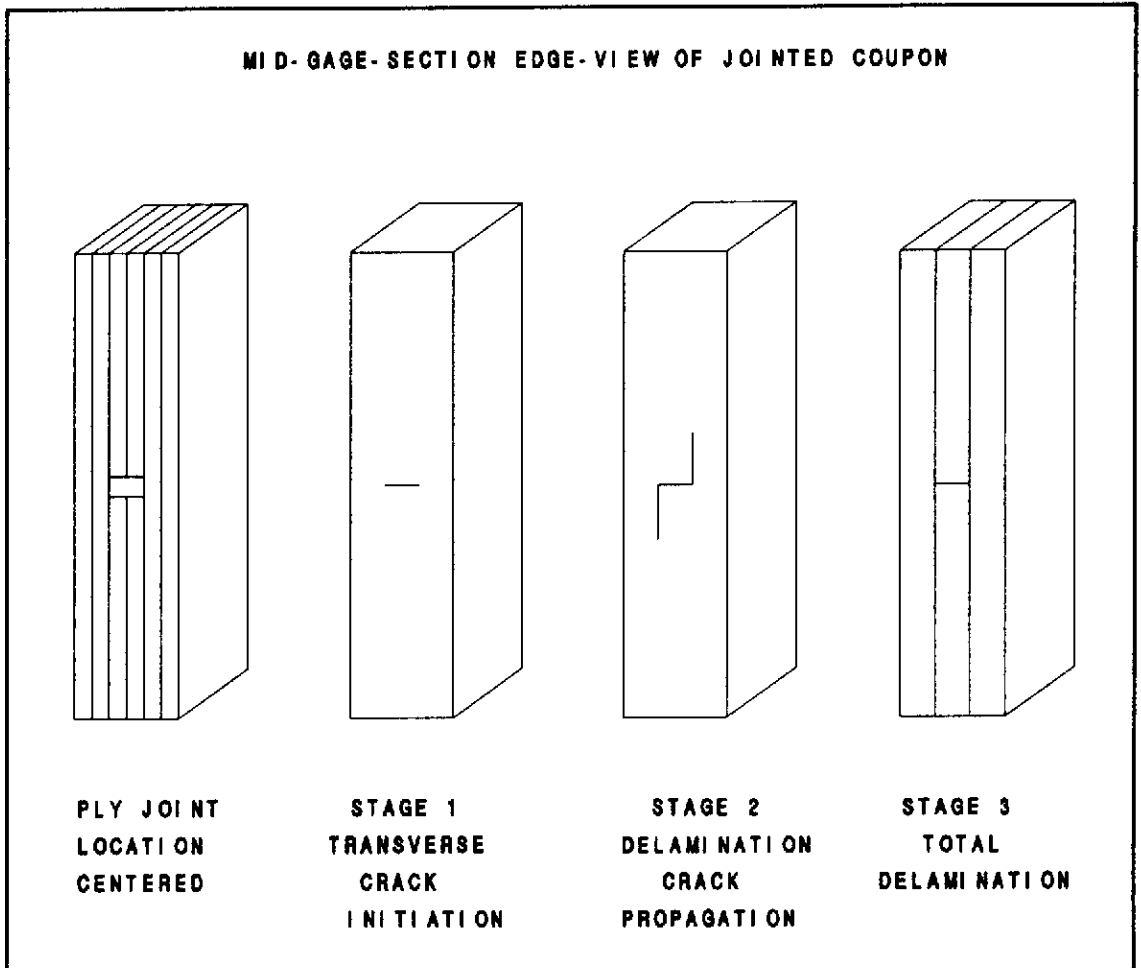
Figure 50. Typical Ply Delamination Pattern for Materials H and J.
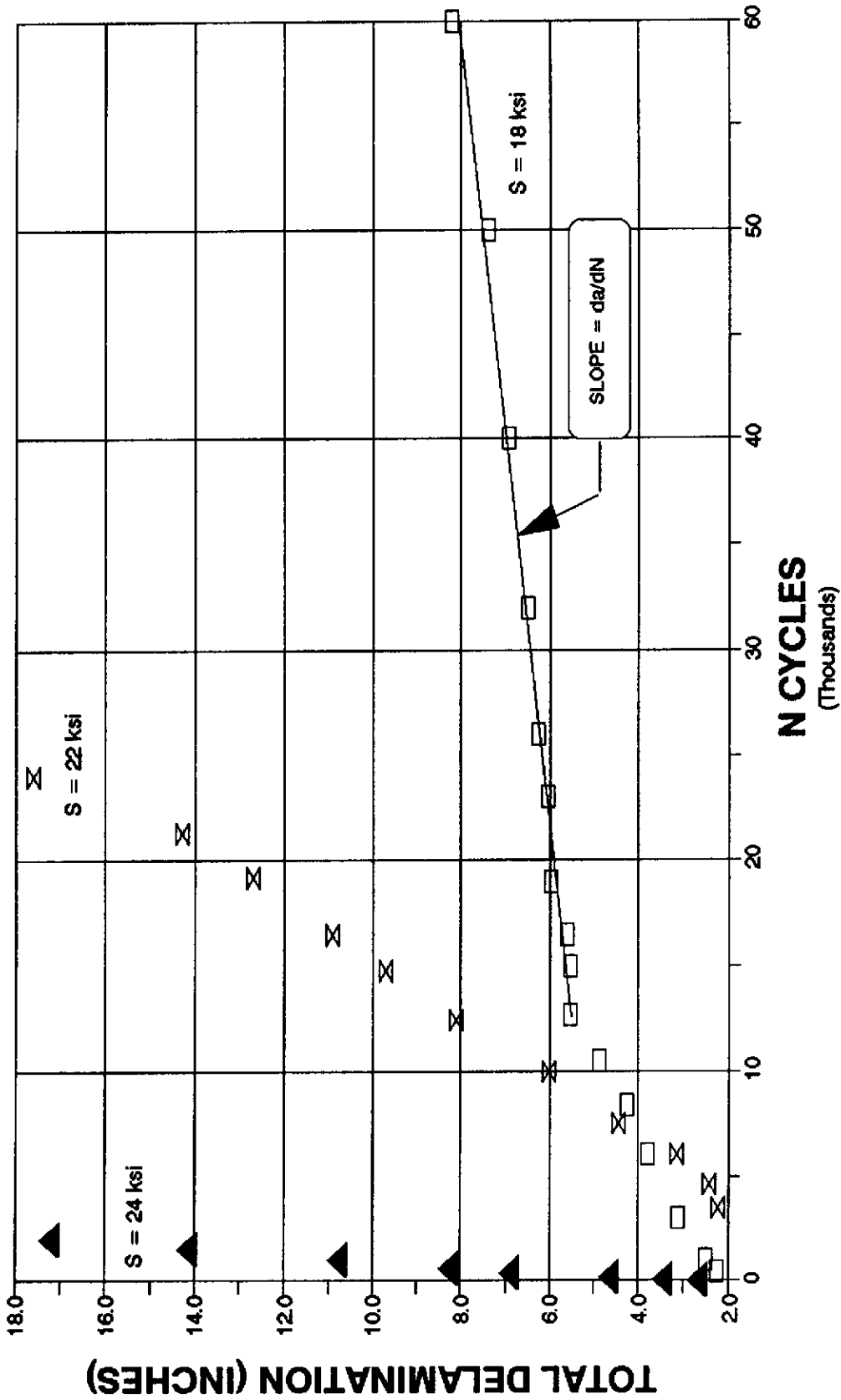
Figure 51. Typical Delamination Crack Length Data for Materials H and J, Triaxial
E-Glass/Polyester with a Center Ply Joint, R = 0.1, 5 to 15 Hz.

120
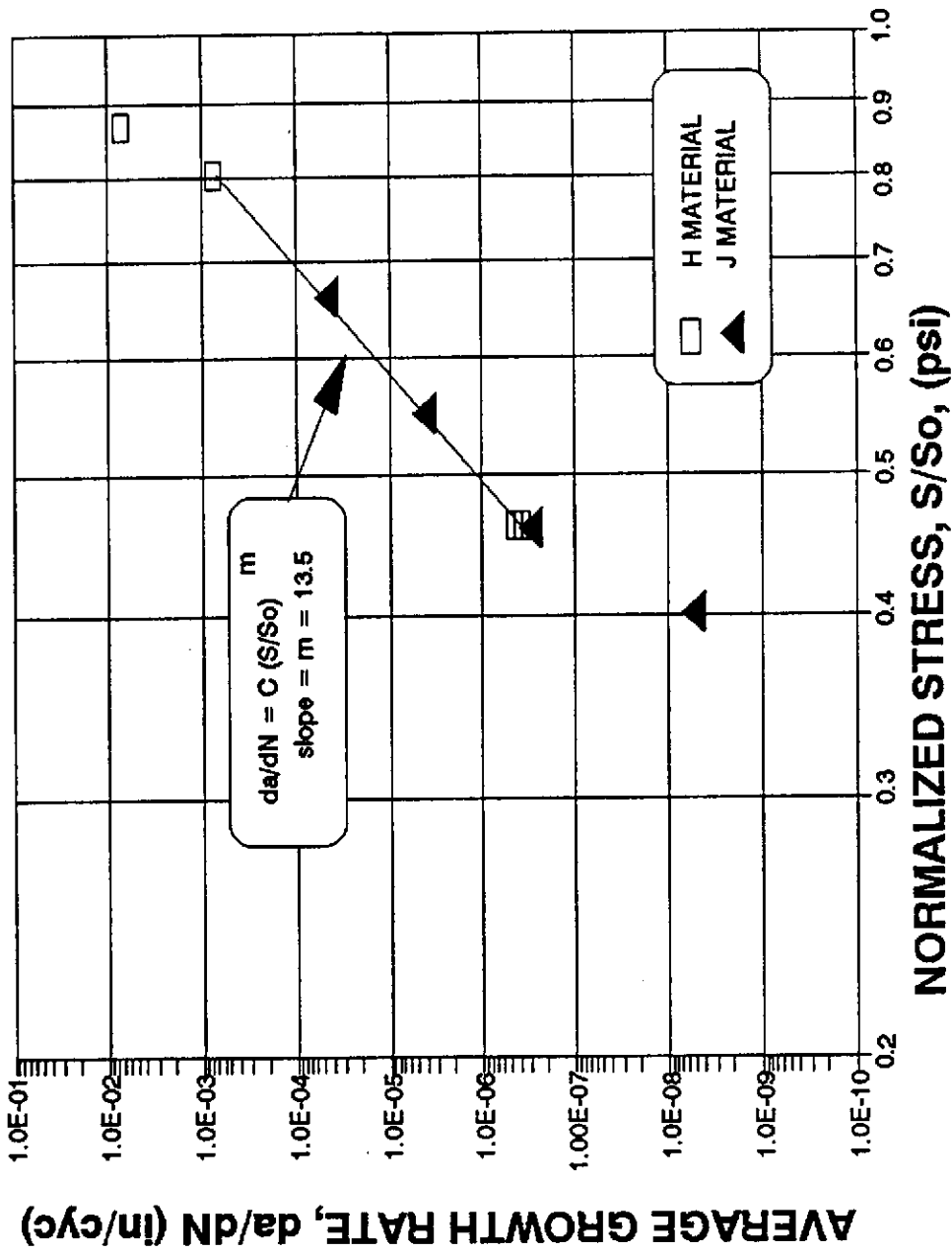
Figure 52. Delamination Crack Growth Data and Paris Law Fit for Materials H and J, Triaxial E-Glass/Polyester with a Central Ply Joint, R=0.1, 5 to 15 Hz.
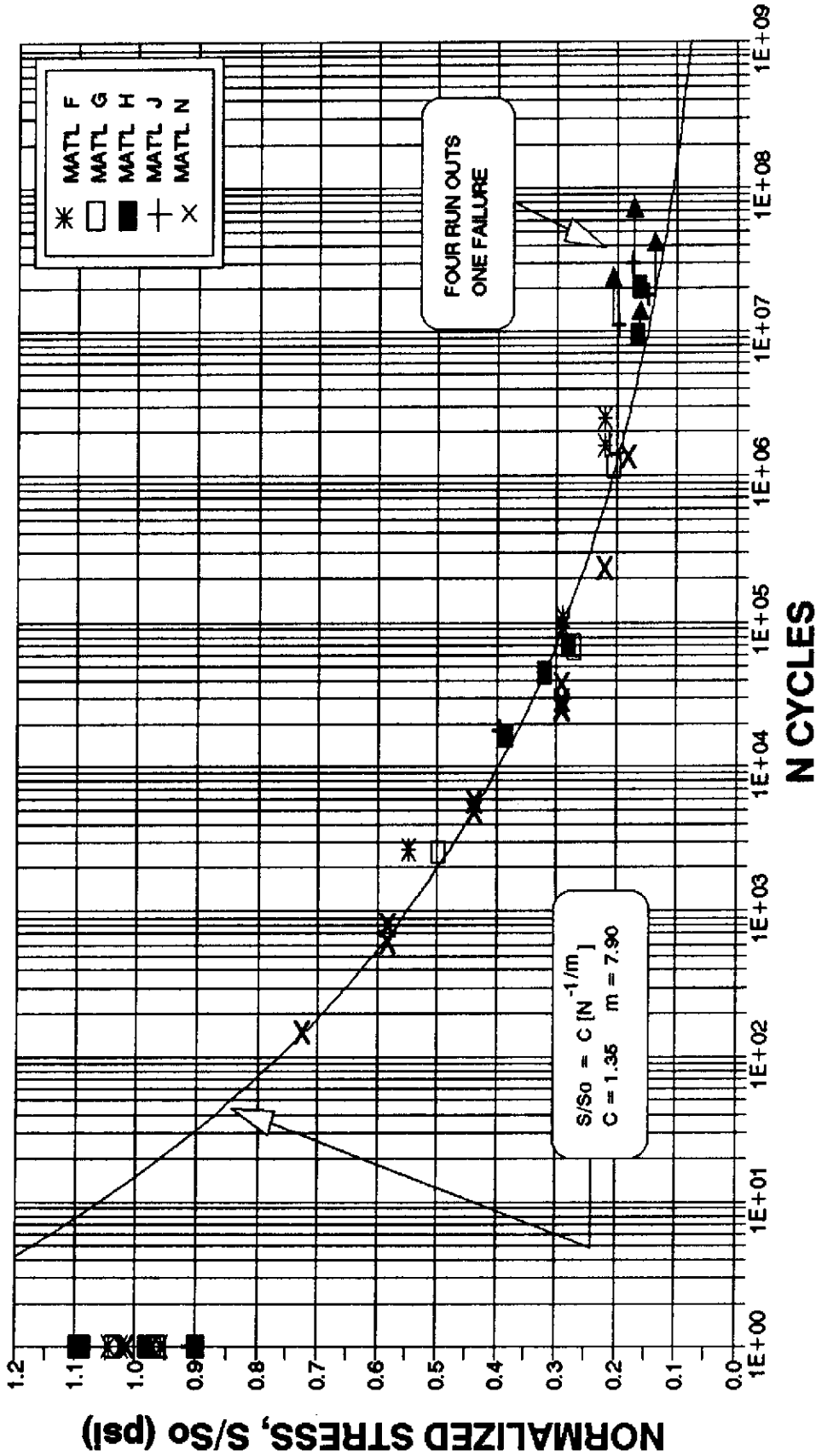
Figure 53. S-N Curve Summary of Triaxial [0/±45] E-Glass/Polyester, R = 0.1, 1 to 15 Hz.
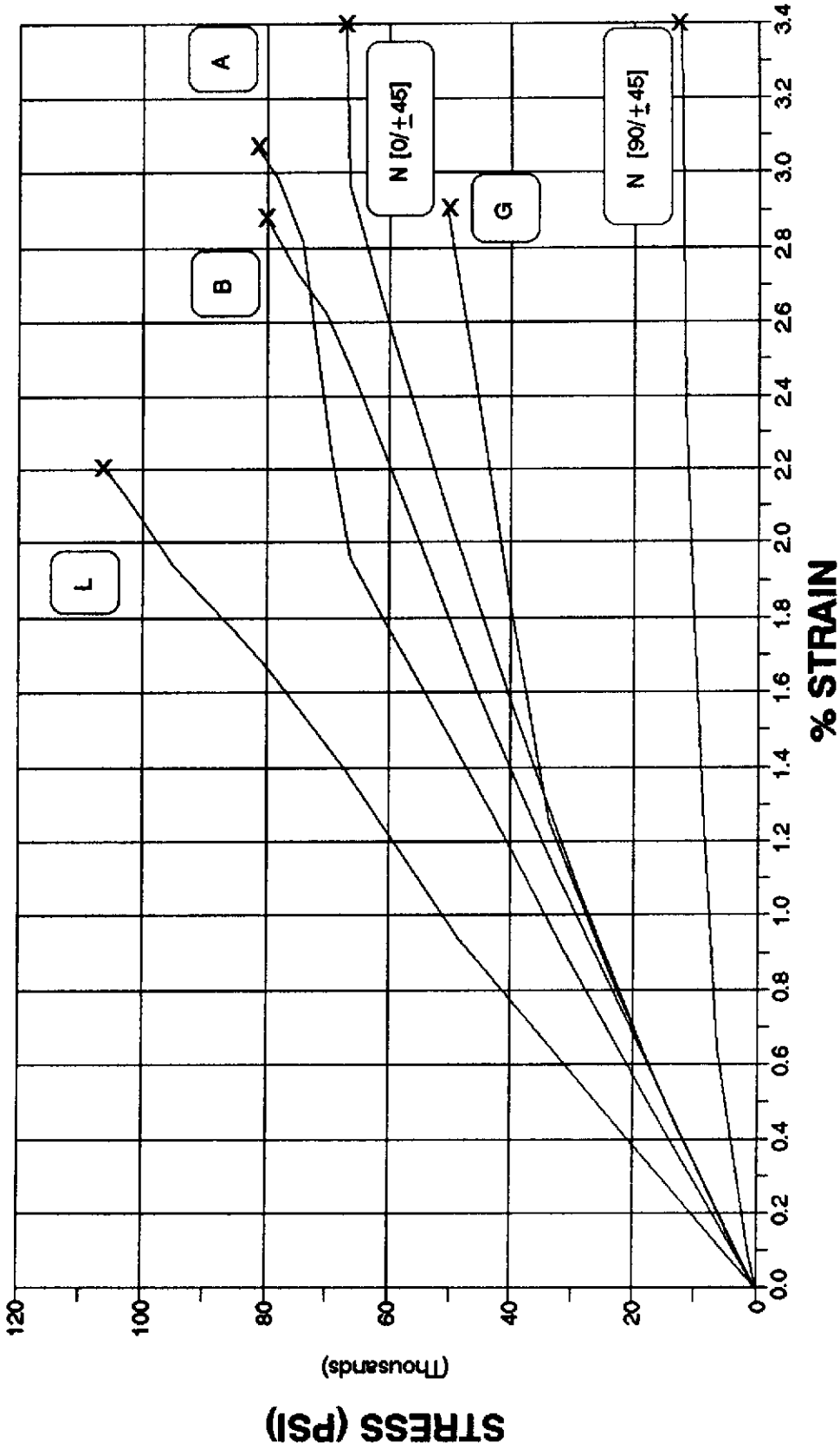
Figure 54. Comparison of Stress-Strain Curves for Various E-Glass Reinforced Materials, 4 or 5 inch Gage Length, 0.25 inch/sec Ramp Rate.
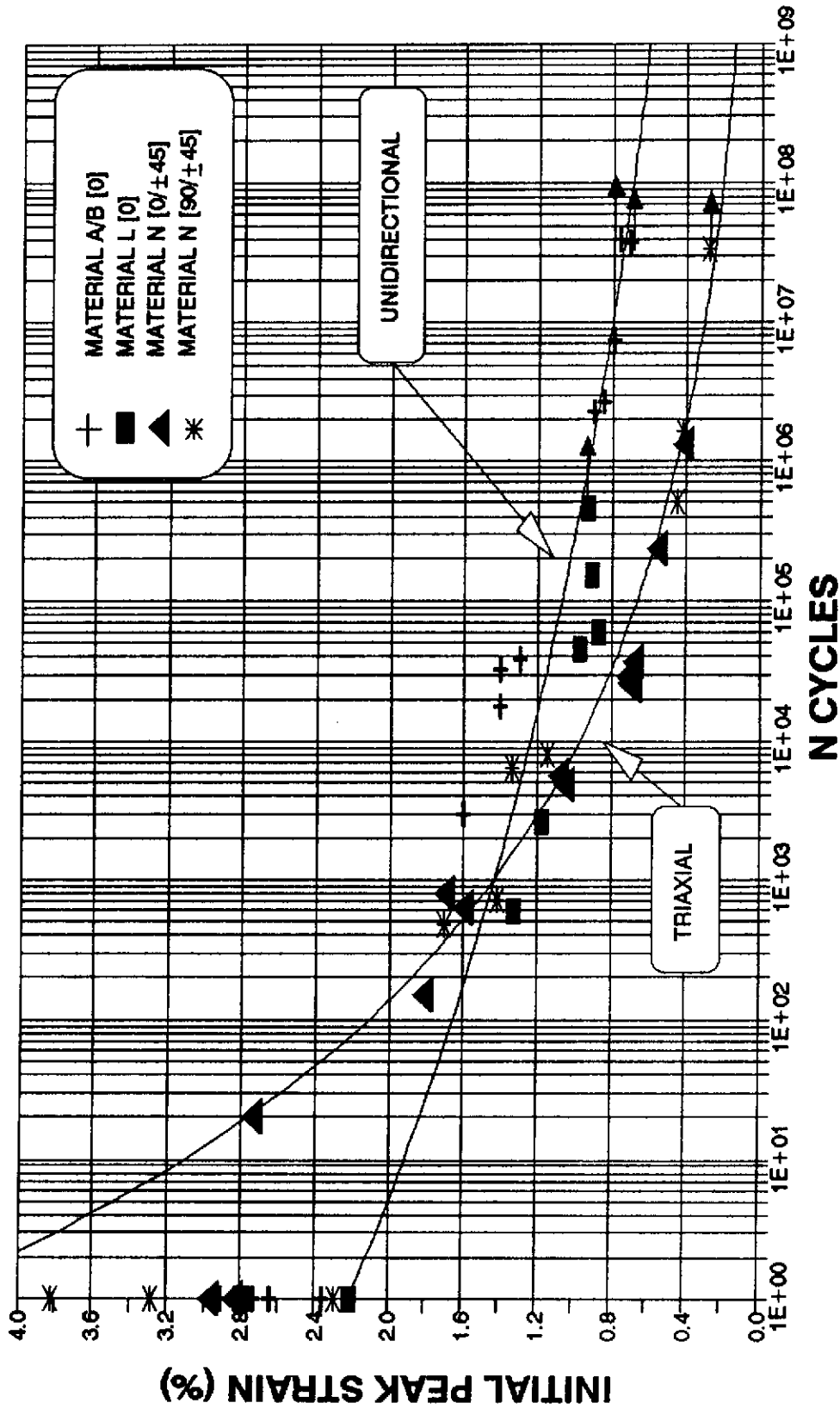
Figure 55. Initial-Strain-Level vs. Cycles-to-Failure Comparison of Various
E-Glass Composites, R = 0.1, 1 to 15 Hz.
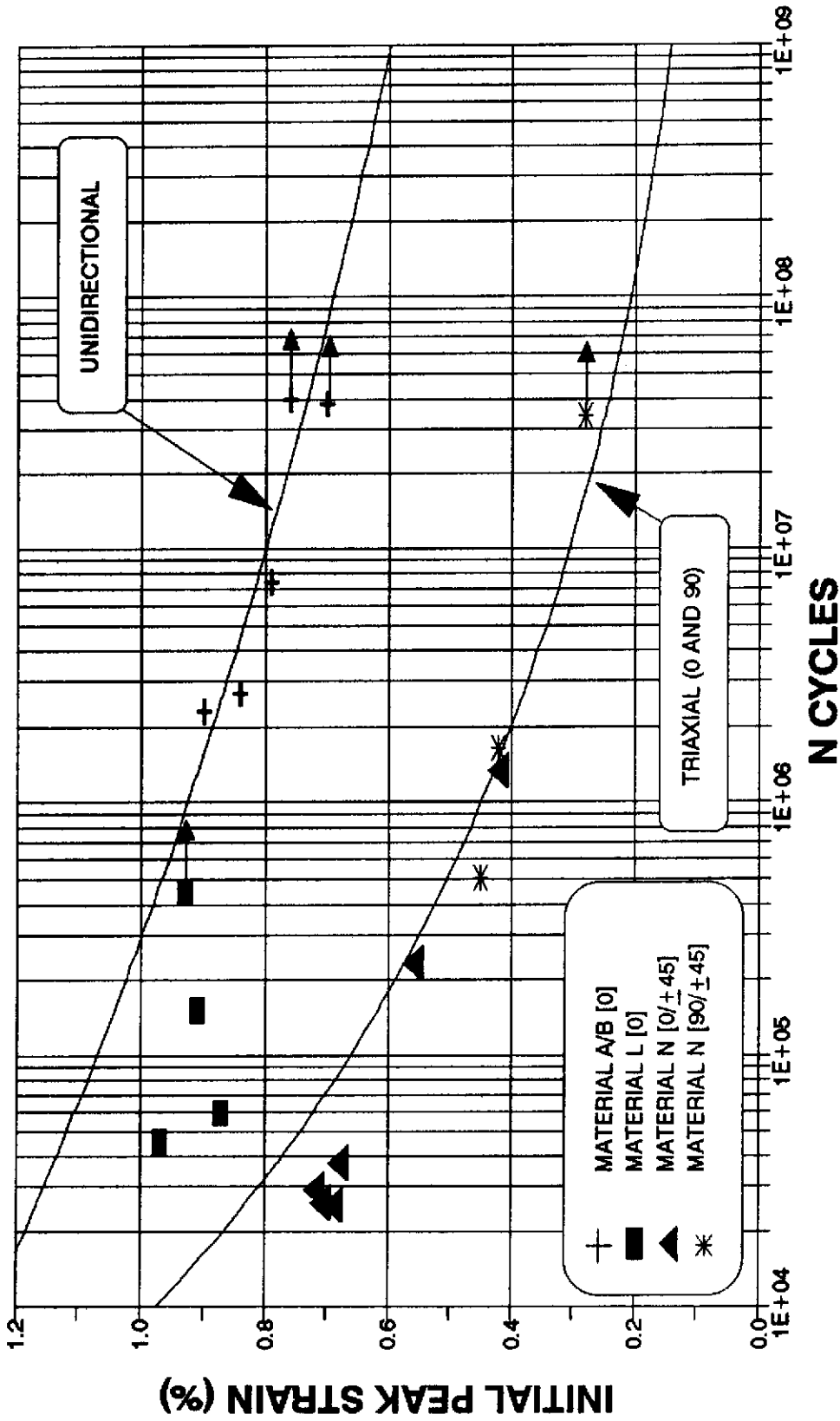
Figure 56. Initial-Strain-Level vs. Cycles-to-Failure Comparison of Various E-Glass Composites, R = 0.1, 1 to 15 Hz.

CHAPTER SEVEN

CONCLUSIONS AND RECOMMENDATIONS

Conclusions

The purpose of this study was to explore the long term cyclic fatigue behavior of fiberglass materials used in wind turbine blades. Test results are given for material stiffness reductions, damage and failure modes, and material lifetimes out to as many as 40 million cycles. Although this range is 40 times greater than existing studies, it represents only a fraction of the hundreds of millions of cycles a wind turbine blade is expected to experience in its lifetime. Still, these data allow a more rational choice of theoretical models for lifetime trends. These trends are then extrapolated to 10^9 cycles to provide an improved basis for blade design and material selection.

The following detailed conclusions relate only to the uniaxial tensile fatigue loading conditions which this study examined: sinusoidal loading at R = 0.1, and ambient conditions.

The unidirectional materials tested herein exhibited fatigue failure trends below the 10%/decade relationship established for this type of material. The reason for the apparent reduction in fatigue resistance may be due to poor

fiber alignment which leads to edge splitting. The data were better fit by a power law relationship which is anticipated where lifetime is dominated by the propagation of matrix/interfacial cracks. The power law exponents (m) which best fit the unidirectional data were in the range of 13.5. The value of 13.5 was also determined from direct measurements of the exponent during interply delamination growth of one of the triaxial reinforced materials. This agreement of exponent values provides a substantial basis for concluding that crack growth along the misaligned fibers dominates the specimen lifetime. However, a more detailed investigation is warranted as it is quite possible that larger composite structures would be much less sensitive to misalignment and edge effects, as is reported for aerospace structures.

Only minor differences were observed between unidirectional reinforced unsaturated vinyl ester and polyester thermoset matrices. More noticeable effects may occur with the multidirectional reinforced materials which are scheduled to be tested. However, as evident in the high cycle results to date, there is little justification for use of the more expensive vinyl ester matrix.

Triaxial reinforced laminates behaved quite differently from the unidirectional composites. The S-N curves for the [0/±45] triaxial composites were uniformly steeper that those for the unidirectional materials. Also, triaxial material failures at high cycles occurred at much lower initial strain

levels than for unidirectional materials. As the initial strain-to-failure ranges were similar for both [0/±45] and [90/±45] triaxial tests, it appears that the scrim induced damage to 0° fibers creates a situation where failure of the ±45° plies leads to rapid failure of the laminate. Additional tests for various types of triaxial reinforcement would be beneficial to finding a material where the failure would be dominated by the 0° reinforcement.

Fatigue tests were also performed on geometries which contained ply terminations and joints. Results of these tests indicate that such discontinuities do not have a noticeable effect on the overall fatigue life. The strength reduction trend from the static tensile limit was the same for all the triaxial materials tested, regardless of this geometric factor.

The triaxial materials also exhibited a significant degradation in stiffness due to fatigue cracking of the ±45° plies. Modulus decreases in the range of 10-40% for [0/±45] and 40-70% for [90/±45] triaxial materials were typical. Unidirectional materials showed much lower reductions, on the order of 10-20%. Overall, the use of triaxial reinforcement is likely to be detrimental to blade performance over the entire range of lifetimes as compared to unidirectional reinforcement, under these loading conditions.

The data provided herein have established a basic foundation for future research in the area of long term cyclic

fatigue behavior of glass fiber reinforced composites. It is the author's sincere hope that such information will help wind turbine blade designers create longer lasting, higher efficiency blades.

Recommendations

The current data have established the basic strength reduction patterns due to cyclic fatigue loading at R=0.1. Actual blade loading conditions should be reviewed in order to provide either a worst case, or a spectrum of load conditions from which this research can proceed: programming of the MTS unit would enable the operator to achieve a loading spectrum for coupon tests.

Complications to the unidirectional material behavior have been incurred by poorly aligned fibers. Either materials with higher degrees of fiber alignment should be obtained, or else the coupon edges should be modified to reduce edge splitting. A possible modification might be to apply a glass-mat/epoxy mixture along the coupon edges. Either method would enable a more confident analysis of the unidirectional trends. Analysis of the data might then answer such questions as (1) does the unidirectional material actually follow the 10%/decade reduction trend, and (2) does the 10%/decade rule apply to the high cycle range? Additional long term fatigue tests would further clarify whether the high cycle curve trends predicted herein are valid, and whether the intersections of the predicted curves actually exist.

As stroke calculations (Do/D) appear to follow the pattern of the strain based modulus, future testing would clarify their relationship; the stroke/strain ratio is theoretically the actual gage length. Specific documentation of strain levels at multiple locations coupon-wide would reduce the effect that nearness to damage had on the single location reading. When coupled with precise data documentation of stroke, damage initiation and propagation locations, and measured grip slippage, the strain output from each test would aid in clarifying the behavior of the active gage length, and the local and overall moduli. These comparisons will depend heavily on accurate data for the initial dynamic strains and strokes at the proper loading conditions.

The use of small coupon fatigue data to design blades and select materials requires justification. Larger coupons cut from actual blades should be studied for comparison. Such tests would examine the static and fatigue behavior of the actual composite blade material (actual blade material thickness, laminate stacking sequences, fiber contents and orientations, with actual fabrication flaws and defects), not material facsimiles. In conjunction with this type of substructure testing, it is essential to establish actual blade data: load conditions at specific blade damage sites from field studies. These data would then be applied to determining suitable loading conditions for the material

fatigue behavior studies of coupons cut from those areas.

Typical fatigue trends for thermoset matrix materials tend to converge at high cycles; although epoxies exhibit higher initial strength, the fatigue trend is steeper and rapidly approaches the trend established by the polyester. However, the introduction of a more expensive reinforcement with a higher fatigue resistance may be cost effective. For example, replacing some of the E-glass fiber reinforcement with carbon fiber reinforcement would produce a stiffer, more fatigue resistant, and lighter blade. Even with the increased initial costs associated with materials and manufacturing, the higher efficiency blade might offset the overall cost. Research and laminate theory calculations could determine effective fiber content and laminate scheduling for various fiber/matrix materials. Fatigue testing could then provide information on the relative improvement in fatigue resistance.

REFERENCES

REFERENCES

1. F.S. Stoddard, "Field Problems With Wind Turbine Rotors", presented to committee on Assessment of Research Needs for Wind Turbine Rotor Materials Technology, National Academy of Sciences, Washington D.C. November 7, 1989.

2. Solar Energy Research Institute, "Wind Energy Technical Information Guide", SERI/SP-220-3555, DE89009462, December 1989.

3. North Wind Power Company, Promotional literature, 1978.

4. J.T. Ryder, "Life Prediction Methodologies for Aerospace Composite Materials", presentation at Montana State University, Bozeman, Montana, May 4 1990.

5. T. Alfrey, E. Gurnee, <u>Organic Polymers</u>, Prentice Hall Inc., 1967.

6. P.K. Mallick, <u>Fiber Reinforced Composites</u>, Marcel Dekker Inc., New York, 1988.

7. Engineered Materials Handbook Volume 2 "Engineering Plastics", ASM International, 1988.

8. Chapter 2 "Unsaturated Polyester Resins" article by Ivor H. Updegraff, American Cyanamid Corporation, Stamford CT.

9. D. Huang, "Tensile Fatigue of Short Fiber Reinforced Composites", MIT Doctoral Thesis, June 1981.

10. N.G. McCrum, C.P. Buckley, C.B. Bucknall, <u>Principles of Polymer Engineering</u>, Oxford Science Publications, 1988.

11. Material Properties List, Class handout J.F. Mandell, Montana State University, 1990.

12. Z. Hashin and A. Rotem, "A Fatigue Failure Criterion For Fiber Reinforced Materials", Journal of Composite Materials , V17, p. 448, 1973.

13. J.F. Mandell, D.D. Huang, F.J.McGarry, "Tensile Fatigue Performance of Glass Fiber Dominated Composites", Composites Technology Review, V3, p. 96, 1981.

REFERENCES-Continued

14. L. Malvern, *Introduction to the Mechanics of A Continuous Medium*, Prentice Hall, 1969.

15. R. Tobler, D. Read, "Fatigue Resistance of a Uniaxial S-Glass/Epoxy Composite at Room and Liquid Helium Temperatures." Journal of Composite Materials, V10, p. 32, 1976.

16. J.F. Mandell, F. McGarry, A. Hsieh, and C Li, "Tensile Fatigue of Glass Fibers and Composites with Conventional and Surface Compressed Fibers", Polymer Composites, V6, 168, 1985.

17. J.F. Mandell, "Fatigue Behavior of short fiber composite materials, submitted 9/86 for chapter 9 of *The Fatigue Behavior of Composite Materials*, Elsevier Sci. Pub. Co. (in press).

18. A.J. Kinloch, R.J. Young, *Fracture Behavior of Polymers*, Elsevier Applied Science, N.Y., 1983.

19. H.T. Hahn, R.Y. Kim, "Fatigue Behavior of Composite Laminate", Journal of Composite Materials, Vol. 10, 1976, p. 156.

20. J.F. Mandell, "Fatigue Behavior of Fibre-Resin Composites" Chapter 4, *Developments in Reinforced Plastics-2*, G. Pritchard Ed.

21. W. Brostow, R. Coneliussen, *Failure of Plastics*, Hanser Publishers, Munich, 1986.

22. J.F. Mandell, F.J. McGarry, D.D, Huang, C.G. Li, "Some Effects of Matrix and Interface Properties on the Fatigue of Short Fiber Reinforced Thermoplastics" Proc 36th Annual Conf. Reinf. Plast./Composites, SPI, 1982, Paper 23-C.

23. J.F. Mandell, Urs Meier, "Effects of Stress Ratio, Frequency, and Loading Time on the Tensile Fatigue of Glass-Reinforced Epoxy." *Long Term Behavior of Composites*, ASTM STP813, 1983, p. 55.

24. R.M. Hertzberg, J.A. Manson, *Fatigue of Engineering Plastics*, Academic Press, N.Y., 1980.

25. J.F. Mandell, J.Y. Tsai, "Effects of Porosity On Delamination of Resin-Matrix Composites", Wright Research Development Center Report Number WRDC-TR-89-3032, April 20 1990.

REFERENCES-Continued

26. R.W. Thresher, "The Status of Wind Turbine Structural Loading and Fatigue Research at SERI", presented to The National Academy of Sciences Review Panel on Wind Turbine Materials, Washington D.C., 1989.

27. T. Tanimoto, S. Amijima, "Progressive Nature of Fatigue Damage of Glass Fiber Reinforced Plastics", Journal of Composite Materials, V9, p. 380, 1975.

28. Engineered Materials Handbook Volume 1 "Composites", ASM International, 1988.

29. D.J. Williams, Polymer Science and Engineering, Prentice Hall Inc., 1971.

30. H. Allcock, F. Lampe, Contemporary Polymer Chemistry 2nd Ed., Prentice Hall, 1990.

31. S. Gaggar, L. Broutman, "Crack Growth Resistance of Random Fiber Composites", Journal of Composite Materials, Vol 9., 1975.

32. J.A. Manson, R.W. Hertzberg, "Fatigue Failure in Polymers" CRC Critical Reviews In Macromolecular Sciences, The Chemical Rubber Company, V. 1, Issue 1, 1972.

33. R. Talreja, Fatigue of Composite Materials, Technomic Pub. Co. Inc., Lancaster PA., 1987.

APPENDICES

APPENDIX A

TEST EQUIPMENT AND PROCEDURES

The MTS 880 machine operates in a closed-loop servo controlled fashion and is comprised of three basic units: the hydraulic pump, the master control unit, and the load frame. As this machine is designed for possible operation in three control modes, accurate monitoring of load, strain, and displacement are possible throughout the test. The strain on the specimen surface is measured through a strain transducer which is then attached to the MTS control panel. Foil strain gages may be bonded directly to the surface or, as in this case, an extensometer device based on strain gages is attached to the specimen. After the extensometer unit is connected to the control unit, calibration is performed with a mechanical micrometer such as the Boeckeler Instruments model 4-MBR.

Displacement is measured through an electronic transducer within the hydraulic actuator unit. With the 880 system, the linear velocity displacement transducer (LVDT) is attached to the bottom of the loading train. The load train begins with a hydraulic piston (actuator), on top of which is attached the lower hydraulic grip housing (see Figure 47). The lower hydraulic grip housing contains removable jaws which clamp onto the test specimen, fixing it to the load train. When hydraulic grip pressure is activated, the housing moves vertically which mechanically forces the jaws to slide horizontally open or closed due to their wedge-shaped design. The material is clamped on its upper end by an identical upper hydraulic grip. (It has been noted that the gravitational

effects on the grip housings may be slightly increasing the gripping pressure on the lower grip, while slightly relaxing the gripping pressure on the upper grip).   The upper grips are then attached to a previously calibrated force transducer (load cell) and supported by the cross-head. During a test, the upper load train (cross head, load cell, and upper grips) remains fixed, while the lower half (the lower grips and the actuator) cycle up and down. Typically, materials with well documented mechanical response are initially tested to verify that both the machine and the operator are functioning properly.

Static Test Method

As the static tensile strength is plotted at one cycle to failure on the S-N curve, static strength tests were performed to establish the fatigue test load range.   ASTM D 3039-76 recommends that static ramp tests (constant displacement rate to failure) be performed at a material strain rate of .02 in/in / min. Equation 6.1 calculates an equivalent displacement rate to be .002 inch/sec for a 6 inch gage length.

$$STRAIN\ RATE = .02\left(\frac{inch}{inch}/\min\right)$$

$$= .02\left(\frac{DISPLACEMENT\ inch}{GAGELENGTH\ inch}/\min\right) \qquad \textbf{A.1}$$

$$RAMP\ RATE = .02\left(\frac{DISP}{GAGE}/\min\right)*6\,(inch)\ GAGE*\left(\frac{\min}{60\ sec}\right)$$

$$= .002\left(\frac{inch}{sec}\right)$$

Initial tests indicated that the suggested standard rate resulted in lower UTS estimates than at the higher strain rate in fatigue tests due to the strain rate sensitivity of the material. Equation 6.2 was developed as a method to determine a ramp rate more in line with the strain rate imposed by a 10 hertz frequency. The result for a 6 inch gage length with a 2% strain to failure requires a ramp rate on the order of 5 in/sec or a strain rate of 50 in/in/min. Although the example assumes a 2% strain value, the static test value should then be used to validate that assumption or adjust the ramp rate.

$$RAMP\ RATE = \frac{(gage\ length)*(strain\ tofailure)}{(\frac{.25 cycles}{tofailure})*(\frac{1\ sec}{10\ cycles})} \quad \textbf{(A.2)}$$

$$= \frac{6*.02}{.025} = 5(\frac{inch}{sec})$$

Static tests were performed by placing the MTS test controller panel in 'stroke control mode' with the function panel set for 'ramp test'. Dry runs with no coupon in the load train verify the performance of the machine to complete the full 0.5 inch stroke in the 0.1 seconds (ramp rate 1) setting. Once satisfied that the machine is functioning properly, the operator engages the safety shutoff limits for maximum and minimum displacements, and zeroes the load and extensometer display readings. The coupon is then placed in the exact center of the hydraulic grips to provide uniform loading. The brackets which locate the exact center are then

removed to prevent damage. Before activating the hydraulic grips, the grip pressure is checked to make certain it is at a maximum 1200 psi. Higher pressure tends to crush the tab region rather than merely prevent slippage. With the specimen gripped, the zero load readings are recorded, and a low stress modulus check is performed. The operator at this point should not re-zero the readout display. As in metals testing, the extensometer and grips may initially slip, and/or the specimen may creep. With this in mind, the operator should take sufficient readings to distinguish between slip and creep. (Allowing time for material relaxation at zero load may help strain and stroke readings to return to zero). If slippage does occur, it can be mathematically removed later.

After documentation of the zero load readings, the function generator is engaged by depressing the start button. The specimen then fails rapidly. After failure, the maximum load and strain stored in the MTS memory are recorded. The specimen is removed, the machine deactivated, and the test documentation is completed.

Fatigue Test Method

Fatigue tests are initiated in the same manner as the static tests, but in load control. The function generator is set in local control, sine wave, and the ramp rates at 1, 5, 10, or 15 hertz depending upon the relative time to failure of tests. (Although lower frequencies may be used in the short time tests in order to gather data, perhaps a more accurate

method would be to run single cycle impulses at 10 or 15 hertz, and record the maximum readouts from memory). Initial static and dynamic modulus checks are made, and after the test has stabilized, the extensometer is removed to prevent damage. The test may be stopped at intervals to provide static modulus checks, but the operator must document the stopping and starting well, as typically load spikes may occur on the initial restart. Dynamic modulus checks with the machine still running may also be performed. In either case the operator should keep in mind that permanent strain may have occurred and that the peak to peak values of load and strain should be used to calculate the modulus, not the global maximum reading.

APPENDIX B

LAMINATE THEORY COMPARISON

Basic Material Properties

The unidirectional material tests can be used to establish basic material property data such as;

V_f = 0.3 :Material A
       Tensile modulus = 3.13 msi
       UTS = 82 ksi
       Fiber modulus = E_L/V_f = 3.13/0.3= **10.4 msi** = E_{1f}
V_f = 0.5 :Material L
       Tensile modulus = 4.76 msi
       UTS = 108 ksi
       Fiber modulus = E_L/V_f = 4.76/0.5 = **9.52 msi** =E_{1f}

Other data required for laminate theory analysis can be found in References such as 6, 24;

Fiber poisson ratio   = **0.22**   = v_f
Fiber transverse modulus = **10.4 msi**= E_{2f}
Matrix tensile modulus   = **0.5 msi**= $E_{1,2m}$
Matrix poisson ratio   = **0.35**   = v_m
Matrix UTS   = 3750 psi

Laminae Analysis

Analysis of the laminae properties with respect to the fiber axis, the 11,22,33 reference frame, where 11 is the fiber direction, may be performed using the equations as shown below [6]:

$$E_{11} = E_{1f}*V_f + E_{1m}*V_m$$

$$E_{22} = \frac{E_{2m}\ (1+\xi\eta_2 V_f)}{1 - \eta_2 V_f}$$

$$\text{where } \eta_2 = \frac{E_{2f}/E_{2m}-1}{E_{2f}/E_{2m}+\xi} \qquad \xi=1,2$$

$$G = \frac{E}{2(1+v)} \quad \text{for both } f,\ m$$

$$\text{where } G_{12} = \frac{G_f*G_m}{G_f*V_m + G_m*V_f}$$

$$v_{12} = v_f*V_f + v_m*V_m$$

Materials F and G Analysis

The triaxial Materials F and G have V_f = 0.3 and are analyzed using the Material A fiber modulus (10.4 msi). The results of the laminae equations are;

$$E_{11} = 3,470,000 \text{ psi}$$
$$E_{22} = 874,527 \text{ psi}$$
$$G_f = 4,262,295 \text{ psi}$$
$$G_m = 185,185 \text{ psi}$$
$$G_{12} = 259,714 \text{ psi}$$
$$v_{12} = 0.245$$

The modulus of the off-axis laminae with respect to the loading direction (the x,y,z coordinate frame), can be found from;

$$\frac{1}{E_{xx}} = \frac{COS^4\theta}{E_{11}} + \frac{SIN^4\theta}{E_{22}} + \frac{1}{4}(\frac{1}{G_{12}} - \frac{2v_{12}}{E_{11}})SIN^2(2\theta)$$

When θ = 45;

$$4\frac{E_{11}}{E_{xx}} = 1 + \frac{E_{11}}{E_{22}} + \frac{E_{11}}{G_{12}} - 2v_{12}$$

Using the above laminae information, E_{xx45} = 0.925 msi. Application of this information to a triaxial laminate which contains 50% ±45°, and 50% 0° reinforcement determines the overall laminate modulus

$$E_{xx} = 0.5 \ E_{11} + 0.5 \ E_{xx(45)}$$
$$= 2.25 \text{ msi}$$

This theoretical value compares well with the actual measured

values for Materials F and G which were 2.54 ± 17% msi.

A laminate theory program was established by Jim Schutz
to perform just such calculations, and provide quick stress
distribution calculations. Of the many equations and sources
on this subject, his program refers to Jones' "Mechanics of
Composite Materials" as a primary reference.

The thin four ply region of Materials F and G were 0.20
inch thick. For the application of a $[0/\pm45/0]_s$ laminate with
individual ply thicknesses of 0.025 inch, the program yields
the following properties;

$$
\begin{aligned}
E_{11} &= 3,470,000 \text{ psi} \\
E_{22} &= 874,527 \text{ psi} \\
v_{12} &= 0.311 \\
G_{12} &= 325,682 \text{ psi} \\
E_{xx} &= 2,274,000 \text{ psi} \\
E_{yy} &= 1,096,000 \text{ psi} \\
v_{xy} &= 0.487 \\
G_{xy} &= 649,800 \text{ psi}
\end{aligned}
$$

According to this program, the ±45° plies will fail in
transverse tension at an applied stress of 28.3 ksi, at which
point the various laminae stresses are;

$$
\begin{aligned}
\text{0° Ply:} \quad & \sigma_{11} = 42,580 \text{ psi} \\
& \sigma_{22} = -1,966 \text{ psi} \\
& \tau_{12} = 0 \text{ psi} \\
\text{45° ply:} \quad & \sigma_{11} = 12,240 \text{ psi} \\
& \sigma_{22} = 3,750 \text{ psi} \quad \longleftarrow \text{Failure} \\
& \tau_{12} = \pm6,029 \text{ psi}
\end{aligned}
$$

At this stress level, equivalent to 1.1% strain, cracks would
develop in the ±45° plies parallel to the fiber direction.
The transverse and shear moduli of the ±45 plies would be
effectively reduced to zero, whereas the longitudinal modulus

would remain relatively unchanged. A conservative estimate assumes the ±45° plies no longer contribute to E_{xx}, and that the laminate modulus therefore drops from 2.27 to 1.74 msi. This correlates fairly well with Figure 26, which indicates that the modulus begins to drop from 3.0 msi at roughly 1.25% strain, reaching a modulus of about 1.7 msi prior to total failure. Under constant displacement, the reduction in modulus would result in a reduction of total stress from 28.3 to 21.7 ksi. The stress carried by the 50% 0° reinforcement increases from 42.58 to 43.39 ksi. Failure occurs when the 0° fiber stress reaches 82 ksi (Material A) under a total or laminate stress of 41 ksi. Experimental UTS values average 54 ksi, so that the prediction totally excluding the ±45's is conservative.

Materials H and J Analysis

The triaxial Materials H and J have V_f = 0.3 and are analyzed using the Material A fiber modulus. The six ply region of Materials H and J were 0.25 inch thick, with 70% 0° reinforcement. For the application of a $[0/0/0/\pm45/0/0]_s$ laminate with individual ply thicknesses of 0.018 inch, the program yields the following properties;

$$E_{11} = 3,470,000 \text{ psi}$$
$$E_{22} = 874,527 \text{ psi}$$
$$\nu_{12} = 0.311$$
$$G_{12} = 325,682 \text{ psi}$$
$$E_{xx} = 2,794,000 \text{ psi}$$
$$E_{yy} = 1,019,000 \text{ psi}$$
$$\nu_{xy} = 0.4252$$
$$G_{xy} = 510,900 \text{ psi}$$

According to this program, the ±45° plies will fail in transverse tension at an applied stress of 31.0 ksi, at which point the various laminae stresses are;

        0° Ply: σ_{11} = 38,140 psi
                   σ_{22} = -1,136 psi
                   τ_{12} =   0 psi
        45° ply: σ_{11} = 12,230 psi
                   σ_{22} =   3,750 psi   <--- Failure
                   τ_{12} = ±5,150 psi

At this stress level, equivalent to 1.1% strain, cracks would develop in the ±45° plies parallel to the fiber direction. The transverse and shear moduli of the ±45 plies would be effectively reduced to zero, whereas the longitudinal modulus would remain relatively unchanged. The conservative approach assuming the ±45° plies to reduce to 0 stiffness calculates a modulus drop from 2.79 to 2.43 msi. Under constant displacement, this results in a laminate stress reduction from 31 to 27 ksi, and an associated 0° fiber stress increase from 38.1 to 38.6 ksi. Total failure occurs when the 0° fibers reach a stress of 82 ksi (Material A) under a laminate stress of 57.4 ksi. Experimental results give an average UTS of 82 ksi and failures occur at the joint. Since this value is based on the entire 6 ply cross-sectional area, a calculation of 4/6 * 82 = 54.7 ksi, gives an approximate value to the actual ply stress in the 4 ply joint region. Thus, the estimate of no ±45 contribution was not conservative enough when coupled with geometric assumptions of the joint region. The added fraction of 0° reinforcement significantly reduces the impact of ±45°

cracking, as well as increase the overall UTS.

Material N [0/±45] Analysis

The triaxial Material N has $V_f = 0.5$ and is analyzed using the Material A fiber modulus (10.4 msi). The four ply material is 0.125 inch thick, with 50% 0° reinforcement. For the application of a $[0/\pm45/0]_s$ laminate with individual ply thicknesses of 0.016 inch, the program yields the following properties;

$$E_{11} = 5,450,000 \text{ psi}$$
$$E_{22} = 1,331,930 \text{ psi}$$
$$v_{12} = 0.285$$
$$G_{12} = 498,610 \text{ psi}$$
$$E_{xx} = 3,557,000 \text{ psi}$$
$$E_{yy} = 1,685,000 \text{ psi}$$
$$v_{xy} = 0.4793$$
$$G_{xy} = 1,017,000 \text{ psi}$$

According to this program, the ±45° plies will fail in transverse tension at an applied stress of 29.3 ksi, at which point the various laminae stresses are;

0° Ply:	σ_{11} =	44,340 psi
	σ_{22} =	-2,178 psi
	τ_{12} =	0 psi
45° ply:	σ_{11} =	12,770 psi
	σ_{22} =	3,750 psi <--- Failure
	τ_{12} =	±6,085 psi

At this stress level, equivalent to 0.8% strain, cracks would develop in the ±45° plies parallel to the fiber direction. The transverse and shear moduli of the ±45 plies would be effectively reduced to zero, whereas the longitudinal modulus would remain relatively unchanged. The conservative estimate

of setting the ±45° ply contribution to E_{xx} equal to zero suggests a modulus reduction from 3.56 to 2.73 msi. Although Figure 37 indicates non-linear behavior to failure, modulus fatigue plots (E/Eo) show good correlation reducing from an initial modulus of 3 msi down 20%. This reduction in modulus would shift the overall stress down from 29.3 to 22.45 ksi and the 0° ply stress up from 44.3 to 44.9 ksi. Total failure occurs when the 0° fibers reach their UTS of 108 ksi at the applied stress of 54 ksi. The results of static strength tests fall about 69 ksi, so again the prediction is conservative ignoring the contributions of the 45 plies. The relative increase in V_f is noticeable both in the higher modulus and UTS, but as expected contributes nothing to the load/modulus shift at ±45 ply failure.

Material N [90/±45] Analysis

The triaxial Material N has V_f = 0.5 and is analyzed using the Material A fiber modulus (10.4 msi). The four ply material is 0.125 inch thick, with 50% 90° reinforcement. For the application of a $[90/±45/90]_s$ laminate with individual ply thicknesses of 0.016 inch, the program yields the following properties;

$$
\begin{aligned}
E_{11} &= 5,010,000 \text{ psi} \\
E_{22} &= 1,318,510 \text{ psi} \\
\nu_{12} &= 0.285 \\
G_{12} &= 494,000 \text{ psi} \\
E_{xx} &= 1,685,000 \text{ psi} \\
E_{yy} &= 3,557,000 \text{ psi} \\
\nu_{xy} &= 0.227 \\
G_{xy} &= 1,017,000 \text{ psi}
\end{aligned}
$$

Back calculating the contribution of the 50% ±45° plies show E_{xx45} to be 1.94 msi. According to this program, the 90° plies will fail in transverse tension at an applied stress of 4.97 ksi, at which point the various laminae stresses are;

```
90° Ply:   σ₁₁ = -2,580 psi
           σ₂₂ =  3,750 psi   <--- Failure
           τ₁₂ =      0 psi
45° ply:   σ₁₁ =  6,780 psi
           σ₂₂ =  1,990 psi
           τ₁₂ = ±1,805 psi
```

At this stress level, equivalent to 0.3% strain, cracks would develop in the 90° plies parallel to the fiber direction. The modulus of the 90 plies would be effectively reduced to zero in the loading direction. Thus, the overall laminate modulus drops from 1.6 msi to (.50*1.94) 0.97 msi. The correlation with Figure 38 is not straight forward as the plot exhibits multiple shifts in modulus.